Mathematical Models of Immune Responses to Infectious Diseases

Samantha H. Erwin

Dissertation submitted to the Faculty of the
Virginia Polytechnic Institute and State University
in partial fulfillment of the requirements for the degree of

Doctor of Philosophy
in
Mathematics

Stanca M. Ciupe, Chair
Lauren M. Childs
Matthias Chung
Lizette Zietsman

March 20, 2017
Blacksburg, Virginia

Keywords: Mathematical biology, theoretical immunology, ordinary differential equations, model validation.

Mathematical Models of Immune Responses to Infectious Diseases

Samantha H. Erwin

ABSTRACT

Infectious diseases are disorders caused by bacteria, viruses, fungi or parasites. Mathematical models provide an extra tool into the study of dynamical interactions between pathogens and the immune responses they solicit. In this dissertation, we present three projects that investigate the mechanisms behind such diseases and the immune responses required for successful disease resolution: a study of HIV and HPV co-infection, a germinal center dynamics model, and a study of monoclonal antibody therapy.

In the first chapter we present the relevant biological background related to infections of human immunodeficiency virus (HIV) and human papilloma virus (HPV). We present information for the cellular and humoral immune response components of the adaptive immune response against these agents, culminating with the known mechanisms behind germinal center formation and their role in antibody function. We then present the concept of monoclonal antibody-based therapeutics.

In chapter 2, we present a background of in-host mathematical models and explain several numerical and analytical techniques used throughout this work, including ordinary differential equations, stability analysis, sensitivity analysis, and parameter estimation.

In chapter 3, we present a model of co-infection with two viruses, HIV and HPV. HIV-infected patients have an increased risk for a variety of co-infections. We focus specifically on the co-infection with HPV. To determine the role of HIV-associated immune suppression in HPV persistence and pathogenesis, we developed a mathematical model of HIV/HPV co-infection. Our model captures known immunological and molecular features, such as impaired HPV-specific effector cell responses and enhanced HPV infection due to HIV. We use the model to determine HPV prognosis in the presence of HIV infection, and identify conditions under which HIV infection alters HPV persistence. The model predicts that the condition leading to HPV persistence during HIV/HPV

co-infection is the permissive immune environment created by HIV, rather than direct HIV/HPV interaction. The model also elucidates the criteria for acute persistence of HPV infection in a co-infected patient undergoing antiretroviral therapy.

In chapter 4, we present our first project involving the development of novel mathematical models to investigate the role of germinal centers during acute and chronic infections. The ability of the immune system to clear pathogens is limited during chronic infections where potent long-lived plasma and memory B-cells are produced only after germinal center B-cells undergo many rounds of somatic hypermutations. We investigate the mechanisms of germinal center B-cell formation by developing mathematical models for the dynamics of B-cell somatic hypermutations. We use the models to determine how B-cell selection and competition for T follicular helper cells and antigen influences the size and composition of germinal centers in acute and chronic infections. We predict that T follicular helper cells are a limiting resource in driving large numbers of somatic hypermutations and present possible mechanisms to overcome this limitation in the presence of non-mutating and mutating antigen.

In chapter 5, we develop a mathematical model of monoclonal antibody therapy. Broadly neutralizing antibodies against HIV are able to act in many different ways in vivo: they can block viral entry, clear plasma virions, or lead to the death of virus-expressing cells. Recently, the 3BNC117 broadly neutralizing antibody has been tested in a Phase I clinical trial as a potential alternative treatment of HIV. We test if 3BNC117 presents with one or a combination of these antiviral effects by developing a pharmacokinetic model of 3BNC117 dynamics and estimating patient's parameters. We use this model together with a viral dynamics model to test the effects of 3BNC117. We fit the viral dynamics model to HIV RNA measurements from patients given antibody therapy and conclude that 3BNC117 elicits both neutralizing and non-neutralizing effects across most patients. We predict that the combined effects of initial CD4 T cell count, initial HIV levels, and virus production are strong indicators of patient's response to 3BNC117 as an immunotherapy. We end by modeling the effect of antibody boosting on the long-term HIV levels.

We conclude this work with a summary of our present conclusions and a discussion of potential extensions of the methods and results described herein. We present further applications of this work in non-human organisms that could enhance the lives and medical treatment of animals in the veterinary industry.

Mathematical Models of Immune Responses to Infectious Diseases

Samantha H. Erwin

GENERAL AUDIENCE ABSTRACT

In this dissertation, we investigate the mechanisms behind diseases and the immune responses required for successful disease resolution in three projects: i) A study of HIV and HPV co-infection, ii) A germinal center dynamics model, iii) A study of monoclonal antibody therapy. We predict that the condition leading to HPV persistence during HIV/HPV co-infection is the permissive immune environment created by HIV, rather than the direct HIV/HPV interaction. In the second project, we develop a germinal center model to understand the mechanisms that lead to the formation of potent long-lived plasma. We predict that the T follicular helper cells are a limiting resource and present possible mechanisms that can revert this limitation in the presence of non-mutating and mutating antigen. Finally, we develop a pharmacokinetic model of 3BNC117 antibody dynamics and HIV viral dynamics following antibody therapy. We fit the models to clinical trial data and conclude that antibody binding is delayed and that the combined effects of initial CD4 T cell count, initial HIV levels, and virus production are strong indicators of a good response to antibody immunotherapy.

To my family: Mom, Dad, Dan, Chloe and Adora. This would not of been possible without you.

Acknowledgments

I would like to thank my advisor, Dr. Stanca Ciupe, for her support and guidance over the past 4 years; you pushed me harder to do things I didn't think I could. Thanks to Dr. Maeve McCarthy for sparking my interest in Mathematical Biology many years ago while I was at Murray State. Your support early on and continued guidance has helped shaped my future goals. To Dr. Terry Herdman for giving me the opportunity to study at Virginia Tech so many years ago and having faith in me. I would like to thank Dr. Joe Ball for showing me how to get your hands dirty in mathematics, and helping me through that first year - it was rough. I would also like to express my gratitude to Dr. Jeff Borggaard who advised my early work in Fluid Dynamics and Dr. Lizettee Zietsman for being a supportive member of all of my academic committees. Also thank you to the rest of my committee for their support in this venture. My gratitude to the Department of Mathematics at Virginia Tech, and Eileen Shugart for helping me develop into the mathematics teacher I am today. I must also thank my colleagues at q-Bio, the people from T-6 at Los Alamos, and the staff at the Center for Talented Youth for 3 wonderful summer experiences.

To all of my friends who have enriched my life during my stay in Blacksburg - Justin Krueger, Kelli Karcher, Tanner Slagel and Holly Grant, just to name a few. A special thanks to Ryan Shifler; we started this journey at visitor's day and we actually made it! To my friends who have kept me entertained outside of graduate school: Rachel Neff, Jennifer Robertson, Mallory Vale and Melodie Weintraut. The horse shows, vacations, and hours of phone calls we've had kept me sane over the past 6 years. I must also thank Daniel Sweeney for the many nights we spent working on dissertations, talking science and for being a sounding board for each other. I can't wait to see what the future holds for us. Most importantly I thank my horse Adora for providing so many needed breaks. To my dog Chloe, you were by my side for nearly every step of this work and losing you this last month was the hardest part of all.

Finally, my family has been a constant source of support, encouragement, and inspiration during my entire life, academic career, and graduate school, you are wonderful. My gratitude to them: Virginia and Ray Bartlett, Melva and Bud Erwin, Karen Sparks, Constance Erwin, Tom and Rebecca Cains & Katherine and Ed Bowling. To my parents, Terri and Randy Erwin, you are the greatest and most supportive parents any person could ask for, thank you for helping me chase all of my dreams.

Contents

List of Tables

List of Figures

Chapter 1

Introduction

1.1 Mathematics in medicine

Mathematical biology is a broad field that studies mathematical applications to medicine and other life sciences [59]. Mathematical medicine is a flourishing area of research that has gained increasing popularity, especially in recent years. There are numerous fields of medicine where mathematics has historically been utilized including population growth, genetics, anatomy, epidemiology, and immunology [12, 55, 76, 80, 121]. The content of this dissertation is centered around the application of mathematics to immunology and virology.

As an elementary example, mathematics may be used to study population growth. Specifically, the growth and decay of bacterial colonies, populations of cancer cells and immune cells can be described using mathematical models. Such models can be divided in to two distinct categories: discrete and continuous. Discrete models are used when the variables undergo discrete processes and continuous models are used when the variables change continuously. Both discrete and continuous models have proven to be useful in expanding our understanding of medicine.

Some of the most well-known contributions at the intersection of medicine and mathematics have led to Noble Prize achievements. The mathematics developed by Allen McLeod Cormack were instrumental in improving early X-ray technology. He used a series of cross sectional images to digitally reconsruct three-dimensional anatomy, in what has since become known as Computer Assisted Tomography [26]. While mathematics has been used to enhance medical technology, it has also proven useful in understanding and describing complex interactions within the body. For example, Alan Lloyd Hodgkin and Andrew Fielding Huxley created one of the first models to successfully capture the complex dynamics of signal propagation in neurons [90]. While their original work was developed using giant squid neurons, the model is now used as the basis for understanding the flow of ionic currents through excitable cell membranes throughout the body [56]. Mutations in a population of bacteria were also investigated using mathematical models that resulted in the development of the Luria-Delbruck fluctuation test. The test itself was developed in 1943 to investigate how variation arises in a population over time [84] and has since found broad applications to evolutionary processes in general. For a more in-depth discussion of these models, and many others, we refer the reader to a complete text book on the topic [59].

This dissertation focuses specifically on the application of differential equations to understanding virological and immunological processes. Specifically we discuss the results from three main research projects: i) a model of human immunodeficiency virus and human papilloma virus coinfection ii) a mathematical model of germinal center formulation and function, and iii) the use of monoclonal antibodies as therapeutics in human immunodeficiency virus infection. In the next sections we will provide a comprehensive overview of the relevant immunological and virological concepts within this dissertation.

1.2 Virology

A virus is a microscopic, infectious agent that inserts itself into biological cells and incorporates its genetic information into the host. In this manner, the host cell synthesizes replicates of the original virus which, in turn, infect other cells. Though organisms across all five taxalogical kingdoms are affected by viruses, viruses themselves cannot replicate independently of their hosts. A typical complete virus particle, or virion, consists of nucleic acids (DNA or RNA) that compose the viral genome enveloped in a protective protein layer called the capsid. A virus may evolve over time, however it does not have its own metabolic processes and locomotion, depending on its host entirely for its propagation [63]. When viruses hijack the cellular machinery of the host, they may cause a variety of infectious diseases, such as the common cold, smallpox, yellow fever, and rabies and may ultimately lead to conditions such as cancer. In the following sections we present an in depth discussion of two specific viruses, human immunodeficiency virus (HIV) and human papillomavirus (HPV).

1.2.1 Human immunodeficiency virus

Human immunodeficiency virus (HIV) belongs to the lentiviruses family, which is a group of viruses that continues to replicate for years before an individual becomes symptomatic. Retroviruses are viruses that exploit the RNA to DNA translation during the cellular process of DNA replication and insert themselves in the host genome [63]. The HIV virus itself is an enveloped retrovirus that contains two copies of its RNA-based genome. The HIV virion is surrounded by an envelop expressing glycoproteins, such as gp41 and gp120, on its surface that help bind the virion to a target cell. There are multiple binding sites on the HIV virion that are used to attach to target cells. Typically, HIV predominately targets CD4 T cells, though dendritic cells and macrophages are also infected [172]. Herein, we refer to CD4 T cells as target cells in our discussion and models of HIV dynamics. It must be noted that binding to a target cell alone is not enough for HIV to enter a target cell; HIV must also express a co-receptor, usually the chemokine receptors CCR5 or CXCR4 [77]. Numerous studies have investigated these co-receptors as potential therapeutic targets [103, 127, 139], however we will ignore them in our work.

After an HIV virion enters a target cell, the viral DNA is integrated into the host cell's genome and forms a provirus. Virus replication is then initiated within the host cell's natural processes, usually an activated CD4 T cell, though infection could occur in a memory CD4 T cell or a dormant macrophage, in which case the infection may remain in a latent phase. Over the course of an HIV infection, rapid mutations occur in the HIV genome while CD4 T cell levels drop. Once infected cells are activated, replication occurs and new virions burst from the infected cell while the immune system attempts to initiate an adaptive immune response [63]. This process is discussed in more detail in Section 1.3.2.

HIV infection generally occurs after the exchange of bodily fluids with an infected individual, usually from sexual intercourse, contaminated needles, or poor medical practices. The first cases have been traced back to infected chimpanzees [144]. In some cases, people may not know they are infected because early onset symptoms resemble mild flu-like symptoms, though they are contagious, which leads to public health concern. This initial phase of HIV infection is the seroconversion phase, it occurs within the first few weeks, CD4 T cells levels drop and antibodies began to appear (more about the development of antibodies in Sections 1.3.1 and 1.3.2). Once this acute infection has passed, CD4 T cell levels rebound, and the viral load is reduced and the patient enters into a state known as the asymptomatic phase or clinical latency. The length of the asymptomatic phase is directly correlated with an individual increase in HIV RNA. Eventually most HIV infected individuals, if untreated, will progress into the symptomatic phase and eventually AIDS [54].

Interestingly, a small population of long term non-progressors exhibit high CD4 T cell levels and low levels of virus, while other individuals that have been exposed to HIV remain uninfected [63]. Understanding how these individuals' immune systems function is a popular topic in modern vaccine development and is discussed in greater detail in Section 1.3.2.

Currently, the primary form of HIV treatment is a combination of antiretroviral therapies (cART). These drugs target two specific HIV replication phases: the provirus synthesis (using a reverse transcriptase inhibitor) and the viral cleaving phase (using a protease inhibitor) [4]. cART is highly effective and patients see rapid viral drop within the first 2 weeks, at which point 99% of the initial viral level is eliminated [119]. After this, viremia is reduced more slowly because the remaining virus is contained in longer-lived cells, such as memory CD4 T cells, dendritic cells and macrophages [119]. A patient's viral load may remain below the limit of detection indefinitely, with occasional viral blips, as long as they remain on cART [25]. However, if a patient stops cART, the infection returns, likely due to latent viral reservoir. Additionally, if a patient does not follow the treatment regimen, it is also possible to develop drug resistance [132]. While current HIV therapy is effective as maintaining reduced viral laves, it is still not capable of clearing the virus. Every year an estimated 1.2 million people die globally and, while this is down from previous years, the need for a cure to this deadly virus is a world health issue [162].

1.2.2 Human papilloma virus

Human papilloma virus (HPV) is a prevalent genital infection that can potentially lead to cervical cancer [41]. Of the more than 40 different types of HPV, 15 are known to cause tumors, and, of those, HPV 16 is responsible for over 50% of these tumors [64]. Close to 80% of women worldwide are infected with HPV and it is detectable in nearly all cervical cancers. Cervical cancer is the second most common cancer worldwide, causing over 250,000 deaths each year [116]. For most people, HPV is cleared within 6-18 months, but some will have viral persistence that may eventually develop cervical cancer [43]. Currently, the only apparent risk factor for HPV persistence is immunodeficiency and HPV type. Understanding the factors that lead to HPV clearance motivates the development of better treatments that may ultimately reduce the prevalence of cervical cancer.

HPV infection occurs in epithelial cells, which form the outer body surfaces that provide a physical barrier between the body and its external environment. The tight junctions that connect the epithelial cells form the structure of this barrier to limit the available routes of infection to potential external pathogens [161]. When the HPV virion is able to pass through the basal layer via a microabraision to the suprabasal layer where replication of the virus occurs, an individual becomes infected with HPV [35]. The HPV virion encodes the proteins E6 and E7 which promote cellular proliferation, progression and apoptosis prevention. Because, HPV only infects the basal layer, and has no viremic phase, there is a limited immune response as the infection becomes established [40].

People with prevalent HPV infections exhibit little or no CD4 T cell response, and have significantly fewer Th1 and Th2 T cells than people who clear the infection [41]. Th1 cells are responsible for the production of cytotoxic T lymphocytes that destroy viral cells, and it is believed that these cells are down regulated by HPV. The Th2 cells initiate an antibody-mediate response, however this response is likely insufficient to clear an HPV infection, but may be helpful for vaccination purposes [41]. Another potential effect of HPV is the activation of Treg cells. HPV-specific Treg cells are found in HPV infected individuals where they are normally responsible for keeping the immune system in check and preventing over immune responses. If HPV up-regulates Treg cells, it could down-regulate Th1 and Th2 cells. While interesting, this particular cascade is only speculative. In general, many of the immune responses in HPV are still poorly understood [41]. In typical infections, B cells are responsible for producing antibodies to attack foreign particles. However, because HPV proteins are expressed entirely in the epithelium, these antibody responses are insufficient [152].

There is no treatment for HPV infection. The current course of management is to treat HPV-associated lesions as the occur and it is inconclusive if these treatments reduce infectiveness [89]. As of May 2017, Gardasil 9 is the only approved vaccine for HPV and it protects against 9 types of HPV: 16, 18, 31, 33, 45, 52, 58 [91]. HPV 16 and 18 cause 70% of cervical cancers, while the next-most frequently types detected were HPV 31, 33, 45, 52 and 58. Due to the complex nature of the infection, its location, and its potential to lead to cancer, vaccination is currently the best course of prevention of HPV [89].

1.3 Immunology

When an individual is infected by a pathogen, its immune system responds by initiating a complex signaling cascade to mitigate the potential damage the foreign invader could cause—an immune response. In some cases, the immune response is highly specific to a particular targeted pathogen, though in other cases, the immune system may respond only broadly.

When a pathogen is introduced into a host organism, the immune response may be classified by how the response is triggered and by its specificity to the invading pathogen. The processes part of the adaptive immune response specifically targets the antigen which may, in some cases, lead to life-long immunity from the pathogen. Innate immune responses are not specific, while adaptive immune responses have high specificity for the invading pathogen [63]. In this work, we will discuss mathematical models we have developed in order to better understand adaptive immune responses. We now focus our discussion to biological background of adaptive immune responses, germinal centers, and antibody production. Later we develop new mathematical models to gain a deeper understanding of germinal centers and the effects of antibodies on infected individuals.

1.3.1 Germinal center development

Lymphocytes, a subgroup of white blood cells, are directly responsible for the adaptive immune response. Lymphocytes can be divided into several types, though our present discussion will largely involve only two: i) B cells that differentiate into plasma cells and secrete antibodies or ii) T cells that either become cytotoxic T cells that kill infected cells or activate B cells and macrophages. Lymphocytes are continually circulated through the lymphatic tissues, lymph nodes, and the spleen where they may encounter an antigen presented by dendritic cells or macrophages that have previously had contact with a pathogen [63].

Naive T cells are cells that have not had contact with antigen-presenting cells. T cells are activated when they interact with an antigen presenting cell, triggering antigen-specific T cell subpopulations

[15, 27]. Each of these subpopulations plays a role in the antigen-specific response. For example, Type 1 T helper cells (Th1) activate macrophages and stimulate antibacterial responses and Type 2 T helper cells (Th2) stimulate B cells to produce antibodies. Additionally, regulatory T cells (Treg) defend against immune system overreaction [135], while Tfh cells regulate the production of long-lived plasma and memory cells [70]. Tfh cells and the specific process of creating long lived plasma and memory cells are of particular interest because it is through long lived plasma and memory cells that long-term immunity against pathogens is developed [28].

During their early interactions with antigen-presenting cells, naive T cells that are fated to become Tfh cells, and are known as pre-Tfh cells [154]. In Figure 1.1 this occurs during step 1 when a naive T cell interacts with a dendritic cell. These pre-Tfh cells are found where T cells and B cells interact (T:B border) and function to prime B cells for proliferation [126] (step 2 in Figure 1.1). During this interaction, pre-Tfh become Tfh cells and migrate into the center of a physiological immune structure known as a germinal center [154] where they themselves interact with B cells [126], (step 3 in Figure 1.1). Finally, during step 4, the germinal center response is initiated.

Germinal centers are areas where B cells undergo rapid proliferation and are divided into two regions: the dark zone where B cells undergo rapid somatic hypermutations and the light zone that is less dense and contains a network of follicular dendritic cells and T follicular helper cells [2]. The follicular dendritic cells in the light zone capture antigen and present it for up to a year in order to allow sufficient time for B cells to recognize and respond to the antigen. The process by which the B cells are selected to respond to the antigen is known as affinity maturation and is driven by the Tfh cells [168]. The mathematical models in this dissertation focus specifically on the somatic hypermutations in the dark zone and the diversity of antigens presented by Tfh cells and to which B cells respond.

More specifically, somatic hypermutation describes the process in which B cells rapidly replicate and, through this replication, are better able to adapt to pathogens within the body. Beyond a simple replication process, somatic hypermutation simultaneously involves the process of affinity

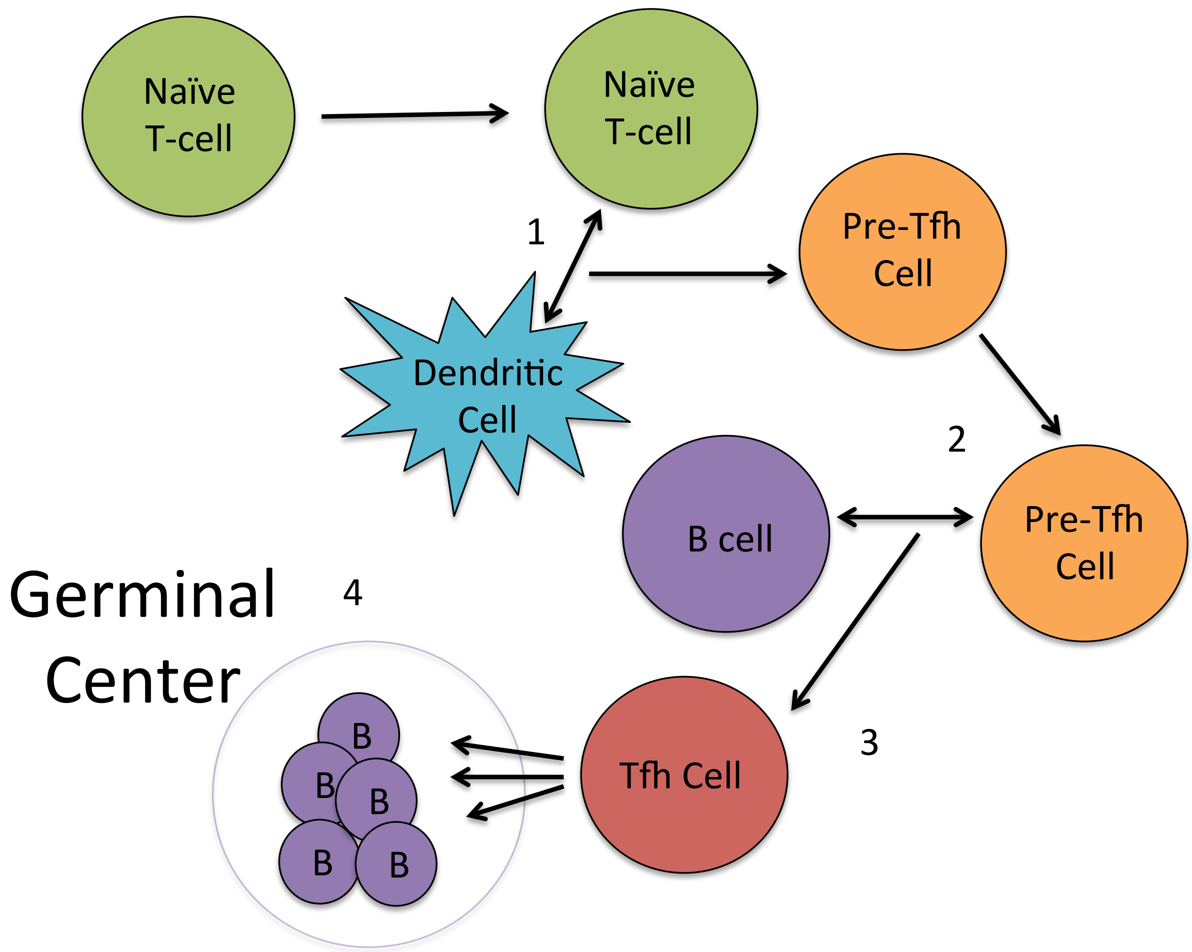

Figure 1.1: The development of the germinal center: (1) Naive CD4 T cells interact with dendritic cells. (2) Upon antigen activation pre-Tfh cells migrate to interact with initial *B* cells. (3) Tfh cells and B cell initiate collaboration develops germinal centers. (4) Tfh promotes B-cell maturation. The germinal center response leads to memory and plasma cell formation [171].

maturation. Affinity maturation describes the process by which B cells enhance their affinity, or tendency to bind, to pathogens within increasing rounds of replication. Together, somatic hypermutation and affinity maturation allow B cells to become increasingly productive in their ability to target and destroy pathogens [2].

Through the processes of somatic hypermutations and affinity maturation, germinal centers create fully differentiated B cells, known as plasma cells, which produce antibodies and memory cells that are specifically formulated to target a specific antigen [168]. Memory cells help to ensure a faster, adaptive immune response during a subsequent encounter with an antigen following an initial exposure. However, in some instances, an immunocompromised patient may never form plasma cells and others may not be able to properly clear a viral infection. Understanding the mechanisms that lead to a successful immune response is imperative to furthering medical research, especially in areas including vaccine development [168] and immunotherapy. Understanding the mechanics of germinal center formation and plasma and antibody production is the first step to understanding how to successfully elicit these responses to enhance an individual's immunological well-being.

1.3.2 Antibodies

In Section 1.3.1 we presented the biology of germinal center development. Germinal centers are structures that are classified as part of the humoral immune response within the overall adaptive immune response. The humoral immune response involves B cell maturation and function that concludes with the production of antibodies. Antibodies are Y shaped molecules that are produced from B cells that mature into plasma [63].

Antibodies have three main functions in the adaptive immune response: neutralization, opsonization, and complement activation. Neutralization occurs when antibodies bind to virions and block them from infecting or destroying cells. Antibodies also cause opsonization which occurs when antibodies coat a pathogen or foreign particle and direct phagocytes to ingest and destroy it. The third function, is activation of the complement system, which enhances the ability of the antibodies and phagocytes to fight infection. In basic infections, an immune response is initiated and the pathogen is cleared, however in some cases the adaptive immune response is not sufficient to clear in an infection. Specifically, for this dissertation, we will discuss inefficient responses in the context of HIV infection [63].

Broadly neutralizing anti-HIV antibodies that develop after many rounds of somatic hypermutation in the germinal center as a result of Tfh and B cell interaction are not usually produced in HIV infection [29]. It has been shown that after several years of infection, 10-30% of infected patients develop antibodies capable of neutralizing a variety of different HIV strains [151] but cannot control the highly mutated HIV in their own bodies which has mutated and has escaped antibody function.

Broadly-neutralizing antibody responses are of interest for vaccine purposes. If a broadly-neutralizing response can be induced during the early stages of an infection, an individual may be able to block the virus spread. In an effort to develop a vaccine that takes advantage of the broad antibody activity, researchers are investigating way to induce broad responses naturally [151]. Moreover, broadly neutralizing antibodies can be used therapeutically through infusion. Recently, researchers have started testing monoclonal antibodies as therapy in already infected patients.

Monoclonal antibodies are antibodies derived from a pure single cell line, pre-determined for a specific substance [158] To manufacture monoclonal antibodies, researchers immunize animals repeatedly with the antigen of interest. The animal must be tested to ensure adequate production of the desired antibody and, following successful testing, the spleen is removed and the cells dissociated *in vitro*. Splenic B cells are fused with myeloma cells to produce a hybridoma that is immortalized in culture while also producing the antibody of interest. Researchers culture each hybridoma individually to generate monoclonal antibodies or all together to generate polyclonal antibodies [45]. Following validation against known pathogen samples, the antibodies may be used in a clinical setting. A polyclonal antibody is significantly easier to create because it is less labor intensive, however there is high variability and large amount on non-specific antibodies are simultaneously generated. Monoclonal antibodies however have high specificity.

To date, there are thousands of monoclonal antibodies derived from a variety of species including mice, donkeys, camels, rabbits, and humans which are available for research and clinical purposes [1]. Monoclonal antibodies have been used in to treat a variety of diseases including tumor necrosis, Chron's disease, rheumatoid arthritis and more [110, 142, 157]. Recently, the testing of monoclonal antibodies has begun in humans as an HIV treatment. While numerous monoclonal antibodies to HIV have been isolated, one particularly exciting antibody is 3BNC117 [138]. 3BNC117 neutralizes 195 out of 237 known HIV-1 strains in 6 different clades. In a recent Phase I clinic trial, 3BNC117 was tested on HIV-positive patients and was able to initially reduce HIV-viremia in all patients before the virus rebounded [19]. In this dissertation we will create a mathematical model to emulate the HIV viral dynamics of this specific clinical trial of 3BNC117 to develop a deeper understanding of the 3BNC117 effects and functions in each patient.

1.4 Manuscripts contained in this dissertation

This dissertation contains material that has been published or is being prepared for publication.

- M Verma*, **S Erwin***, V Abedi, S Hoops, R Hontecills, A Leber, J Bassaganya Riera and SM Ciupe. Modeling the mechanisms by which HIV-associated immunosuppression influences HPV persistence at the oral mucosa. PLoS One, 12(1), 2017.
- **S Erwin** and SM Ciupe. Germinal center dynamics during non-chronic and chronic disease. Math Biosci Eng, 14(3): 655-71, 2017.
- **S Erwin**, EF Cardozo, AS Perelson and SM Ciupe. Modeling HIV dynamics following 3BNC117 antibody infusion. [In-Preparation].

* Denotes equal contribution

In Chapter 1, I review virology and immunology. In Chapter 2, I present the mathematical tools used throughout our studies. In Chapter 3, we present the model of HIV and HPV co-infection dynamics; this work was developed in collaboration with individuals at the Biocomplexity Institute of Virginia Tech. In Chapter 4, I describe a model I developed along with the guidance of Dr. Stanca Ciupe to capture the germinal center dynamics following interactions between B cells and T follicular helper cells. In Chapter 5, I discuss a model of HIV dynamics following an infusion of 3BNC117 which was developed with guidance from Dr. Fabian Cardozo, Dr. Stanca Ciupe, and Dr. Alan Perelson.

Chapter 2

Basic concepts in mathematical models of infectious diseases

The first immunological models, developed in 1960s, are stochastic models of immune responses and antibody production [50, 87]. These were followed in the 1990s by virus dynamic models which investigate how viruses, such as human immunodeficiency [121], hepatitis B [23, 30, 112, 176], and influenza viruses [8, 13, 148], interact with the immune system. These models have been expanded to incorporate the concepts of immunity to pathogens through inclusion of immune responses such as cellular [21, 149] and humoral immune responses [5, 22, 24, 111, 112, 160]. Of particular interest to my work are models of antibody production inside germinal centers [61, 92]. Modeling approaches have provided, and will continue to provide, invaluable insight into complex immunological interactions making theoretical immunology one of the fastest growing subfields in mathematical biology [39].

The models utilized in the dissertation are systems of ordinary differential equations. Ordinary differential equations are used in biological applications when changes overlap continuously. That is, a variable's rate of change may by proportional to its production, death, infection, clearance and so on. Models that describe infections inside an individual are called in-host models. In the next section we will provide a brief history of in-host models and the mathematical tools used to evaluate such models.

2.1 In-host modeling

Through in-host modeling, researchers have gained a better understanding of the mechanisms that lead to chronic and acute infections following infection with a variety of pathogens. While in host models may vary based on the pathogen and host characteristics, the basic model, which was first used for HIV in-host modeling, is the most widely used model and has been adapted for a variety of diseases [121]. This model contains 3 cell populations: target cells, T, infected cells, I, and virus cells, V:

$$\begin{aligned} \frac{dT}{dt} &= s - dT - \beta TV, \\ \frac{dI}{dt} &= \beta TV - \delta I, \\ \frac{dV}{dt} &= pI - cV. \end{aligned} \tag{2.1}$$

Target cells are produced at a constant rate s, die at rate d and become productively infected at rate β, proportional to the interaction between target cells and the virus. Infected cells die at rate δ and produce virions at rate p. Virions are cleared at rate c [121]. This model has since been varied for HIV to account for bursting such that, $p = N\delta$, because virus is released at the end of an infected cell's life [32].

Some viral models consider a latent phase of infection, which occurs when a host has been infected but the symptoms have not appeared yet. To model this phase, called the eclipse phase, a variable E was included in the model. Target cells become infected at rate β, proportional to the interaction between target cells and the virus, to become latent cells, E. E then becomes productively infected cells, I, at rate k. The rest of the I and V dynamics are the same as in the basic model [11, 148].

The system is given by:

$$\begin{aligned}
\frac{dT}{dt} &= s - dT - \beta TV, \\
\frac{dE}{dt} &= \beta TV - kE, \\
\frac{dI}{dt} &= kE - \delta I, \\
\frac{dV}{dt} &= pI - cV.
\end{aligned} \tag{2.2}$$

A variation of the basic model has also been used to model acute infections. An acute infection is short in lifespan, such as dengue and influenza, and the infection resolves within a month [111]. To demonstrate the short course of the virus, the production and death rates of the target cells are ignored and the target population becomes $\frac{dT}{dt} = -\beta TV$.

The basic model has also been adapted to include immune responses. The cellular immune response leads to increased killing of infected cells by cytotoxic T-lymphocytes (CTL). To incorporate the CTL response in (2.1) an equation for CTLs, E, is added and the system becomes:

$$\begin{aligned}
\frac{dT}{dt} &= s - dT - \beta TV, \\
\frac{dI}{dt} &= \beta TV - \delta I - \mu IE, \\
\frac{dV}{dt} &= pI - cV, \\
\frac{dE}{dt} &= \alpha I - d_E E.
\end{aligned} \tag{2.3}$$

In this model, the CTL cells are activated a rate, α, proportional to I, and decay at rate d_E. The CTL cells kill the infected cells at rate μ [21]. Similarly, an adaptation to (2.1) can account for the humoral immune response.

The humoral immune response leads to production by B lymphocytes of antibodies who can have both neutralizing and non-neutralizing effects. These are incorporated by assuming that β is reduced to $\frac{\beta}{1+\alpha A}$ and that viral clearance is increased to $cV + c_A VA$. It is also assume antibodies are produced at rate k_p and die at rate d_A. The system describing these dynamics is given by:

$$
\begin{aligned}
\frac{dT}{dt} &= s - dT - \frac{\beta}{1+\alpha A} TV, \\
\frac{dI}{dt} &= \frac{\beta}{1+\alpha A} TV - \delta I, \\
\frac{dV}{dt} &= pI - cV - c_A VA, \\
\frac{dA}{dt} &= k_p AV - d_A A.
\end{aligned}
\tag{2.4}
$$

In this brief review we have introduced the basic model, and variations of the model to include latent infection, acute infection, cellular immune response and humoral immune response. Throughout this dissertation we utilize and develop different variations of the basic model. We also use a variety of tools to validate our model analytically and numerically. A brief background of these tools is presented in the remainder of this chapter.

2.2 Stability analysis

Steady state solutions of a system of differential equations are solution that do not depend on time. Or, precisely the rate of change for each state variable is zero. Utilizing the basic model (2.1) as an example, we set the derivatives equal to zero

$$
\begin{aligned}
0 &= s - d\bar{T} - \beta \bar{T}\bar{V}, \\
0 &= \beta \bar{T}\bar{V} - \delta \bar{I}, \\
0 &= p\bar{I} - c\bar{V}.
\end{aligned}
\tag{2.5}
$$

We solve for $(\bar{T},\bar{I},\bar{V})$ and find the two steady states:

$$(\bar{T_1},\bar{I_1},\bar{V_1}) = (s/d,0,0), \tag{2.6}$$

$$(\bar{T_2},\bar{I_2},\bar{V_2}) = (\frac{\delta c}{\beta p},\frac{s\beta p-d\delta c}{\beta pc},\frac{\delta\beta p-d\delta c}{\beta\delta c}). \tag{2.7}$$

The first solution represents a disease free steady state, and the second represents a chronic infection. The stability of a steady state, $(\bar{T},\bar{I},\bar{V})$ is determined by the signs of the eigenvalues of the Jacobian matrix. If all eigenvalues are negative or have negative real parts then $(\bar{T},\bar{I},\bar{V})$ is stable. Model (2.1) has the Jacobian:

$$J = \begin{pmatrix} -d-\beta V & 0 & -\beta T \\ \beta V & -\delta & \beta T \\ 0 & p & -c \end{pmatrix}. \tag{2.8}$$

Next, compute the eigenvalues by solving $det(J_{s_1}-\lambda I)=0$ where,

$$J|_{s_1} = \begin{pmatrix} -d & 0 & -\beta\frac{s}{d} \\ 0 & -\delta & \beta\frac{s}{d} \\ 0 & p & -c \end{pmatrix}. \tag{2.9}$$

Thus

$$det(J|_{s_1}-\lambda I) = (-d-\lambda)[(-\delta-\lambda)(-c-\lambda)-\frac{\beta ps}{d}] \tag{2.10}$$

and $\lambda_1=-d$ is negative. Next, we investigate the eigenvalues of the small system where

$$(-\delta-\lambda)(-c-\lambda)-\frac{p\beta s}{d}=0. \tag{2.11}$$

The remaining eigenvalues $\lambda_{2,3}$ are strictly negative if

$$1 - \frac{\beta sp}{cd\delta} > 0, \tag{2.12}$$

or

$$R_0 = \frac{\beta sp}{cd\delta} < 1. \tag{2.13}$$

Since these are the eigenvalues for the disease free steady state, then if (2.13) holds then the steady state, S_1 is stable.

This is the R_0 of (2.1). The reproductive number, R_0, represents the average number of secondary infections caused by a single infected cell in a naive population. In many models, R_0 is used as an indicator to how a disease will spread throughout a host. If $R_0 < 1$ then the infection will eventually clear, and if $R_0 > 1$ then an infection will persists. In our example, if the production rates are less than the death rates combined then the infection will clear. During model development, stability analysis is one of the first steps to ensure the model has reasonable characteristic of the infection. The next tools discussed in model development are sensitivity analysis and parameter estimation.

2.3 Sensitivity analysis

A sensitivity analysis determines the effect a parameter, q, has on a solution. If a small change in a parameter leads to large changes in the solution, we call the parameter sensitive. Instead of manually varying the parameters, a semi-relative sensitivity analysis shows how much a population will change if a parameter is doubled at a particular time. Sensitivity functions are derived with respect to an arbitrary parameter q by differentiating the system with respect to q and assuming each function is dependent on q and t.

As an example, we again use (2.1) for a sensitivity analysis and investigate the semi-relative sensitivities of the system with respect to β. The corresponding sensitivity system is:

$$\begin{aligned}
\frac{dT_\beta}{dt} &= -dT_\beta - TV - \beta T_\beta V - \beta TV_\beta, \\
\frac{dI_\beta}{dt} &= TV + \beta T_\beta V + \beta TV_\beta - \delta I_\beta, \\
\frac{dV_\beta}{dt} &= pI_\beta - cV_\beta.
\end{aligned} \tag{2.14}$$

These sensitivity solutions can be viewed as the Fréchet derivatives in the direction of the chosen parameter. For a specific parameter, the value of the sensitivity function indicates the rate of change in the state at time, t. The semi-relative sensitivity solution are calculated but multiplying the chosen parameter by the sensitivity solutions [14]. For example if we look at βT_β at a specific time t, we will know how much T changes at t if β is doubled. The underlying ideas of formulating the sensitivity equations are rooted in perturbation theory. The sensitivity solutions are the coefficients of the first order Taylor series for the original function where the parameter is treated as an independent variable.

2.4 Parameter estimations

Not all parameters are known experimentally, and through parameter identification we can validate our model and learn more about interactions within our system. Frequently we want to connect parameter b to observed data, y with a model f

$$f(b) = y. \tag{2.15}$$

For our work, f is always a solution of an ODE system, b is usually a vector to estimate, based on a given vector of data, y. The process of finding b given y is an inverse problem. In our work the data and model are both functions of time, so we are solving continuous inverse problems. It is common to refer to problems with a small number of parameters as "parameter estimation problems" and problems with large numbers of parameters as "inverse problems" [7].

In this dissertation we use two techniques to estimate parameters: Nonlinear regression and Markov chain Monte Carlo simulation.

2.4.1 Nonlinear regression

Generally, finding a curve that fits a data set is referred to as regression. Specifically, the statistical technique nonlinear regression, helps to describe experimental data that has nonlinear relationships.

To implement the nonlinear regression method, we use the `nlinfit` tool in MATLAB to estimate the parameters and calculate the normalized relative mean squared error. Let n be the number of data points, $\mathbf{b}$ the vector of parameters to be determined, y_i the data at time t_i and $f(t_i, \mathbf{b})$ is the function at time t_i and parameters $\mathbf{b}$. The MATLAB tool `nlinfit` minimizes the objective function,

$$J = \sum_{i=1}^{n} [\log(y_i) - \log(f(t_i, \mathbf{b}))]^2. \tag{2.16}$$

Also let M be the number of estimated parameters. The mean squared error is calculated by the $\mathscr{L}^2$ norm squared for the difference between the data vector, $\mathbf{y}$, and the estimation $f(\mathbf{t}, \mathbf{b})$ at the respective time normalized all over the difference between the number of data points and number of estimated parameters:

$$MSE = \frac{||\mathbf{y} - f(\mathbf{t}, \mathbf{b})||_2^2}{n - M}. \tag{2.17}$$

2.4.2 Markov chain Monte Carlo

Markov chain Monte Carlo (MCMC) is a sampling method that uses successive random selections to estimate parameters in complex models. To implement this algorithm we utilized the MCMC toolbox for MATLAB. Again we assume y_i the data at time t_i and $f(t_i, \mathbf{b})$ is an ODE solution at time t_i and parameters $\mathbf{b}$. The MCMC toolbox uses the sum of square errors given by:

$$\chi^2 = \sum_{i=1}^{n} \frac{(y_i - f(t_i, \mathbf{b}))^2}{2\sigma^2} \tag{2.18}$$

where σ is an estimate of the data error. The MCMC toolbox also utilizes the Gaussian likelihood function,

$$P(y|\mathbf{b}) = e^{-\chi^2}. \tag{2.19}$$

The Gaussian likelihood function estimates the probability that a specific set of parameters represents the data. The likelihood function is inversely proportional to the error. The MCMC toolbox employs a version of the Metropolis Algorithm to do a maximum likelihood estimation. The Metropolis Algorithm begins with an initial parameter guess, $\mathbf{b}_1$ and generates new proposed parameter set, $\mathbf{b}_2$. It computes the likelihood ratio:

$$\frac{P(y|\mathbf{b}_2)}{P(y|\mathbf{b}_1)} = e^{(-\chi_2^2 + \chi_1^2)}, \tag{2.20}$$

which is a positive real number. Where, $\chi_1^2 = \sum_{i=1}^{n} \frac{(y_i - f(t_i, \mathbf{b}_1))^2}{2\sigma^2}$ and $\chi_2^2 = \sum_{i=1}^{n} \frac{(y_i - f(t_i, \mathbf{b}_2))^2}{2\sigma^2}$. The algorithm picks a number at random from a unifrom distribution between 0 to 1; if the number is smaller than the ratio the algorithm replaces $\mathbf{b}_2$ with $\mathbf{b}_1$. This method is repeated, and a chain of values is generated, known as the Markov Chain [106].

In this chapter, we have provided a brief summary of the tools used in this work. We will now move our discussion to specific research problems and the models we developed using these tools.

Chapter 3

Modeling the mechanisms by which HIV-associated immunosuppression influences HPV persistence at the oral mucosa

In this work I share first authorship with Meghna Verma. I performed all of the numerical simulations, created all figures and performed the analysis. Meghna wrote most of the original introduction of the submitted paper, and we developed the conclusion together. The introduction and conclusion have been modified in this dissertation; additional explanations have been added as well. Dr. Stanca M. Ciupe oversaw in the computational components and Dr. Josep Bassaganya-Riera fostered the initial idea behind the project. All team members assisted in editing the final manuscript. The paper has been published in Plos One [165].

3.1 Abstract

Human immunodeficiency virus (HIV)-infected patients are at an increased risk of co-infection with human papilloma virus (HPV), and subsequent malignancies such as oral cancer. To determine the role of HIV-associated immune suppression on HPV persistence and pathogenesis, we developed a mathematical model of HIV/HPV co-infection and used it to investigate the mechanisms underlying the modulation of HPV infection and oral cancer by HIV. Our model captures known immunological and molecular features such as impaired HPV-specific effector T helper 1 (Th1) cell responses, and enhanced HPV infection due to HIV. We used the model to determine HPV prognosis in the presence of HIV infection, and identify conditions under which HIV infection alters HPV persistence in the oral mucosa. The model predicts that conditions leading to HPV persistence during HIV/HPV co-infection are the permissive immune environment created by HIV and molecular interactions between the two viruses. The model also determines when HPV infection continues to persist in the short run in a co-infected patient undergoing antiretroviral therapy. Lastly, the model predicts that under efficacious antiretroviral treatment HPV infections will decrease in the long run due to the restoration of CD4 T cell levels.

3.2 Introduction

At the time of writing, over 1.2 million people in the United States are infected with human immunodeficiency virus (HIV). These individuals have impaired defenses against other pathogens due to deficient immune responses. Currently, there is no known cure for HIV and management of the infection consists primarily of administration of combination antiretroviral therapy (cART), which has transformed HIV treatment and drastically reduced morbidity and mortality [3, 48]. cARTs are 99% effective; however drug resistance has been reported in up to 60% of the patients studied due to non-compliance with the prescribed treatment regimens and/or HIV viral mutation [51].

Moreover, while treatment can reduce the HIV infection below detectable levels, cART treatment regimens must be strictly followed to avoid viral rebound from activation of latent reservoirs.

While acquired immunodeficiency syndrome (AIDS) is a well-known risk for HIV patients, HIV also increases the risk of developing co-infection from other pathogens, including viruses (papillomavirus, herpesviruses, flaviviruses) and bacteria (Helicobacter pylori, Salmonella typhimurium, Chlamydophila pneumonia) [33]. Specifically, recent epidemiological data suggests that HIV patients have an increased risk of developing human papillomavirus (HPV)-induced cancers, including oropharyngeal cancer, invasive cervical cancer, anogenital cancer, and anal cancers [34, 38, 44, 46, 102, 125]. Interestingly, the direct biochemical connections between these two virus remains largely unknown due to two distinctly different sites of infection.

Both HIV and HPV infections are increased in individuals with high-risk sexual behavior and multiple sexual partners. It has been hypothesized that HIV patients who have lower CD4 T cell counts have a higher prevalence of oral HPV infection and more prevalent oncogenic expressing HPV [9]. HIV-induced immunosuppression further increases the risk of HPV-associated cancer due to a weakened immune system and a subsequent impaired immune response to HPV, as well as the interaction between the two viruses, can increase the risk of severe HPV infections in HIV patients [69, 155, 166].

HIV infection mainly targets CD4 T cells, though infection can occur in memory CD4 T cell or dormant macrophages [81]. The decrease in CD4 T cell levels is a validated biomarker of immunosuppression in HIV patients [65] and over the course of an HIV infection, rapid mutations occur in the HIV genome while CD4 T cell levels drop. On the other hand, HPV infection occurs in epithelial cells when the HPV virion is able to pass through the basal layer via a microabraision to the suprabasal layer where replication of the virus occurs and an individual becomes infected with HPV [35]. Because, HPV only infects the basal layer, and has no viremic phase, there is a limited immune response as the infection becomes established [40]. The immunological changes caused by HIV decreases the overall immune responses against HPV. Subsequently, HIV infection may increase the overall risk for oral HPV, though the mechanisms by which such reduction in CD4 T cell levels affect the immune response against HPV remain largely unknown.

Besides the effect of immunosuppression, interactions at the molecular level between HIV and HPV may have an affect on the pathogenesis of the secondary infection. HIV genes *tat*, *rev* and *vpr* have been reported to potentially affect HPV pathogenesis. Specifically, HIV protein tat, secreted from HIV infected intra-epithelial immune cells, plays a role in the disruption of epithelial tight junctions, facilitating entry of HPV into the mucosal epithelium [161].

To gain new insights into the underlying mechanistic interactions between HIV and HPV, in an HIV/HPV co-infection we developed a mathematical model of HIV and HPV interactions. Building on previous models of individual HIV [121] and HPV [107] infections, the model captures the molecular interactions between HIV and HPV due to *tat* and the effect of progressive depletion of CD4 T cells in HIV/HPV co-infection. Using the model, we aim to investigate if the prevalence of oral HPV infection is increased in HIV-infected individuals. We demonstrate how the dynamics of HIV/HPV co-infection changes under the influence of cART. The findings can be used to enhance our understanding of HIV/HPV co-infection dynamics and propose new theories that can be applied to reverse residual inflammation in individuals under the effect of cART.

3.3 Materials and methods

3.3.1 Mathematical model of HIV infection

We model the interaction between HIV and CD4 T cells as in [121, 123]. Briefly, we consider the interaction between three populations: i) target CD4 T cells (T), ii) productively infected CD4 T cells (I), and iii) HIV (V). Target cells are produced at rate s, die at rate d, and become productively infected at rate β proportional to the interaction between target cells and the virus. Infected cells produce N_1 virions throughout their lifetime, which are released through bursting, and die at rate

δ. The virus is cleared at a rate c_1 per day. The following system of ordinary differential equations (ODE) represents these dynamics:

$$
\begin{aligned}
\frac{dT}{dt} &= s - dT - \beta TV, \\
\frac{dI}{dt} &= \beta TV - \delta I, \\
\frac{dV}{dt} &= N_1 \delta I - c_1 V,
\end{aligned}
\tag{3.1}
$$

with initial conditions $T(0) = T_0$, $I(0) = I_0$, and $V(0) = V_0$.

The effect cART has been modeled as a reduction of the virus infectivity in the presence of reverse transcriptase inhibitors to $\beta(1-\varepsilon_{RT})$ and a reduction in the production of infectious virions in the presence of protease inhibitors to $N_1(1-\varepsilon_{PI})$. Here $0 \leq \varepsilon_{RT}, \varepsilon_{PI} \leq 1$ are the drug efficacies. [122, 123].

The model in the presence of cART becomes (see Fig. 3.1):

$$
\begin{aligned}
\frac{dT}{dt} &= s - dT - (1-\varepsilon_{RT})\beta TV, \\
\frac{dI}{dt} &= (1-\varepsilon_{RT})\beta TV - \delta I, \\
\frac{dV}{dt} &= (1-\varepsilon_{PI}) N_1 \delta I - c_1 V,
\end{aligned}
\tag{3.2}
$$

with initial conditions $T(0) = T_0$, $I(0) = I_0$, and $V(0) = V_0$. Note that models (3.1) and (3.2) do not take into account the HIV latent reservoirs, of long-lived resting CD4 T cells with integrated HIV in their genome [20].

3.3.2 Mathematical model of HPV infection

We model HPV in-host dynamics as in [107]. This is the only within host model to represent HPV dynamics using a system of ODEs. It was originally developed to understand the evolutionary

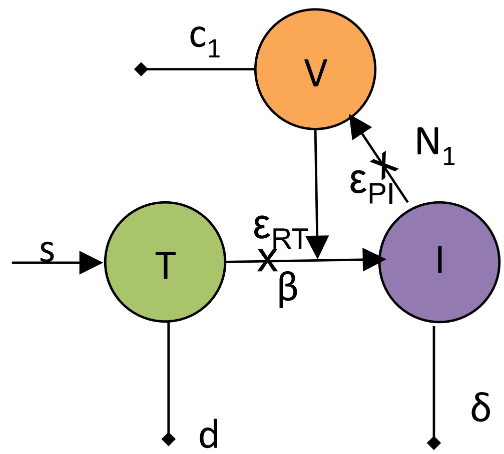

Figure 3.1: **HIV Diagram** A diagram for the HIV models (3.1) and (3.2).

selection process in response to an HPV vaccine. In the original HPV work, they focus on the oncogenic expression and how it changes in a vaccinated and unvaccinated host. For our work, we only consider the within host model of an unvaccinated host.

We consider the interaction between four populations: i) HPV infected basal epithelial cells (Y_1), ii) the HPV infected transit-amplifying cells, in the suprabasal epithelial layer (Y_2), iii) HPV (W) and iv) HPV-specific cytotoxic T lymphocytes (CTL) (E). We assume that N_2 is the total concentration of epithelial cells at the beginning of HPV infection and the basal layer is formed of uninfected basal epithelial cells, targeted by HPV. Upon HPV infection, the basal epithelial cells become infected Y_1 when HPV interacts with uninfected cells at rate ψ. We denote the difference $N_2 - Y_1$ as the concentration of uninfected epithelial cells. The basal infected cells, Y_1 traverse up through the epithelial column and transform into Y_2 cells, which move further into the suprabasal epithelial layer [35, 108]. The Y_2 cells become transit-amplifying cells which start assembling virions to be released at the surface [36, 134]. Therefore, both Y_1 and Y_2 cells are HPV infected cells but differentially located in the epithelial cell layer, wherein Y_2 cells are assumed to have higher expression of the oncogenes E6 and E7 compared to Y_1 [107]. For simplification, we assume that the uninfected cells and infected cells have an equal probability of interaction with the HPV virions irrespective of the spatial architecture of the tissue.

A more generalized model which takes into account the infectivity and layer transition terms, or one which would consider spatial structures for epithelial cells in different layers requires extensive knowledge of numerous parameters, which are currently unknown. We assume that the infection is density dependent with ϕ representing the uninfected cell concentration where the infection is half-maximal. We assume that infected cell populations Y_1 and Y_2 differ in terms of the oncogene expression such that the Y_2 (located in the suprabasal epithelial layer) have higher oncogene expression compared to Y_1 cells (located in the basal epithelial layer) [163]. The rate of oncogene expression of the HPV type present in an infected cell, given by ε controls the conversion of Y_1, into the transit-amplifying infected cells, Y_2. Cells, Y_2, grow at rate $r\varepsilon$, proportional to their own density and die at rate μ. Due to higher expression of oncogenes, the transit-amplifying cells, Y_2 divide more before death, compared to the basal infected cells Y_1. Since, both infected cell population have an expression of oncogene, as in [107], both types of infected cells produce free virions, W, at production rates k_1 and k_2, that are released through bursting. For simplicity, we consider an equal virion production rate of $k_1 = k_2 = k$. The HPV virions are cleared at rate c_2 [107]. The c_2 clearance rate captures the antibody clearance rate implicitly.

The clearance of HPV in the infected cells is associated with a successful immune response that includes the trigger of innate immune responses targeted against the virions released from the surface as well as infected cells [134]. In addition to the innate immune responses, the HPV-specific CTLs recruited during the adaptive immune response aid in the elimination of the infected basal cells [105]. Here, we assume that, after encountering transit-amplifying infected cells Y_2, effector cells specific to HPV, E, expand with a maximum per capita rate ω and carrying capacity K. This carrying capacity is an addition to the original work [107]. In the current model, the CTL response E is initiated only by Y_2 cells which have higher oncogene E6 expression [109, 143] compared to Y_1.

We disregard the differential CTL response against the infected cell populations and consider that HPV-specific CTL population E kills both classes of infected cells at the same rate a, since both infected cells populations express oncogenes E6 and E7 [105, 134]. Additionally, the model does not take into account the virus specific gene expression at any particular epithelial site. Finally, the functional differences in E6 and E7, which are major determinants of HPV pathogenicity between HPV types [40], are also neglected.

The following system of differential equations represents these dynamics (see Fig. 3.2):

$$\begin{aligned}
\frac{dY_1}{dt} &= \psi W \frac{N_2 - Y_1}{\phi + N_2 - Y_1} - \varepsilon Y_1 - \mu Y_1 - a Y_1 E, \\
\frac{dY_2}{dt} &= \varepsilon Y_1 + r\varepsilon Y_2 - \mu Y_2 - a Y_2 E, \\
\frac{dW}{dt} &= \mu(k_1 Y_1 + k_2 Y_2) - c_2 W, \\
\frac{dE}{dt} &= \omega Y_2 E (1 - \frac{E}{K}),
\end{aligned} \tag{3.3}$$

with initial conditions $Y_1(0) = Y_{10}$, $Y_2(0) = Y_{20}$, $W(0) = W_0$, and $E(0) = E_0$.

3.3.3 Co-infection model

The effect of *tat* protien

The only known connection between HIV and HPV is the viral protein *tat*. HIV-protein *tat* enhances HIV transcription and initiates T cell death and eventually enhances HIV patients toward AIDS progression. This protein is responsible for enhanced HPV infection as well. When secreted from HIV-infected intraepithelial immune cells, *tat* is known to play an important role in the disruption of epithelial tight junctions, thereby facilitating the entry of HPV into the mucosal epithelium [161]. We model the *tat* induced proliferation of epithelial cells by increasing N_2 to $N_2(1 + pV)$ where p is the effect of *tat* protein secreted by an HIV virion, V, *i.e.*,

$$\frac{dY_1}{dt} = \psi W \frac{(1 + pV)N_2 - Y_1}{\phi + (1 + pV)N_2 - Y_1} - \varepsilon Y_1 - \mu Y_1 - a Y_1 E. \tag{3.4}$$

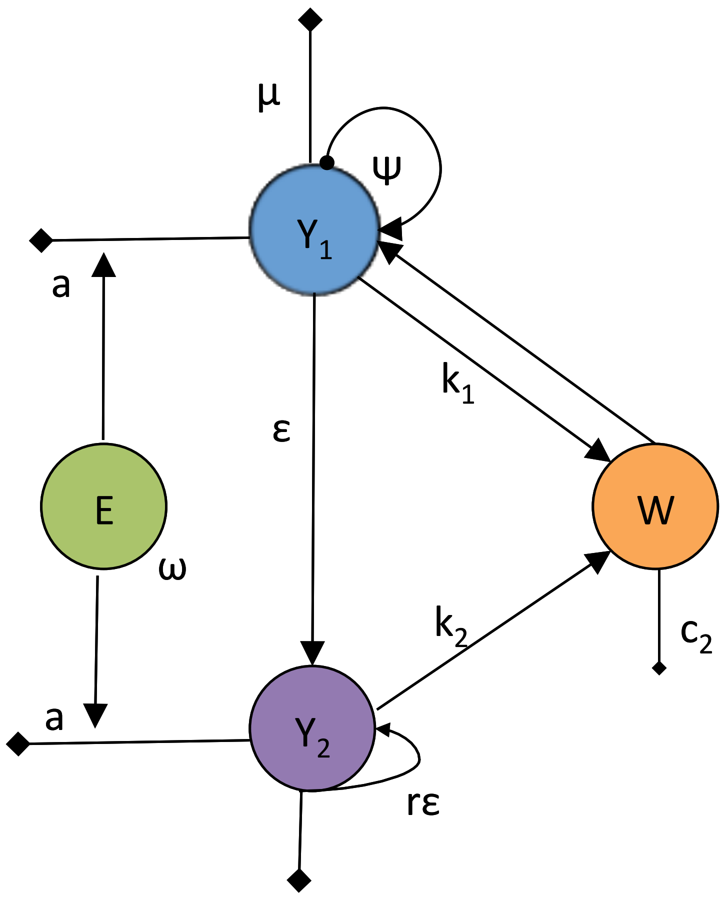

Figure 3.2: **HPV Diagram** A diagram for HPV model (3.3).

The effect of immunosuppression

In a healthy human, CD4 T cells are kept constant however a hallmark of HIV infection is the loss of CD4 T cell levels. During infection, CD4 T cell levels drop in connection with high HIV levels. CD4 T cell loss results in impaired mechanisms and overall immunodeficiency and specifically, CD4 T cell-mediated immune responses against other pathogens such as HPV are suppressed. CD4 naïve T cells are depleted in mucosal tissues in all the stages of HIV infection [20, 49] and progressive decline of CD4 T cells affects the differentiation process of naïve CD4 T cells into the different subsets. Such a subset, Th1, is known to play a major role in immune responses against HPV [143] through induction of cell-mediated immunity in the presence of IL-2, IL-12 and IFN-γ cytokines [136].

To model the decrease in the availability of CD4 T cell population due to HIV; and the subsequent effect of such loss on HPV-specific CTL (E) responses, we assume that the carrying capacity of the E population decreases in an immunosuppressed patient. In particular, we represent K as the carrying capacity of CTLs and thus the maximum E population. We make K a function of CD4 T cell population, such that K is given by, $K = K(T) = bT$, where T are the uninfected CD4 T cells in model (3.1). While, inevitably we choose a linear relationship to represent the connection between the carrying capacity of E and the CD4 T cells population, we also considered a quadratic relationship such that $K(T) = bT^2$. One downfall to our model is the carrying capacity of the CTL response is lower than in the original model [107]. While this could of improved with a quadratic relationship, the biological explanation of a quadratic relationship between the CTL carrying capacity and the CD4 T cells is nonexistent. Therefore, we modeled it such that when T decreases during the progressive loss of CD4 T cell, T, $K(T)$, the maximum carrying capacity decreases at a linear rate. We assume that the CTL carrying capacity is directly proportional to the amount of CD4 T cells. Other modeling options, such as a T dependent source with a death term were explored, however the maximum proliferation term $K(T)$ best explained the homeostatic mechanistic behavior of the CTLs.

The co-infection model becomes (see Fig. 3.3):

$$
\begin{aligned}
\frac{dT}{dt} &= s - dT - \beta TV, \\
\frac{dI}{dt} &= \beta TV - \delta I, \\
\frac{dV}{dt} &= N_1 \delta I - c_1 V, \\
\frac{dY_1}{dt} &= \psi W \frac{(1+pV)N_2 - Y_1}{\phi + (1+pV)N_2 - Y_1} - \varepsilon Y_1 - \mu Y_1 - aY_1 E, \\
\frac{dY_2}{dt} &= \varepsilon Y_1 + r\varepsilon Y_2 - \mu Y_2 - aY_2 E, \\
\frac{dW}{dt} &= \mu(k_1 Y_1 + k_2 Y_2) - c_2 W, \\
\frac{dE}{dt} &= \omega Y_2 E \left(1 - \frac{E}{K(T)}\right),
\end{aligned}
\tag{3.5}
$$

with initial conditions $T(0) > 0$, $I(0) > 0$, $V(0) > 0$, $Y_1(0) = Y_{10}$, $Y_2(0) = Y_{20}$, $W(0) = W_0$, and $E(0) = E_0$ where $t = 0$ is the time of co-infection.

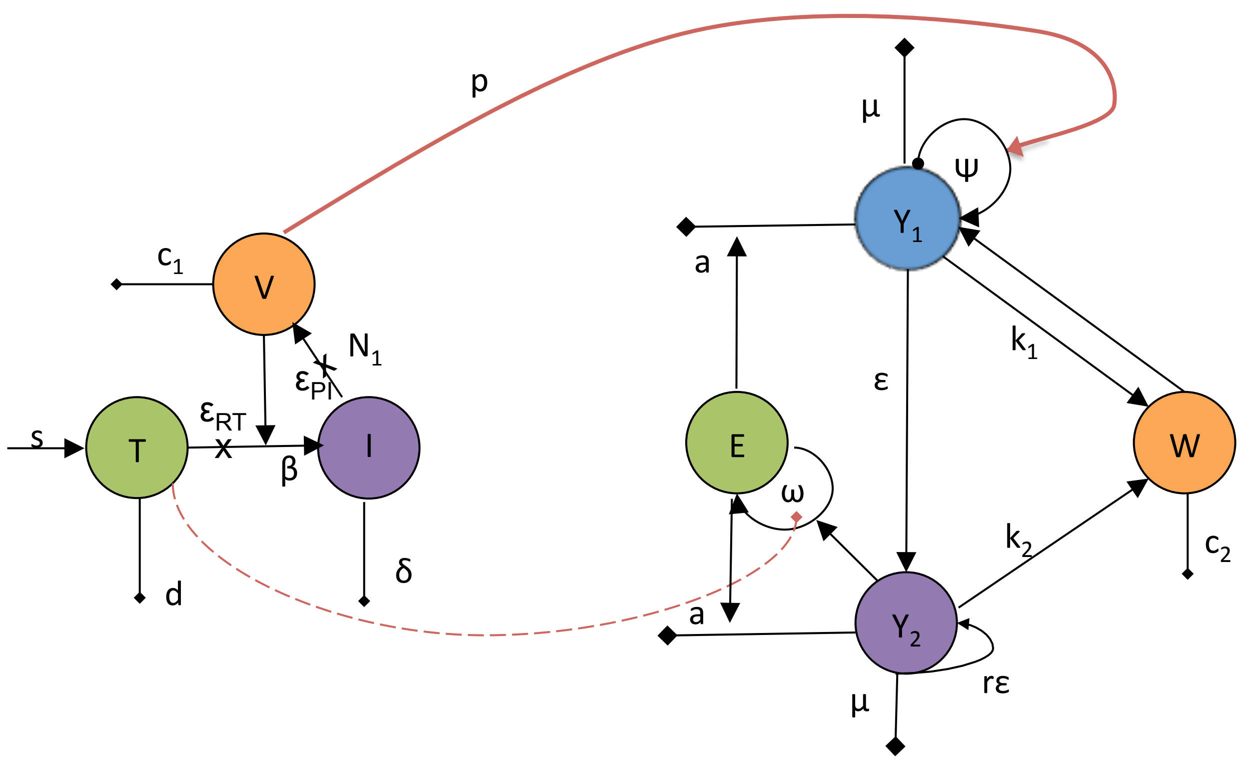

Figure 3.3: **HIV HPV diagram** A diagram for the co-infection model (3.5).

3.4 Results

3.4.1 HIV/HPV co-infection clinical trial

In a recent clinical trial, researchers studied the effect of cART on HIV/HPV co-infected patients. The study explored the changes that occur in oral HPV DNA detection among cART-naive HIV-positive adults over the first 24 weeks. The study also did a 48 week follow up. In the trial, 388 participants enrolled prior to the start of cART; throat wash specimens were collected at pre-screening, entry, between 12-18 weeks and at 24 weeks. CD4 T cell counts were measured at entry, week 4, 12-18, 24 and 48. The average CD4 T cell count was 3.3×10^5 cells/ml and average HIV RNA was 4.8×10^4 copies/ml at the start of the study [145].

The study found that despite highly effective cART there was no reduction in overall oral HPV DNA prevalence after 12-24 weeks of cART. In fact 70 participants had detectable HPV DNA at screening and 93 participants had HPV DNA after 24 weeks of cART. Initially 3% had oral warts, and after that 48 week follow up an additional 2.5% of patients had developed oral warts. This was observed even though the patients had a reduced number of oral sexual partners during the course of the study. Interestingly, patients with new types of HPV DNA, had a higher rebound in CD4 T cell levels, which may suggest activation of latent HPV infection. This was the first study to examine the connection between the initiation of cART and HPV persistence in oral sites [145].

3.4.2 Analytical results

We analytically investigate the properties of the co-infection model (3.5) at a chronic HIV steady state. As described, our model only captures the effect HIV has on HPV dynamics and, hence, we can simplify model (3.5) to include the four HPV equations, and constant $\bar{T} = 3.3 \times 10^5$, $\bar{I} = \frac{c_1 \bar{V}}{N_1 \delta} = 2.4 \times 10^3$, and $\bar{V} = 4.8 \times 10^4$ values, i.e. $(\bar{T}, \bar{I}, \bar{V})$, are at a steady state. We also assume

$k_1 = k_2 = k$ as listed in Table 3.1. The reduced model is:

$$\begin{aligned}
\frac{dY_1}{dt} &= \psi W \frac{(1+p\bar{V})N_2 - Y_1}{\phi + (1+p\bar{V})N_2 - Y_1} - \varepsilon Y_1 - \mu Y_1 - aY_1 E,\\
\frac{dY_2}{dt} &= \varepsilon Y_1 + r\varepsilon Y_2 - \mu Y_2 - aY_2 E,\\
\frac{dW}{dt} &= \mu(kY_1 + kY_2) - c_2 W,\\
\frac{dE}{dt} &= \omega Y_2 E\left(1 - \frac{E}{\bar{K}}\right).
\end{aligned} \tag{3.6}$$

System (3.6) has three steady states: A virus free steady state,

$$S_0 = (0,0,0,E), \tag{3.7}$$

a chronic immuno tolerant HPV steady state,

$$S_1 = (\hat{Y_1}, \hat{Y_2}, \hat{W}, 0), \tag{3.8}$$

where,

$$\hat{Y_1} = \frac{Acr(\varepsilon+\mu) + Bk\mu\psi(1-r)}{-k\mu\psi r + c\varepsilon r + c\mu r + k\mu\psi}, \tag{3.9}$$

$$\hat{Y_2} = \frac{-Acr(\varepsilon+\mu) + Bk\mu\psi(r-1)}{r(-k\mu\psi r + c\varepsilon r + c\mu r + k\mu\psi)}, \tag{3.10}$$

$$\hat{W} = \mu k \frac{Acr(\varepsilon+\mu)(r-1) - Bk\mu\psi(r-1)^2}{rc(-k\mu\psi r + c\varepsilon r + c\mu r + k\mu\psi)}, \tag{3.11}$$

with $A = (1+p\bar{V})N_2$ and $B = \phi + (1+p\bar{V})N_2$, and chronic immuno competent HPV steady state,

$$S_2 = (\bar{Y_1}, \bar{Y_2}, \bar{W}, \bar{E}), \tag{3.12}$$

where,

$$\begin{aligned}
\bar{Y}_1 &= (A\bar{K}^2a^2c + A\bar{K}^2ac\mu - A\bar{K}ac\varepsilon r - B\bar{K}ak\mu\psi - B\bar{K}k\mu^2\psi + B\varepsilon k\mu\psi r \\
&\quad + A\bar{K}ac\varepsilon\mu + A\bar{K}ac + A\bar{K}c\varepsilon\mu + A\bar{K}c\mu^2 - Ac\varepsilon^2 r - Ac\varepsilon\mu r - B\varepsilon k\mu\psi)/ \qquad (3.13) \\
&\quad (\bar{K}^2a^2c + \bar{K}^2ac\mu - \bar{K}ac\varepsilon r - \bar{K}ak\mu\psi - \bar{K}k\mu^2\psi + \varepsilon k\mu\psi r + \bar{K}ac\varepsilon \\
&\quad + \bar{K}ac\mu + \bar{K}c\varepsilon\mu + \bar{K}c\mu^2 - c\varepsilon^2 r - c\varepsilon\mu r - \varepsilon k\mu\psi), \\
\bar{Y}_2 &= \varepsilon(A\bar{K}^2a^2c + A\bar{K}^2ac\mu - A\bar{K}ac\varepsilon r - B\bar{K}ak\mu\psi - B\bar{K}k\mu^2\psi + B\varepsilon k\mu\psi r \\
&\quad + A\bar{K}ac\varepsilon + A\bar{K}ac\mu + A\bar{K}c\varepsilon\mu + A\bar{K}c\mu^2 - Ac\varepsilon^2 r - Ac\varepsilon\mu r - B\varepsilon k\mu\psi)/ \\
&\quad (\bar{K}^3a^3c + 2\bar{K}^3a^2c\mu + \bar{K}^3ac\mu^2 - 2\bar{K}^2a^2c\varepsilon r - \bar{K}^2a^2k\mu\psi - 2\bar{K}^2ac\varepsilon\mu r \qquad (3.14) \\
&\quad - 2\bar{K}^2ak\mu^2\psi - \bar{K}^2k\mu^3\psi + \bar{K}ac\varepsilon^2r^2 + 2\bar{K}a\varepsilon k\mu\psi r + 2\bar{K}\varepsilon k\mu^2\psi r \\
&\quad - \varepsilon^2k\mu\psi r^2 + \bar{K}^2a^2c\varepsilon + \bar{K}^2a^2c\mu + 2\bar{K}^2ac\varepsilon\mu + 2\bar{K}^2ac\mu^2 + \bar{K}^2c\varepsilon\mu^2 \\
&\quad + \bar{K}^2c\mu^3 - 2\bar{K}ac\varepsilon^2 r - 2\bar{K}ac\varepsilon\mu r - \bar{K}a\varepsilon k\mu\psi \\
&\quad - 2\bar{K}c\varepsilon^2\mu r - 2\bar{K}c\varepsilon\mu^2 r - \bar{K}\varepsilon k\mu^2\psi + c\varepsilon^3r^2 + c\varepsilon^2\mu r^2 + \varepsilon^2k\mu\psi r), \\
\bar{W} &= [Ac(\bar{K}^2a^2 + \bar{K}^2a\mu - \bar{K}a\varepsilon r + \bar{K}a\varepsilon + \bar{K}\varepsilon\mu + \bar{K}a\mu + \bar{K}\mu^2 - \varepsilon^2 r - \varepsilon\mu r) \\
&\quad - Bk\mu\psi(\bar{K}a + \bar{K}\mu + \varepsilon - r\varepsilon)\mu k](\bar{K}a + \bar{K}\mu - \varepsilon r + \varepsilon)/ \\
&\quad c(\bar{K}^3a^3c + 2\bar{K}^3a^2c\mu + \bar{K}^3ac\mu^2 - 2\bar{K}^2a^2c\varepsilon r - \bar{K}^2a^2k\mu\psi - 2\bar{K}^2ac\varepsilon\mu r \qquad (3.15) \\
&\quad - 2\bar{K}^2ak\mu^2\psi - \bar{K}^2k\mu^3\psi + \bar{K}ac\varepsilon^2r^2 + 2\bar{K}a\varepsilon k\mu\psi r + 2\bar{K}\varepsilon k\mu^2\psi r \\
&\quad - \varepsilon^2k\mu\psi r^2 + \bar{K}^2a^2c\varepsilon + \bar{K}^2a^2c\mu + 2\bar{K}^2ac\varepsilon\mu + 2\bar{K}^2ac\mu^2 + \bar{K}^2c\varepsilon\mu^2 \\
&\quad + \bar{K}^2c\mu^3 - 2\bar{K}ac\varepsilon^2 r - 2\bar{K}ac\varepsilon\mu r - \bar{K}a\varepsilon k\mu\psi - 2\bar{K}c\varepsilon^2\mu r - 2\bar{K}c\varepsilon\mu^2 r \\
&\quad - \bar{K}\varepsilon k\mu^2\psi + c\varepsilon^3r^2 + c\varepsilon^2\mu r^2 + \varepsilon^2k\mu\psi r), \\
\bar{E} &= \bar{K}. \qquad (3.16)
\end{aligned}$$

To investigate the asymptotic stability of S_0 we compute the Jacobian for model (3.6):

$$\mathscr{J}=\begin{bmatrix} -\psi W\frac{\phi}{(\phi+(1+p\bar{V})N_2-Y_1)^2}-\varepsilon-\mu-aE & 0 & \psi\frac{(1+p\bar{V})N_2-Y_1}{\phi+(1+p\bar{V})N_2-Y_1} & -aY_1 \\ \varepsilon & r\varepsilon-\mu-aE & 0 & -aY_2 \\ \mu k & \mu k & -c_2 & 0 \\ 0 & \omega E(1-\frac{E}{\bar{K}}) & 0 & \omega Y_2-2\omega aY_2\frac{E}{\bar{K}} \end{bmatrix}. \tag{3.17}$$

At S_0,

$$\mathscr{J}(S_0)=\begin{bmatrix} -\varepsilon-\mu-E-\lambda & 0 & \Omega & 0 \\ \varepsilon & r\varepsilon-\mu-E-\lambda & 0 & 0 \\ \mu k & \mu k & -c_2-\lambda & 0 \\ 0 & \omega E(1-\frac{E}{\bar{K}}) & 0 & -\lambda \end{bmatrix}, \tag{3.18}$$

where $\psi\frac{(1+p\bar{V})N_2}{\phi+(1+p\bar{V})N_2}=\Omega$. The corresponding characteristic equation is:

$$\begin{aligned}(-\lambda)\Big[\lambda^3+\lambda^2(c_2-\varepsilon r+2aE+\varepsilon+2\mu)+\lambda[c_2(\varepsilon+\mu+aE)\\ +c_2(-\varepsilon r+aE+\mu)-\Omega\mu k+(-\varepsilon-\mu-aE)(\varepsilon r-aE-\mu)]\\ +(\varepsilon+\mu+aE)c_2(\mu+aE-r\varepsilon)-\varepsilon\mu k\Omega\Big]=0.\end{aligned} \tag{3.19}$$

One eigenvalue is 0.

By Routh-Hurwitz criterion, all other eigenvalues are negative when $a_1>0$, $a_3>0$ and $a_1a_2>a_3$, where,

$$a_1 = c_2-\varepsilon r+2aE+\varepsilon+2\mu, \tag{3.20}$$

$$\begin{aligned}a_2 &= c_2(\varepsilon+\mu+aE)+c_2(-\varepsilon r+aE+\mu)\\ &\quad -\Omega\mu k+(-\varepsilon-\mu-aE)(\varepsilon r-aE-\mu),\end{aligned} \tag{3.21}$$

$$a_3 = (\varepsilon+\mu+aE)c_2(\mu+aE-r\varepsilon)-\varepsilon\mu k\Omega. \tag{3.22}$$

$a_1 > 0$ always since $r < 1$. $a_3 > 0$ when

$$\frac{\Omega k\mu}{c_2} < \frac{(\varepsilon+\mu+aE)(-\varepsilon r+aE+\mu)}{(\varepsilon+\mu+aE-r\varepsilon)}. \tag{3.23}$$

Finally, $a_1a_2 - a_3 > 0$ when $a_3 > 0$ (not shown).

Condition (3.23) translates to

$$\frac{\psi k\mu(1+p\bar{V})N_2}{c_2(\phi+(1+p\bar{V})N_2)} < \frac{(\varepsilon+\mu+aE)(-\varepsilon r+aE+\mu)}{(\varepsilon+\mu+aE-r\varepsilon)}, \tag{3.24}$$

which means that when the HPV infection rate times the HPV production rate (in the presence of HIV) is less than the combined effect of effector cells and natural death rate of HPV, HPV will be cleared.

3.4.3 Numerical results

Using the co-infection model (3.5) we numerically simulate disease scenarios in order to understand the dynamics of HPV infection in a co-infected individual. A recent clinical trial has investigated the effect of HIV in HPV infection in the presence and absence of combination antiretroviral therapy [145]. The levels of oral HPV DNA in the co-infected patients, which was monitored for 24 weeks after the start of cART, remained elevated throughout therapy [145]. To determine the possible mechanisms of HPV persistence, we investigate models (3.5) and (3.6) for the relative contributions of co-infection factors: *tat*, as given by pV, and immunosuppression, as given by $K(T)$.

Parameter values

Parameter values from previously published studies are utilized here, as follows. Equilibrium values for HIV RNA per ml and HIV-specific uninfected CD4 T cells per ml were reported in an

HIV/HPV co-infection study to be $\bar{V} = 4.8 \times 10^4$ virions per ml and $\bar{T} = 3.3 \times 10^5$ cells per ml [145]. Using previous estimates, we assume that uninfected and infected HIV specific CD4 T cells die at rates $d = 0.01$ per day [100] and $\delta = 1$ per day [113]. HIV burst size is $N_1 = 467$ virions per cell [21] and its clearance rate is $c_1 = 23$ per day [131]. Since the patient is in a chronic HIV steady state, we derive $\bar{I}$, β and s from steady state conditions, $\bar{I} = \frac{c_1 \bar{V}}{N_1 \delta}$, $\beta = \frac{c_1}{\bar{T} N_1}$ and $s = d\bar{T} + \beta \bar{V} \bar{T}$, to be $\bar{I} = 2.4 \times 10^3$ cells per ml, $\beta = 1.5 \times 10^{-7}$ ml per cell per day and $s = 5.6 \times 10^3$ cells per ml per day. For the HPV interactions, we assume that epithelial cells are infected at rate $\psi = 0.0067$ per day, HPV infected cells (Y_1) and self-proliferating cells (Y_2) die naturally or through CTL killing at rates $\mu = 0.048$ per day and $a = 0.01$ ml per cell per day, respectively. Self-proliferating cell growth rate is $r = 0.1$ per day. HPV burst size is $k = k_1 = k_2 = 1000$ virions per cell and its clearance rate is $c_2 = 0.05$ per day [107]. CTL proliferate at rate $\omega = 10^{-3}$ ml per cell per day [107]. Finally, initial conditions are $Y_{10} = 1$ cells per ml, $Y_{20} = 0$ cells per ml, $W_0 = 0$ virion per ml, and $E_0 = 0.01$ cells per ml. These parameters are summarized in Table 3.1.

We assume that the *tat*-effect, given by $p\bar{V}$, ranges between zero and 20, to account for up to 20-fold increase in the target epithelial cells due to co-infection. The immunosuppression factor, given by $K(\bar{T}) = b\bar{T}$ ranges between $K(\bar{T}) = 35$ per ml and $K(\bar{T}) = 1$ per ml to account for changes in available CTL concentrations between an HPV infection and HIV/HPV co-infection. Lastly, the oncogene expression ε ranges from zero to one.

The viral dynamics of HPV infected individuals

We first study the dynamics of HPV infection in the absence of HIV, as given by model (3.6) with $\bar{I} = \bar{V} = 0$ cells per ml, and $\bar{T} = 10^6$ cells per ml. We let $\varepsilon = 0.5$ cells per ml, $K = 35$ cells per ml ($b = 3.5 \times 10^{-5}$), and the other parameters as listed in Table 3.1. While the original HPV model [107] investigated $\varepsilon = 0.1$ to $\varepsilon = 1$ in the unvaccinated host model, for most of this work we fix ε. A higher ε models an increased oncogene expression rate, or more cell divisions. For now we fix $\varepsilon = 0.5$ and investigate changes in this parameter in the presence of cART. Under these

Table 3.1: **Parameters**

Parameter	Value	Description	Reference
s	5.6×10^3 ml^{-1} day^{-1}	CD4 T cell recruitment rate	see text
β	1.5×10^{-7} ml^{-1} day^{-1}	HIV infection rate	see text
d	0.01 per day	Uninfected CD4 T cell death rate	[100]
δ	1 day^{-1}	Infected CD4 T cells death rate	[113]
N_1	467 virions	HIV burst size	[21]
c_1	23 day^{-1}	HIV clearance rate	[131]
ε_{RT}	varied	Reverse transcriptase efficacy	see text
ε_{PI}	varied	Protease inhibitor efficacy	see text
$\bar{T}$	3.28×10^5 ml^{-1}	Uninfected CD4 T cells at equilibrium	[145]
$\bar{I}$	2.4×10^3 ml^{-1}	Infected CD4 T cells at equilibrium	see text
$\bar{V}$	4.8×10^4 ml^{-1}	HIV at equilibrium	[145]
N_2	10^4 ml^{-1}	Total concentration of epithelial cells	[107]
ϕ	10^6 ml^{-1}	Epithelial cell concentration for which infection is half-maximal	[107]
ψ	0.0067 day^{-1}	HPV infection rate	[107]
μ	0.048 day^{-1}	Epithelial cell death rate	[107]
r	0.1 day^{-1}	Self-proliferating cells recruitment rate	[107]
ε	varied	Oncogenic expression	see text
ω	10^{-3} ml cell^{-1} day^{-1}	CTL expansion rate	[107]
K	varied	CTL carrying capacity	see text
a	0.01 day^{-1}	CTL killing rate	[107]
$k_1 = k_2$	1000 virions	HPV burst size	[107]
c_2	0.05 day^{-1}	HPV clearance rate	[107]

assumptions, model (3.6) predicts HPV and CTL levels similar to those in [107]. In particular, HPV reaches a maximum of 1.4×10^5 copies per ml at day 174 and eventual clearance (see Fig. 3.4, panel b, green line). The CTL expansion is delayed 80 days, and reaches equilibrium values of 27 cells per ml by day 240 (see Fig. 3.4, panel b, purple line). Self-proliferating cells with high oncogenic gene expression, Y_2 are 12 times higher than cells with low oncogenic expression, Y_1 (see Fig. 3.4, panel a). This result is dependent on the oncogene expression rate ε.

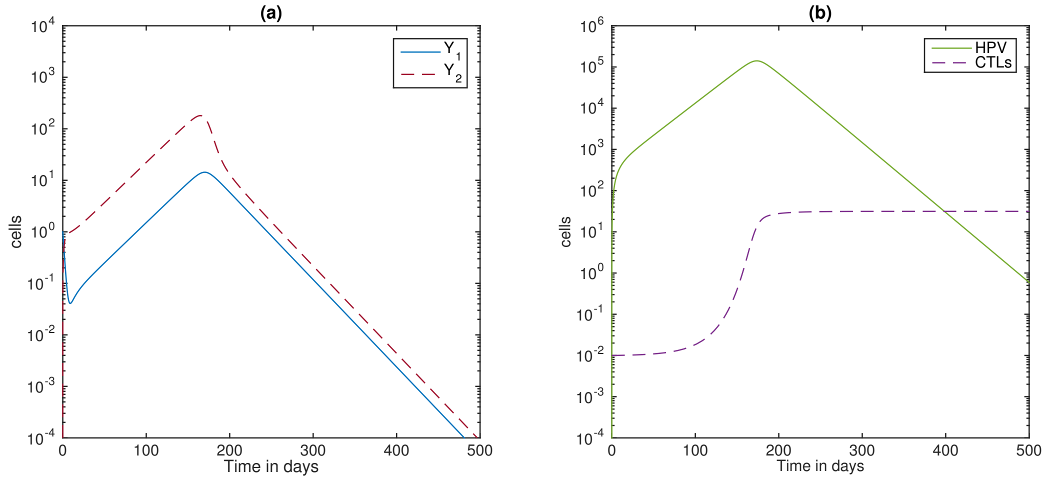

Figure 3.4: **HPV infection** (a) Infected cells Y_1 (blue line) and Y_2 (red line); (b) HPV W (green line) and CTL E (purple line) for $\varepsilon = 0.5$ and $K = 35$ per ml per day. All the other parameters are listed in Table 3.1.

The viral dynamics of HIV/HPV co-infected individuals

We start by assuming that the *tat* effect leads to a doubling of available target epithelial cells, *i.e.* $N_2(1 + p\bar{V}) = 2N_2$. Prior to considering the fixed amount of available target epithelial cells, $2N_2$, we also considered including the exact production of *tat* by an HIV-infected individual. However, individuals produce unique amounts of *tat* and in some cases it is thought to be produced logistically. While we investigated including this in our model, ultimately we decided at most, *tat* could double the available target epithelial cells; biologically it seems unreasonable that *tat* would increase epithelial targets more than double.

We account for HIV induced immunosuppression in an HIV/HPV co-infected individual, by changing $K(\bar{T})$ as follows. We have shown in the previous section that an HIV-naïve individual has a CTL carrying capacity $K(\bar{T}) = 35$ cells per ml, where $\bar{T} = 10^6$ CD4 T cells per ml and $b = 3.5 \times 10^{-5}$. We keep this b value and decrease the $\bar{T}$ number to i) $\bar{T} = 5 \times 10^5$ cells per ml, corresponding to average chronic HIV CD4 T cell numbers [120]; ii) $\bar{T} = 3.3 \times 10^5$ cells per ml as in the HIV/HPV co-infection study [145]; and iii) $\bar{T} = 2 \times 10^5$ cells per ml, corresponding to AIDS.

Under these assumptions and parameters listed in Table 1, model (3.6) predicts HPV clearance in case (i) and HPV persistence in cases (ii) and (iii). In case (i), HPV reaches a maximum of 2.4×10^5 copies per ml at day 128 and clears by day 1050. In cases (ii) and (iii), HPV virus reaches steady state values of 3.5×10^6, and 6.7×10^7 DNA per ml after 20 years and 2.1 years, respectively (see Fig. 3.5, panel a). CTL levels decrease to 17.5, 11.5 and 7 cells per ml for cases (i), (ii), and (iii), respectively (see Fig. 3.5, panel b).

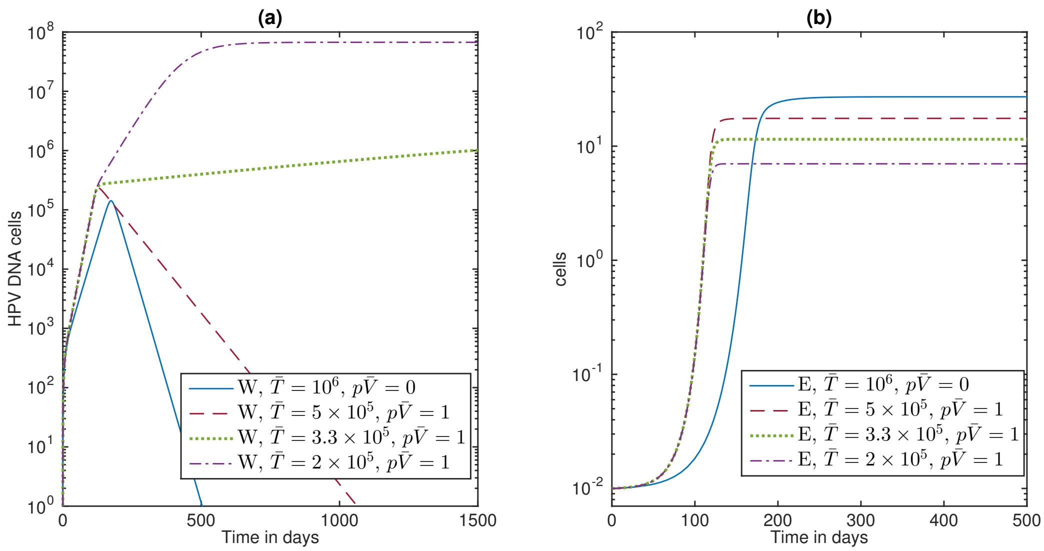

Figure 3.5: **HIV/HPV co-infection** (a) HPV W and (b) CTL E as given by model (3.5) for $\varepsilon = 0.5$, parameters listed in Table 3.1 and $\bar{T} = 10^6$ (blue lines); $\bar{T} = 5 \times 10^5$ (red lines); $\bar{T} = 3.3 \times 10^5$ (green lines); and $\bar{T} = 2 \times 10^5$ (purple lines).

To determine the relative contributions of the *tat* effect and immunosuppression in the transition between HPV clearance and HPV persistence, we derived a bifurcation diagram showing the asymptotic dynamic of HPV as given by model (3.6) when both $p\bar{V}$ and $K(\bar{T})$ are varied. As expected, an increase in the available epithelial cells requires a larger CTL population for the clearance to occur (see Fig. 3.6). In particular, if the *tat* effect is increased 100%, such that $1 + p\bar{V} = 2$, then the CTL carrying capacity has to be $K > 11.9$ cells per ml for clearance to occur. Moreover, a carrying capacity as low as $K(\bar{T}) = 7$ cells per ml is enough to ensure HPV clearance in the HIV-naïve case, 80% lower than the considered base value of $K(\bar{T}) = 35$ cells per ml. If we increase $p\bar{V}$ then the required level $K(\bar{T})$ to ensure clearance of HPV infection also increases. The trade off between $p\bar{V}$ and $K(\bar{T})$ is given in Figure 3.6. For example, based on the bifurcation plot, (Figure 3.6), if

$p\bar{V} = 8$ or an 800% increase in available epithelial targets, then the CTL carrying capacity has to be $K(\bar{T}) > 51$ cells per ml for clearance to occur.

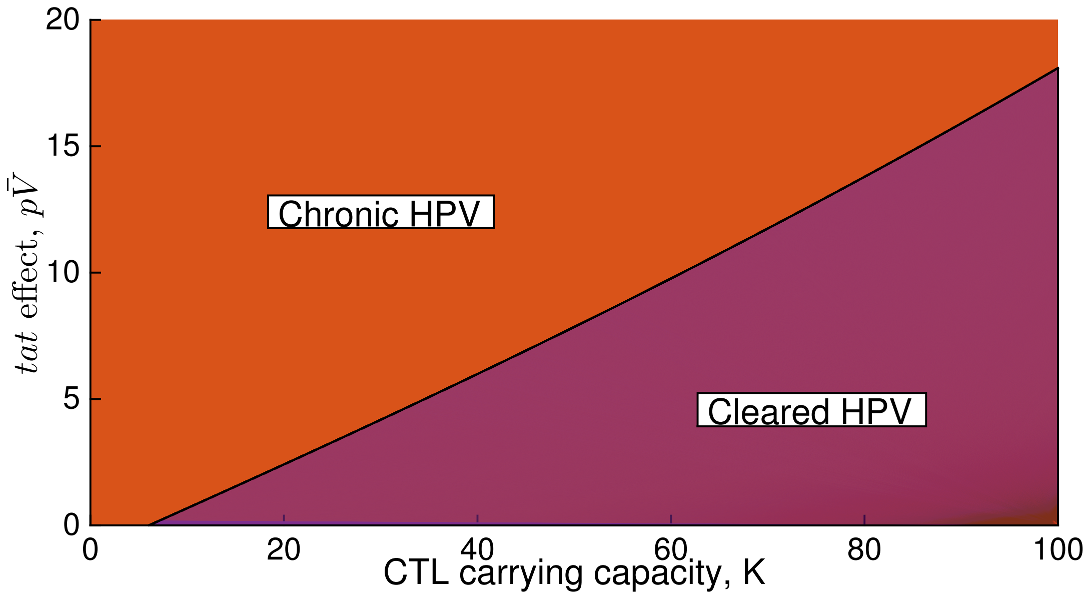

Figure 3.6: **Bifurcation Diagram** A bifurcation diagram showing parameters regions of cleared (blue area) versus chronic (orange area) HPV (W) as the *tat* effect $p\bar{V}$ and CTL carrying capacity $K(\bar{T})$ vary. Here, the criterion for HPV clearance is given by equation (3.24) for $\varepsilon = 0.5$ and parameters listed in Table 3.1.

Changing oncogene expression rates

We have considered that the oncogenic expression is $\varepsilon = 0.5$. In an HIV-naïve host, this corresponds to self-proliferating cells Y_2 exceeding the Y_1 cells 12-times (see Fig. 3.4, panel a). In [107], the authors showed that in an HIV-naïve, HPV-unvaccinated individual, a decrease in the oncogenic expression ε leads to slower growth of Y_1, Y_2 and W, a delayed and weak CTL response E and, consequently, a delayed HPV clearance. To determine whether this effect is carried over in an HIV/HPV co-infected patient we compared clearance regions for $\varepsilon = 0.1$, $\varepsilon = 0.5$ and $\varepsilon = 0.9$ for varying $p\bar{V}$ and $K(\bar{T})$ values (see Fig. 3.7, panel a). We find that the clearance regions (defined as the area under the curve) are higher for low ε values, similar to the results from an HIV naïve patient [107].

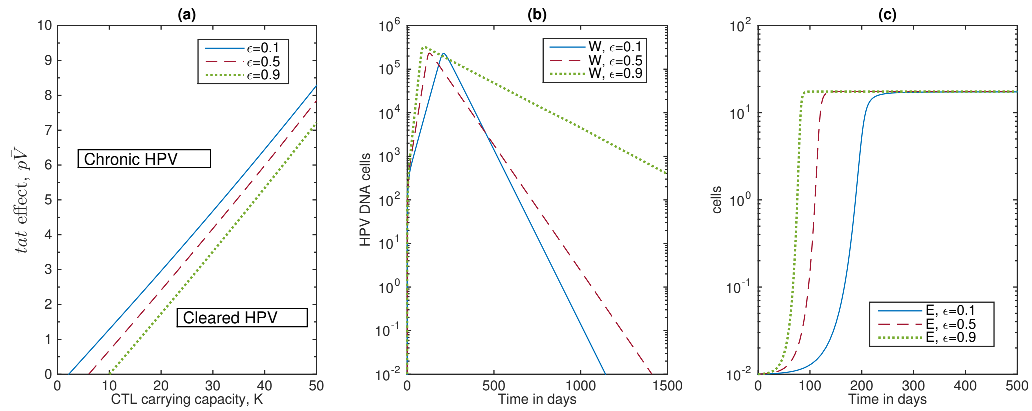

Figure 3.7: **Varying oncogene expression rates** (a) Bifurcation diagram showing cleared W (area under the curve)versus chronic W (are above the curve) as the *tat* effect $p\bar{V}$ and CTL carrying capacity $K(\bar{T})$ vary; (b) HPV W; and (c) CTL E as given by model (3.6) for parameters listed in Table 3.1 and $\varepsilon = 0.1$ (blue lines), $\varepsilon = 0.5$ (red lines), and $\varepsilon = 0.9$ (green lines).

To determine the timing of clearance, we fixed the *tat* effect to $1 + p\bar{V} = 2$ and the CTL carrying capacity to $K(\bar{T}) = 17.5$ cells per ml and determined the changes in W and E dynamics for various values of ε (see Fig. 3.7, panels b and c). We find that HPV levels are slightly higher for high oncogenic expression, ε, and they take significantly longer to get cleared (see Fig. 3.7, panel b). This happens in spite of the fact that CTL level grow faster for high oncogenic expression (see Fig. 3.7, panel c).

The effect of cART on an HIV/HPV co-infection

We previously introduced a recent trial that investigated the dynamics of oral HPV DNA in HIV/HPV co-infected individuals undergoing cART, see Section 3.4.1, [145]. We use model (3.5) to determine the tat effect pV, CTL numbers $K(T)$, and oncogenic expression ε that can explain this observation.

The patients in [145], have $\bar{T} = 3.3 \times 10^5$ uninfected CD4 T cells per ml and $\bar{V} = 4.8 \times 10^4$ HIV RNA per ml at day $t = 0$, when cART begins. We assume that drug efficacy are $\varepsilon_{RT} = 0.95$, $\varepsilon_{PI} = 0.5$ and the oncogenic factor is $\varepsilon = 0.5$. If the co-infection with HPV is not included *i.e.* $p\bar{V} = 0$ and $K(\bar{T}) = 35$, then HIV RNA levels decrease to below limit of detection (of 50 copies per ml) in 6.5 days. CD4 T cell concentration increases to a maximum of 5.6×10^5 cells per ml by day 329 (161 days after the end of the study). Finally, HPV is cleared in 688 days (see Fig. 3.8).

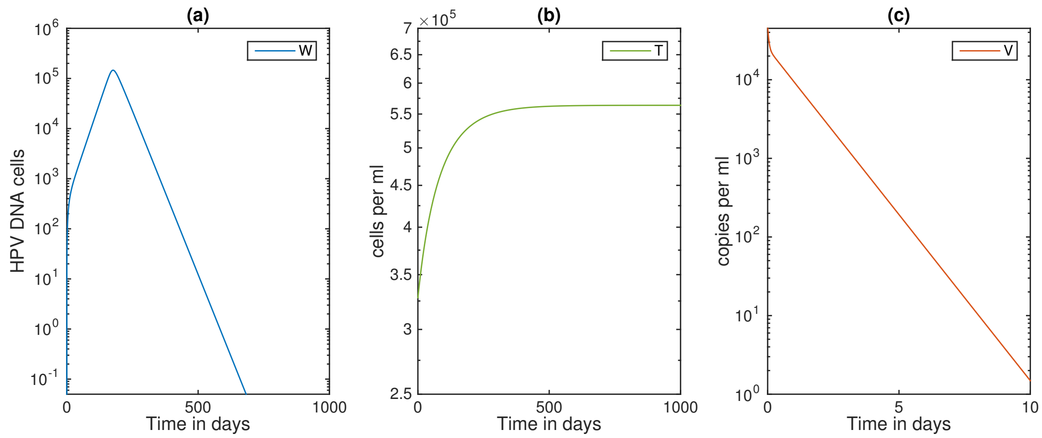

Figure 3.8: **HIV/HPV dynamics during cART and HPV infection not included** (a) HPV W; (b) CD4 T cells (T); (c) HIV as given by model (3.5) under cART. Here, $\varepsilon = 0.5$, $\varepsilon_{RT} = 0.95$, $\varepsilon_{PI} = 0.5$, and all other parameters are listed in Table 3.1. Initial conditions are $T_0 = 3.3 \times 10^5, I_0 = 2.4 \times 10^5, V_0 = 4.8 \times 10^4, Y_{10} = 1, E_0 = 0.01, Y_{20} = W_0 = 0$, and $t = 0$ is the start of cART.

We next add the effects of co-infection under the setup of the oral co-infection trial [145]. If $p\bar{V} = 1$ and $K(T) = 11.5$ (corresponding to CD4 T cell concentration of $\bar{T} = 3.3 \times 10^5$ per ml), then HPV is cleared under cART conditions $\varepsilon_{RT} = 0.95$ and $\varepsilon_{PI} = 0.5$. The timing of the clearance depends on two factors: the HPV stage and the level of CD4 T cells at the start of cART. If the HPV infection occurs at the same time as the start of cART, then the HPV levels increase to a peak value of 1.4×10^5 DNA per ml and stay elevated throughout the 24 weeks of study (see Fig. 3.9, panel a). HPV starts to decay at day 180 (see Fig. 3.9, panel a, zoomed out graph) when CD4 T cells reached 5.2×10^5 cells per ml (see Fig. 3.9, panel b) which is the low level of CD4 T cell counts for healthy individuals.

In contrast, if HPV infection reached a chronic state at the start of cART, then cART helps to initiate HPV decay by day 8 (see Fig. 3.10, panel a), when the CD4 T cell population is still low, *i.e.*, $T = 3.5 \times 10^5$ cells per ml (see Fig. 3.10, panel b). It is worth noting that cART removes HIV, and consequently the *tat* effect, but it does not control how fast CD4 T cells re-populate the blood compartment.

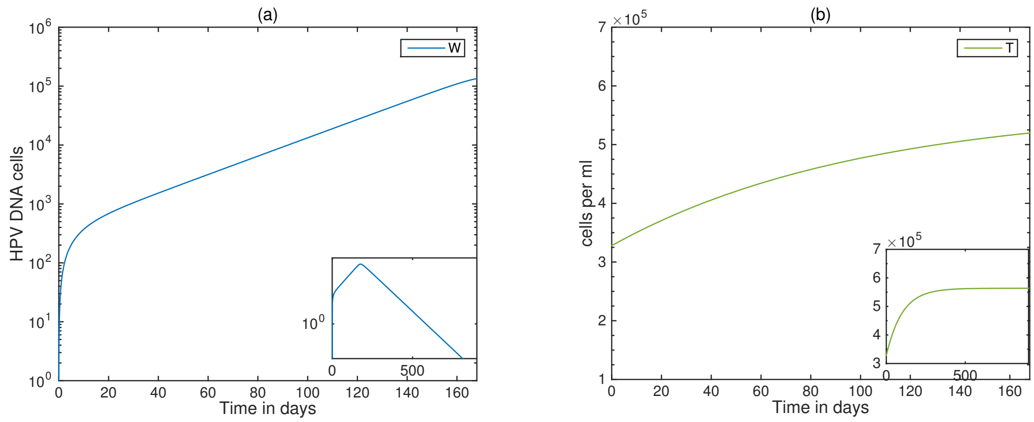

Figure 3.9: **HIV/HPV dynamics when cART and HPV infection coincide** (a) HPV W; (b) CD4 T cells (T) as given by model (3.5) under cART. Here, $\varepsilon = 0.5$, $\varepsilon_{RT} = 0.95$, $\varepsilon_{PI} = 0.5$, and all other parameters are listed in Table 3.1. Initial conditions are $T_0 = 3.3 \times 10^5, I_0 = 2.4 \times 10^5, V_0 = 4.8 \times 10^4, Y_{10} = 1, E_0 = 0.01, Y_{20} = W_0 = 0$, and $t = 0$ is the start of cART. Over the first 24 weeks HPV persists (panel a), and in the long term HPV is cleared (zoomed out panel a).

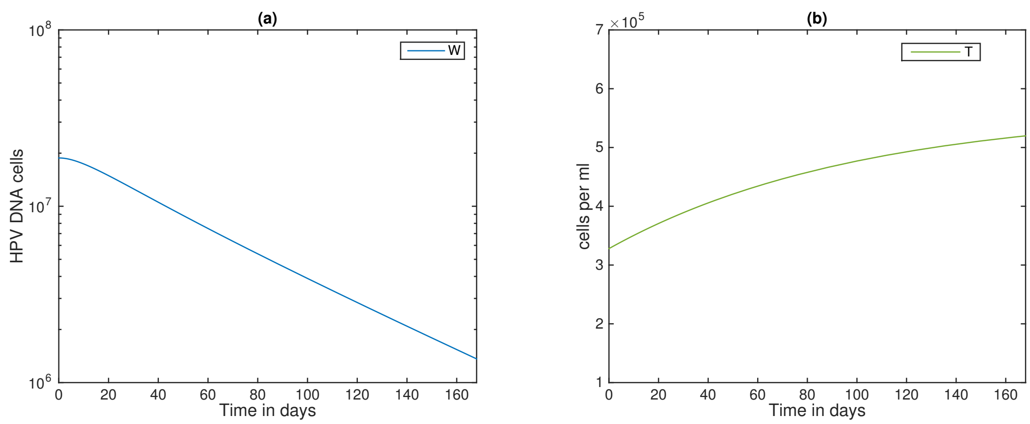

Figure 3.10: **HIV/HPV dynamics when HPV is chronic at the start of cART** (a) HPV W; (b) CD4 T cells T as given by model (3.5) under cART. Here, $\varepsilon = 0.5$, $\varepsilon_{RT} = 0.95$, $\varepsilon_{PI} = 0.5$, and all other parameters are listed in Table 3.1. Initial conditions are $T_0 = 3.3 \times 10^5, I_0 = 2.4 \times 10^5, V_0 = 4.8 \times 10^4, Y_{10} = 3.2 \times 10^3, Y_{20} = 1.6 \times 10^4, W_0 = 1.8 \times 10^7, E_0 = 0.01$, and $t = 0$ is the start of cART.

Moreover, we found two instances when HPV stays chronic in the presence of cART, namely strong drug efficacy, $\varepsilon_{RT} = 0.95$ and $\varepsilon_{PI} = 0.5$, and AIDS level CD4 T cells, $\bar{T} \leq 1.7 \times 10^5$ cells per ml; and inefficient drug therapy, $\varepsilon_{RT} = 0.2$ and $\varepsilon_{PI} = 0$ and intermediate CD4 T cell levels $\bar{T} \leq 2.6 \times 10^5$ cells per ml.

Lastly, we investigated how the dynamics of HPV in a co-infected individual undergoing cART change with the oncogenic expression ε. We found that HPV levels stay high throughout the first 24 weeks of cART, but are eventually cleared for all levels of oncogenic expression (see Fig. 3.11, panel a). This is due to the fact that the dynamics of CD4 T cells are not affected by the oncogenic expression (see Fig. 3.11, panel b). HPV has lower peak levels but longer time until clearance for low oncogenic expression, $\varepsilon = 0.1$ (see Fig. 3.11, panel a, blue line) compared to high oncogenic expression $\varepsilon = 0.9$ (see Fig. 3.11, panel a blue line).

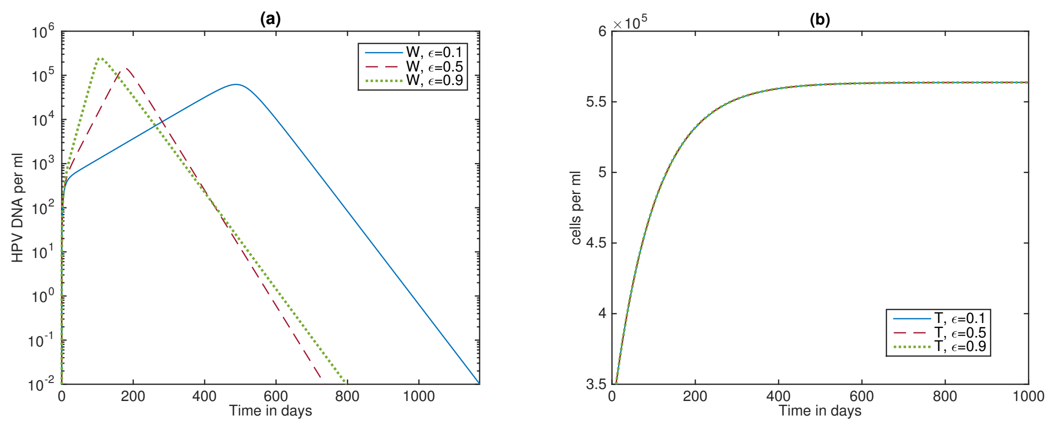

Figure 3.11: **Effect of oncogene expression rates and cART on HIV/HPV co-infections** (a) HPV W; (b) CD4 T cells T as given by model (3.5) under cART. Here, $\varepsilon = 0.1$ (green line); $\varepsilon = 0.5$ (red line); $\varepsilon = 0.9$ (blue line), $\varepsilon_{RT} = 0.95$, $\varepsilon_{PI} = 0.5$, and all other parameters are listed in Table 3.1. Initial conditions are $T_0 = 3.3 \times 10^5, I_0 = 2.4 \times 10^5, V_0 = 4.8 \times 10^4, Y_{10} = 1, E_0 = 0.01, Y_{20} = W_0 = 0$ and $t = 0$ is the start of cART.

Increased CD4 T cell count and HPV DNA production

An intriguing finding in [145] showed higher frequency of HPV DNA in individuals with the strongest rebound in absolute CD4 T cell count post cART [145]. To investigate possible underlying mechanisms explaining this unexpected finding, we considered two virtual patients: patient 1 has a rebound to 6.5×10^5 cells per ml CD4 T cell count as in [145], and patient 2 has a rebound to 5.6×10^5 cells per ml. We further assume that patient 1 has high oncogenic expression level $\varepsilon = 0.9$ per day, and patient 2 has low oncogenic expression level $\varepsilon = 0.1$ per day. This increase in oncogene expression leads to higher HPV DNA production in patient 1 (see Fig 3.12 panel a, solid blue vs dashed green line) in spite of its better cART outcome (see Fig 3.12, panel b, solid blue versus dashed green lines).

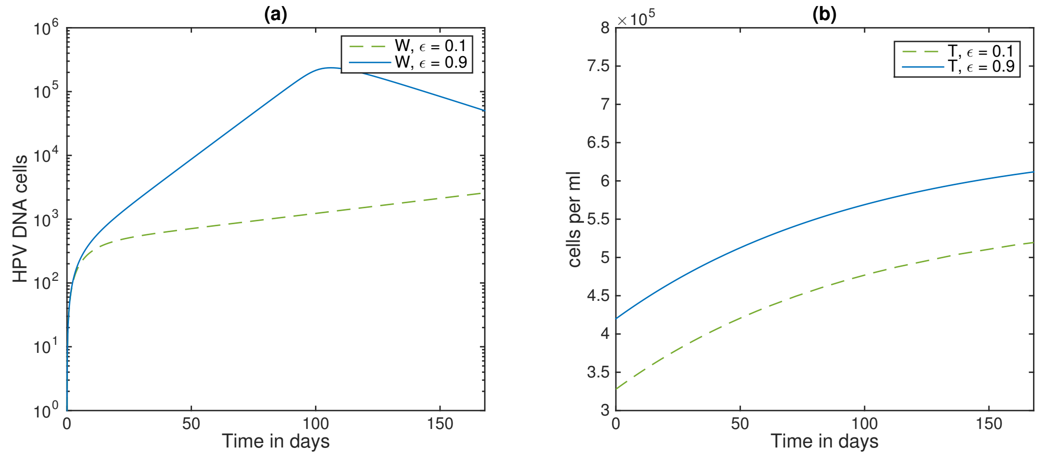

Figure 3.12: **Effect of oncogene expression rates and cART on HIV/HPV co-infections** (a) HPV W; (b) CD4 T cells T as given by model (3.5) under cART. Here, $\varepsilon = 0.1$ (green dashed line), $\varepsilon = 0.9$, $\varepsilon_{RT} = 0.95$, $\varepsilon_{PI} = 0.5$ and all other parameters are listed in Table 3.1. Initial conditions are $T_0 = 3.3 \times 10^5$ (green dashed line) or $T_0 = 4.5 \times 10^5$ (blue solid line), $I_0 = 2.4 \times 10^5, V_0 = 4.8 \times 10^4, Y_{10} = 1, E_0 = 0.01, Y_{20} = W_0 = 0$ and $t = 0$ is the start of cART.

Exploring the inclusion of uninfected basal cells in the HIV/HPV co-infection

We also investigated the properties of the co-infection model using the large model developed in the original HPV work's supplementary material [107]. The extended model includes the population of uninfected basal epithelial cells, X, which are born at rate $\lambda(t)$ and die at rate μ. HPV, W, interacts with uninfected basal epithelial cells, X, at rate ψ to produce infected cells, Y_1. We assume that the infection is density dependent with ϕ representing the uninfected cell concentration where the infection is half-maximal. Below is the expanded co-infection model wherein we included the effect of tat, pV, with the birth of uninfected basal epithelium. The term $(1+pV)\lambda(t)$ accounts for the production of epithelial cells that are susceptible for HPV infection. The rest of the co-infection dynamics are described in the previous text.

The expanded co-infection model becomes:

$$
\begin{aligned}
\frac{dT}{dt} &= s - dT - (1-\varepsilon_{RT})\beta TV, \\
\frac{dI}{dt} &= (1-\varepsilon_{RT})\beta TV - \delta I, \\
\frac{dV}{dt} &= (1-\varepsilon_{PI})N_1\delta I - c_1 V, \\
\frac{dX}{dt} &= (1+pV)\lambda(t) - \mu X - \psi W \frac{x}{\phi + X} \\
\frac{dY_1}{dt} &= \psi W \frac{X}{\phi + X} - \varepsilon Y_1 - \mu Y_1 - aY_1 E, \\
\frac{dY_2}{dt} &= \varepsilon Y_1 + r\varepsilon Y_2 - \mu Y_2 - aY_2 E, \\
\frac{dW}{dt} &= \mu(k_1 Y_1 + k_2 Y_2) - c_2 W, \\
\frac{dE}{dt} &= \omega Y_2 E\left(1 - \frac{E}{K(T)}\right),
\end{aligned}
\tag{3.25}
$$

with initial conditions $T(0) > 0$, $I(0) > 0$, $V(0) > 0$, $X(0) > X_1$, $Y_1(0) = Y_{10}$, $Y_2(0) = Y_{20}$, $W(0) = W_0$, and $E(0) = E_0$ where $t = 0$ is the time of co-infection.

Since, *tat* is known to play an important role in the disruption of epithelial tight junctions, thereby facilitating the entry of HPV into the mucosal epithelium [134]. We compare the dynamics of model (3.25) against those of main model (3.5) for the same tat effect $(1+pV) = 2$. When considering HIV induced immunosuppression in HIV/HPV co-infected individuals with different CD4 T cells levels of i) $T = 10^6$ cells per ml, corresponding to a healthy patient ii) $T = 5\times10^5$ cells per ml, corresponding to average chronic HIV CD4 T cell numbers [145]; iii) $T = 3.3\times10^5$ cells per ml as in the HIV/HPV co-infection study [145]; and iv) $T = 2\times10^5$ cells per ml, corresponding to AIDS; the extended model (3.25) has similar results as the reduced model (3.5) (see (a) in Fig. 3.13).

Similarly, when we considered the effects of co-infection under the setup of the oral co-infection trial [145] for $pV = 1$ and $K(T) = 11.5$ cells (corresponding to CD4 T cell concentration of $T = 3.3\times10^5$ per ml) we found that both model (3.25) and (3.5) give similar results. In particular,

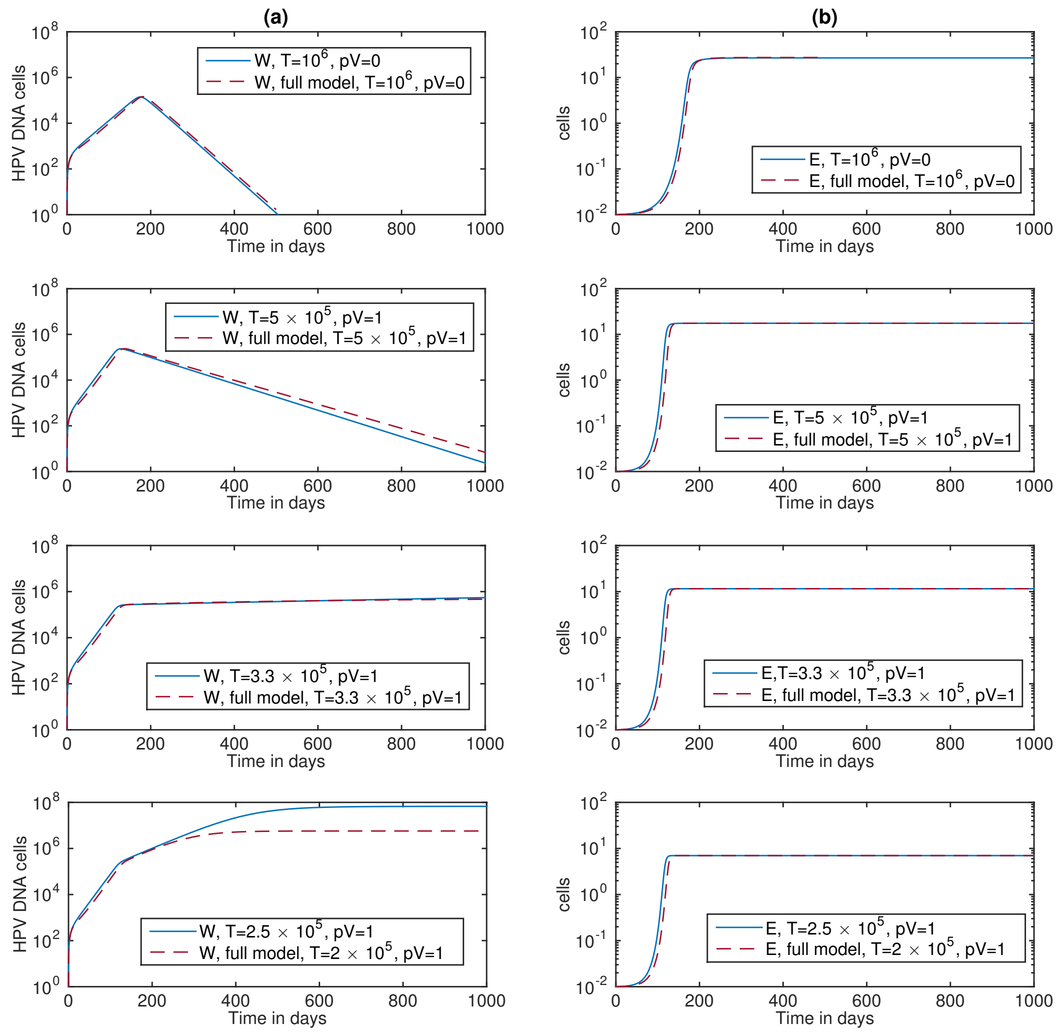

Figure 3.13: **HIV/HPV co-infection model comparison** (a) HPV W and (b) CTL E as given by model (3.5), solid blue lines and model (3.25), dashed red lines, for $\varepsilon = 0.5$ per day, parameters are listed in Table 3.1 for different $\bar{T}$ levels- $\bar{T} = 10^6$ cells per ml (first row); $\bar{T} = 5x10^5$ cells per ml (second row); $\bar{T} = 3.3x10^5$ cells per ml (third row); and $\bar{T} = 2x10^5$ cells per ml (fourth row).

HPV is cleared under cART conditions $\varepsilon_{RT} = 0.95$ and $\varepsilon_{PI} = 0.5$ and the timing of the clearance depends on two factors: the HPV stage and the level of CD4 T cells at the start of cART (see (B) in Fig. 3.14). In conclusion we found the difference to be negligible and used to the co-infection model (3.5) throughout this work.

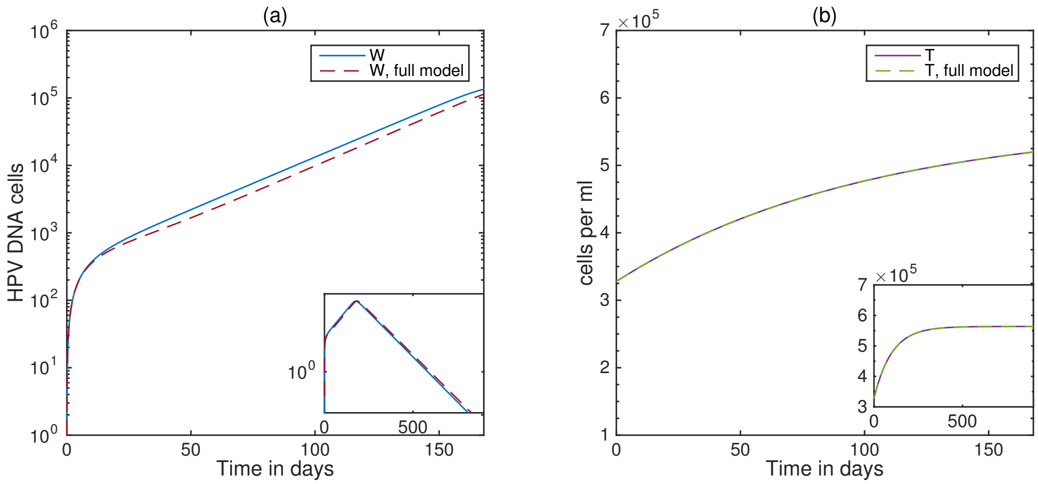

Figure 3.14: **HIV/HPV dynamics when cART and HPV infection coincide** (a) HPV W; (b) CD4 T cells (T) as given by model (3.5) solid blue lines and model (3.25) dashed red lines under cART. Here, $\varepsilon = 0.5$, $\varepsilon_R T = 0.95$, $\varepsilon_{PI} = 0.5$, and all other parameters are listed in Table 3.1 and $t = 0$ is the start of cART. Over the first 24 weeks HPV persists (panel a), and in the long term HPV is cleared (zoomed out panel a).

3.5 Discussion

This work is one of the first HIV/HPV co-infection models that investigates the dynamics of HPV in HIV infected individuals. Our model aims to explain the mechanistic interactions leading to HPV persistence in co-infected individuals even after the start of cART, as reported experimentally. Indeed, a recent study reported an increased prevalence of oral HPV infection in an HIV-infected cohort, where HPV DNA levels in the patients were not reduced following treatment with antiretroviral therapy [145]. This results is corroborated by other studies, suggesting that HPV may be present chronically in oral sites among HIV patients on antiretroviral therapy [18, 37].

To address the possible interactions leading to HPV persistence, we highlighted specific scenarios presenting an increased persistence of HPV due to the permissive immune environment created in an HIV-infected individual. Among the HIV infected individuals, those who had CD4 T cells levels corresponding to average chronic HIV CD4 T cell levels were more likely to clear HPV than those who had CD4 T cell levels as in an HIV/ HPV oral co-infection clinical study [145] or those who had CD4 T cell levels corresponding to AIDS. These results are dependent on the oncogenic expression levels, with HPV DNA levels increasing and taking a longer time to clear for high oncogenic expression levels. Interestingly, for high oncogenic expressions HPV clearance is delayed despite the faster expansion of CTL levels. This is due to an increase in the amount of HPV transit-amplifying cells.

We used the model to study the impact of cART in HIV/HPV co-infected individuals and compared the findings with those from the clinical study [145] which showed elevated HPV levels throughout the 24 weeks of cART. Our study showed that for the CD4 T cell levels in [145], HPV will eventually clear in an HIV/HPV co-infected individual receiving potent cART. The timing of the viral clearance, however, is determined by the timing of cART compared to the timing of HPV co-infection. When cART is started shortly after HPV infection, then HPV will expand and not be controlled in the 24 weeks of cART described in [145]. This is due to the fact that the CTL expansion and control of HPV is delayed due to both recruitment and size limitation observed when CD4 T cell reconstitution following cART is delayed. If, however, the cART starts at the peak anti-HPV CTL response, then HPV is cleared as soon as CD4 T cell reconstitution allows for the adequate CTL levels for control of HPV infection. The results are independent of the molecular effects induced by *tat*, which are removed when HIV is removed, and therefore do not influence HPV clearance.

This work is one of the first HIV/HPV co-infection models that investigates the dynamics of HPV in HIV-infected individuals. The only other published HIV/HPV co-infection model is a transitional probability-based model [71], which was used to study the relationship between immune status and the probability of the type of HPV clearance in HIV infected patients. The model [71] showed that HPV clearance was mainly based on the level of CD4 T cell count. The main difference between our findings compared to [71] stems from the fact that the current model takes into account that HPV clearance not only depends on the levels of CD4 T cell count but also the stage of HPV infection. Our results are consistent with observed associations between immunosuppression and HPV persistence in several clinical studies [9, 10, 145, 161].

The present modeling study should be evaluated in the context of several limitations. Our model does not take into account the spatial structure of the epithelial tissue. A generalized model that takes in to account the consider spatial structures for epithelial cells in different layers, requires extensive knowledge of numerous parameters, that are currently unknown. The second limitation concerns the immune clearance of lesions caused by HPV infections, which can lead to asymptomatic or latent infections with possibility of increased virion production upon immunosuppression [47, 86, 133, 153]. This further necessitates the need for consideration of both the cellular environment and the site of infection which are important determinants of virus activity [40]. Third, the simplistic modeling approach employed in the current modeling study does not take into account the feedback from the HPV to HIV infection. Due to absence of feedback from HPV to HIV, we disregard the effects of cART induced immune reconstitution. Additionally, our study does not consider the activation of latent HIV reservoirs post cART, which may contribute to the emergence new HPV genotype infections in co-infected individuals as shown in [145].

Additionally, the findings of this study and associated limitations guarantees and necessitates inclusion of latent T cell reservoirs which are involved in the activation of residual cART induced immune reconstitution. Furthermore, incorporating the immune activation in the T cells under the effect of cART during a HIV/HPV co-infection would corroborate the findings regarding the presence of new detectable HPV DNA.

In summary, we developed a novel mathematical and computational model of HIV/HPV co-infection and used it to present hypotheses for the mechanisms underlying HPV persistence in HIV/HPV co-infected individuals. Our model can be applied to studying interactions between HIV and other widespread microbes to gain a better mechanistic understanding, guide the rational for the design of clinical trials, and accelerate the path to safer and more effective vaccines and therapeutics. We use this study as an alternative approach to determining how overall CD4 T cell levels influence HPV prognosis in an HIV-infected individual. Overall, a better understanding of the cell specificity of HIV infection integrated with the cellular environment in HPV infection would facilitate the development of more effective therapeutic strategies in HIV/HPV co-infections.

Chapter 4

Germinal center dynamics during acute and chronic infection

This work was jointly authored with Dr. Stanca M. Ciupe. I created the model, figures, and numerical simulations with guidance from Dr. Stanca M. Ciupe. This section extends upon the original publication to include, model development, additional methods for parameters estimations, stability analysis and recent developments.

4.1 Abstract

The ability of the immune system to clear pathogens is limited during chronic virus infections where potent long-lived plasma and memory B-cells are produced only after germinal center B-cells undergo many rounds of somatic hypermutations. In this paper, we investigate the mechanisms of germinal center B-cell formation by developing mathematical models for the dynamics of B-cell somatic hypermutations. We use the models to determine how B-cell selection and competition for T follicular helper cells and antigen influences the size and composition of germinal centers in acute and chronic infections. We predict that the T follicular helper cells are a limiting

resource in driving large numbers of somatic hypermutations and present possible mechanisms that can revert this limitation in the presence of non-mutating and mutating antigen.

4.2 Introduction

The production of high-affinity antibodies capable of broad neutralization, viral inactivation, and protection against viral infections or disease requires activation, expansion, and maturation of B-cells into virus specific long-lived plasma and memory cells [173]. Germinal centers (GC) are the anatomical structures in which B-cells undergo somatic hypermutation, immunoglobulin class switching, and antigen-specific selection [118]. Somatic hypermutations are random and, therefore, the emergence of non-autoreactive, high-affinity B-cell clones requires strong selection through competition for survival signals [175]. The exact nature of these survival signals is poorly understood. T follicular helper (Tfh) cells have been identified as an important factor in driving B-cell hypermutation inside germinal centers [171]. Indeed, recent experiments have identified correlations between the density, function, and infection status of Tfh cells and the development of mature germinal centers [83, 124, 128, 129, 146, 169, 170].

Determining the characteristics of germinal centers such as their formation, size, and composition is important in understanding the protective mechanisms against pathogens that induce chronic infections. During HIV infections, only approximately 15 to 20% of chronically infected subjects develop antibodies with neutralization breadth [98, 151]. These antibodies are highly mutated compared to antibodies induced by most viral infections *in vivo* [164] or through vaccination [101]. For example, the high-affinity human antibody VRC01, which neutralizes 90 % of HIV-1, has 70-90 somatic mutations [174] compared to the natural 5-10 somatic mutations [73]. The mechanisms that allow for the production of protective antibodies in some patients but not others are still under investigation [17, 53, 74, 75, 150].

Mathematical models have been used in the past to investigate the mechanisms responsible for B-cell somatic hypermutations inside the germinal centers [52, 66, 68, 85, 93, 94, 95, 114, 130, 146]. Early studies hypothesized that re-entry into new GCs of B-cells from previous GCs may explain the affinity maturation process [66, 114]. Others showed that affinity maturation requires cyclic transition of B-cells between the two anatomical structures of the germinal center: the dark and light zones [52, 68, 85, 93, 94, 95]. The models that incorporate dark and light zones investigated the role of molecular mechanisms such as competition for Tfh cells [95, 130, 146], antigen on the surface of follicular dendritic cells [147], binding sites [68], and clonal competition [141] in facilitating movement between the two zones. Lastly, they investigated internal and external stimuli that lead to germinal center termination [96, 104]. These studies have not considered the mechanisms behind the emergence of large number of B-cell somatic hypermutations inside germinal centers as seen in some HIV patients [174]. Nor did they present hypotheses behind the absence of broadly neutralizing antibodies in the majority of HIV patients. Understanding the mechanistic interactions inside GCs that lead to production of plasma cells capable of producing antibodies with neutralization breadth forms the focus of this paper.

To address this, we develop mathematical models of germinal center formation that investigate the role of B-cell competition, Tfh cells, and antigen in inducing large numbers of B-cell somatic hypermutations, as seen in the few HIV patients that produce broadly neutralizing antibodies. We first develop a deterministic model of Tfh cell-B cell interactions to determine how B-cell selection and competition influences GC formation in acute infections. We fit the model to published germinal center B-cell data to estimate parameters. We then investigate the mechanisms that allow for emergence of highly mutated B-cell clones that are capable of protecting against chronic infections with non-mutating antigen, i.e. substances that do not mutate but stimulate antibody generation. Finally, we investigate how our predictions change when we consider antigenic mutation.

For a non-mutating pathogen, we predict that when only a few rounds of somatic hypermutations are needed for the clearance of a pathogen, as in acute infections, the Tfh cells are not limiting the emergence of high affinity B-cell clones. When large numbers of somatic hypermutations arise, however, a limitation in the number of Tfh cells may prevent B-cell clones of higher affinity from emerging and becoming the dominant B-cell population inside the germinal centers. Moreover, we predict that for a mutating pathogen which drives the somatic hypermutation of B-cells, emergence of B clones of highest affinity may be hindered not only through a limitation in the number of Tfh cells but also by the speed of the viral mutation.

4.3 Model of germinal center formation

We develop a mathematical model of B - Tfh cell dynamics which considers the interaction between the naive CD4 T cells (N), non-mutating antigen (V), pre-Tfh cells (H), Tfh cells (G), primed follicular B-cells (B_0), GC B-cells that have undergone i rounds of somatic hypermutations (B_i), and plasma cells (P). Here $1 \leq i \leq n$ and n represents the maximum number of B-cell clones inside a single germinal center.

N cells are produced at rate s_N and die at per capita rate d_N and, upon encountering specific antigen V, migrate to the T:B cell border and become pre-Tfh cells H at rate α_N. H cells either migrate to GCs following interaction with primed follicular B-cells B_0 and differentiate into Tfh cells G at rate γ, or die at per capita rate d_H. G cells are lost through natural death at per capita rate d_G. Moreover, we assume that competition between B-cell clones B_i for Tfh cell-induced stimulation is limiting G population growth at rate η. This competition, in return, will limit the number of B-cells inside GCs and their transition between clones of higher affinity for the pathogen.

Primed follicular B-cells B_0 (B blasts) die at rate d and, upon interaction with pre-follicular helper cells H, move inside germinal centers where they undergo affinity maturation. We assume that each stage of affinity maturation requires Tfh cell help at the same rate σ and that each population B_i produces α offsprings B_{i+1}, for $1 \leq 1 \leq n-1$ [171]. B_is die at the same per capita rate d as B blasts. Lastly, cells in clone B_n leave germinal centers at rate κ to become plasma cells P capable of removing a non-mutating antigen V at rate μ.

The system describing these interactions is given by:

$$\frac{dN}{dt} = s_N - d_N N - \alpha_N V N, \tag{4.1a}$$
$$\frac{dH}{dt} = \alpha_N V N - d_H H - \gamma H B_0, \tag{4.1b}$$
$$\frac{dG}{dt} = \gamma H B_0 - d_G G - \eta G \sum_{i=1}^{n} B_i, \tag{4.1c}$$
$$\frac{dB_0}{dt} = -dB_0 - \sigma B_0 H, \tag{4.1d}$$
$$\frac{dB_1}{dt} = \alpha \sigma B_0 H - \sigma B_1 G - dB_1, \tag{4.1e}$$
$$\frac{dB_i}{dt} = \alpha \sigma B_{i-1} G - \sigma B_i G - dB_i, \tag{4.1f}$$
$$\frac{dB_n}{dt} = \alpha \sigma B_{n-1} G - dB_n - \kappa B_n, \tag{4.1g}$$
$$\frac{dP}{dt} = \kappa B_n, \tag{4.1h}$$
$$\frac{dV}{dt} = -\mu V P, \tag{4.1i}$$

for $1 \leq i \leq n-1$ with initial conditions $N(0) = s_N/d_N$, $B(0) = B_0$, $V(0) = V_0$ and all other populations are initially absent. Our goal is to determine the dynamical evolution of the total B-cell population in a single germinal center based on the availability of Tfh cells. We focus on the size and composition of B-cells in the germinal center,

$$B_t = \sum_{i=1}^{n} B_i, \tag{4.2}$$

for acute infections and for chronic infections where many rounds of affinity maturation lead to development of broadly neutralizing antibody-producing plasma cells, as seen in a few HIV infections [98, 151].

4.4 Tfh-B-cell dynamics during acute infections

In acute infections, B clones undergo between 5 and 10 steps of affinity maturation [73, 104, 115]. Without loss of generality, we set $n = 8$. We assume that 1% of naive CD4 T cells are recruited by the antigen V, therefore $N(0) = 10^6$ cells per ml [149]. Studies have shown that mature B-cell clones inside germinal centers are the progeny of as little as 3 precursor blasts [67, 72]. Therefore, the initial blast population is $B(0) = 3$ cells.

The B_t data was collected from young, pathogen free mice. The splenic germinal center B-cells' temporary responses to a T-dependent antigen were measured [58], therefore providing germinal center B-cell dynamics throughout an acute infection. The antigen V is the density of sheep red blood cells (sRBC) per ml injected into the mouse, $V(0) = 2 \times 10^8$ sRBC per ml. It elicits a B-cell expansion inside a germinal center and subsequent antigen clearance. Lastly, we assume that at the time of the infection, all the other populations are absent, *i.e.* $H(0) = G(0) = 0$ cells per ml and $P(0) = B_i(0) = 0$ cells, for $1 \leq i \leq n$.

In our model, the per capita death rates of all CD4 T cells are equal, $d_N = d_H = d_G = 0.01$ per day [149], and the naive CD4 T cell population is at equilibrium at the beginning of infection, *i.e.*, $s_N = d_N \times N_0 = 10^4$ cells per ml per day. Naive CD4 T cells N are activated by antigen V at rate α_N and move to the follicules and become pre-Tfh cells H. Since the pre-follicular T cell density is around 10^4 cells per ml and the ratio between G and H cells ranges between 2 and 4 in the first 10 days of germinal center formation [146], we adjust parameters $\alpha_N = 1.8 \times 10^{-11}$ ml per day per cell and $\gamma = 2$ per cell per day to reflect this fact.

B-cells in each B clone die at rate $d = 0.8$ per day [67], independent of affinity maturation class i. Since the dynamics of V and P do not affect the Tfh-B cell interactions, we randomly assign values for parameters $\kappa = 1.2$ per day and $\mu = 2$ per cell per day, the plasma cell production rate and antigen removal rate, respectively. We will later analyze the effect of varying these rates. A summary of initial conditions and fixed parameters is presented in Table 4.1.

Name	Value	Units	Description	Citation
s_N	10^4	cells per ml per day	Naive CD4 T cell recruitment rate	[149]
d_N	0.01	per day	Naive CD4 T cell death rate	[149]
α_N	1.8×10^{-11}	ml per day per cell	Pre-Tfh cell production rate	
d_H	0.01	per day	Pre-Tfh cell death rate	[149]
d_G	0.01	per day	Tfh cell death rate	[149]
d	0.8	per day	B-cell death rate	[67]
κ	1.2	per day	Plasma cells production rate	
γ	2	per cell per day	Pre-Tfh cell differentiation rate	[146]
μ	2	per cell per day	Antigen removal rate	
η	10^{-5}	per cell per day	Tfh competition rate	
$N(0)$	10^6	cells per ml	Initial amount of CD4 T cells	[149]
$H(0)$	0	cells per ml	Initial amount of Pre-Tfh cells	
$G(0)$	0	cells per ml	Initial amount of Tfh cells	
$B_0(0)$	3	cells	Initial amount of B-cells	[67, 72]
$B_i(0)$	0	cells	Initial amount of B-cell clones	
$P(0)$	0	cells	Initial amount of plasma cells	
$V(0)$	2×10^8	per ml	Initial amount of non-mutating antigen	[58]

Table 4.1: Variables and fixed parameter values.

We estimate the remaining parameters α, the B-cell offspring production rate, and σ, the B-cell transition rate, by fitting the total B_t population as given by (4.11), in the presence of competition for Tfh cell signaling, *i.e.* $\eta = 10^{-5}$ per cell per day, to published germinal center B-cell data [58, 104]. We used `nlinfit` in MATLAB R2014b (The MathWorks Inc., Natick, MA). The estimates and confidence intervals for α and σ are presented in Table 4.2.

Name	Units	Value	Description	Confidence Intervals
α		27.469	B-cell offspring production rate	[14.015 40.924]
σ	ml per cell per day	1.1×10^{-5}	Affinity maturation rate	[4.8×10^{-6} 1.7×10^{-5}]

Table 4.2: Parameter estimates and confidence intervals.

4.4.1 Stability analysis

We analytically investigate the properties of the germinal center model (5.4) when $n = 2$ but this can easily be expanded for any n. The system (5.4) has two steady states:
An infection free steady state,

$$S_0 = (\frac{s_N}{d_N}, 0, 0, 0, 0, 0, 0, P, 0) \tag{4.3}$$

or, a chronic infection steady state,

$$S_1 = (\bar{N}, \frac{s_N - d_N\bar{N}}{d_H}, 0, 0, 0, 0, 0, 0, \frac{s_N - d_N\bar{N}}{\alpha_N\bar{N}}), \tag{4.4}$$

where $\bar{N}$ is the naive CD4+ T cell level. S_0 exists when germinal center leads to plasma formation and the pathogen has cleared. S_1 exists when a germinal center did not lead to plasma formation and the pathogen is not cleared. To investigate the asymptotic stability of S_0 we compute the Jacobian for model (5.4):

$$\mathscr{J} = \begin{bmatrix} -d_N - \alpha_N V & 0 & 0 & 0 & 0 & 0 & 0 & 0 & -\alpha_N N \\ \alpha_N V & -d_H - \gamma B_0 & 0 & -\gamma H & 0 & 0 & 0 & 0 & \alpha_N N \\ 0 & \gamma B_0 & -d_G - \eta \sum_{i=1}^{n} B_i & \gamma H & -\eta G & -\eta G & -\eta G & 0 & 0 \\ 0 & -\sigma B_0 & 0 & -d - \sigma H & 0 & 0 & 0 & 0 & 0 \\ 0 & \alpha\sigma B_0 & -\sigma B_1 & \alpha\sigma H & -\sigma G - d & 0 & 0 & 0 & 0 \\ 0 & 0 & \alpha\sigma B_{i-1} - \sigma B_i & 0 & \alpha\sigma G & -\sigma G - d & 0 & 0 & 0 \\ 0 & 0 & \alpha\sigma B_{n-1} & 0 & 0 & \alpha\sigma G & -d - \kappa & 0 & 0 \\ 0 & 0 & 0 & 0 & 0 & 0 & \kappa & 0 & 0 \\ 0 & 0 & 0 & 0 & 0 & 0 & 0 & -\mu V & -\mu P \end{bmatrix} \tag{4.5}$$

At S_0,

$$
\mathscr{J}|_{S_0} - \lambda I = \begin{bmatrix}
-d_N-\lambda & 0 & 0 & 0 & 0 & 0 & 0 & 0 & \frac{-\alpha_N s_N}{d_N} \\
0 & -d_H-\lambda & 0 & 0 & 0 & 0 & 0 & 0 & \frac{\alpha_N s_N}{d_N} \\
0 & 0 & -d_G-\lambda & 0 & 0 & 0 & 0 & 0 & 0 \\
0 & 0 & 0 & -d-\lambda & 0 & 0 & 0 & 0 & 0 \\
0 & 0 & 0 & 0 & -d-\lambda & 0 & 0 & 0 & 0 \\
0 & 0 & 0 & 0 & 0 & -d-\lambda & 0 & 0 & 0 \\
0 & 0 & 0 & 0 & 0 & 0 & -d-\kappa-\lambda & 0 & 0 \\
0 & 0 & 0 & 0 & 0 & 0 & \kappa & -\lambda & 0 \\
0 & 0 & 0 & 0 & 0 & 0 & 0 & 0 & -\mu P-\lambda
\end{bmatrix} \tag{4.6}
$$

and

$$
\det(\mathscr{J}|_{S_0} - \lambda I) = (-d_N-\lambda)(-d_H-\lambda)(-d_G-\lambda)(-d-\lambda)^3(-d-\kappa-\lambda)(-\mu P-\lambda)\lambda. \tag{4.7}
$$

In this system all non-zero eigenvalues are negative, and the zero eigenvalue corresponds to the free plasma population which we assume is long living and as such does not have a death term in our model. Thus S_0 is stable.

At S_1

$$
\mathscr{J}|_{S_1} - \lambda I = \begin{bmatrix}
\frac{d_N\bar{N}-s_N}{\bar{N}} - d_N - \lambda & 0 & 0 & 0 & 0 & 0 & 0 & 0 & -\alpha_N\bar{N} \\
-\frac{d_N\bar{N}-s_N}{\bar{N}} & -d_H-\lambda & 0 & \frac{\gamma(\bar{N}d_N-s_N)}{d_H} & 0 & 0 & 0 & 0 & \alpha_N\bar{N} \\
0 & 0 & -d_G-\lambda & -\frac{\gamma(\bar{N}d_N-s_N)}{d_H} & 0 & 0 & 0 & 0 & 0 \\
0 & 0 & 0 & -d-\frac{\sigma(\bar{N}d_N-s_N)}{d_H}-\lambda & 0 & 0 & 0 & 0 & 0 \\
0 & 0 & 0 & -\frac{\alpha\sigma(\bar{N}d_N-s_N)}{d_H} & -d-\lambda & 0 & 0 & 0 & 0 \\
0 & 0 & 0 & 0 & 0 & -d-\lambda & 0 & 0 & 0 \\
0 & 0 & 0 & 0 & 0 & 0 & -d-\kappa-\lambda & 0 & 0 \\
0 & 0 & 0 & 0 & 0 & 0 & \kappa & -\lambda & 0 \\
0 & 0 & 0 & 0 & 0 & 0 & 0 & -\frac{\mu(d_N\bar{N}-s_N)}{\bar{N}} & -\lambda
\end{bmatrix} \tag{4.8}
$$

and

$$\det(\mathscr{J}|_{S_1} - \lambda I) = (\frac{\bar{N}d_N - S_N}{\bar{N}} - d_N - \lambda)(-d_H - \lambda)(-d_G - \lambda)(-d - \lambda)^2 \dots \quad (4.9)$$
$$(-d - \kappa - \lambda)(\frac{(\bar{N}d_N - s_N)\sigma}{d_H} - d - \lambda)\lambda^2.$$

S_1 is stable when $\bar{N} < d/\sigma + s_N/d_N$, given that $d_H = d_N$.

4.4.2 Numerical results

The dynamics of all variables of system (5.4) over time for parameters in Tables 4.1 and 4.2 are shown in Figure 4.1. The number of offspring produced by each B-cell clone is $\alpha = 27.5$ and the transition rate is $\sigma = 1.1 \times 10^{-5}$ ml per cell per day. Competition for Tfh cell help does not affect the fit and B_t dynamics. Indeed, when η, the competition parameter, is decreased from 10^{-5} to 0 per cell per day and $\sigma = 1.1 \times 10^{-5}$ ml per cell per day the estimate for α, the B-cell offspring production rate, decreases by less than 1.5% to $\alpha = 27.1$. Therefore, we predict that the Tfh cell population is not inhibiting the emergence of B-cells that underwent the maximum 8 rounds of somatic hypermutation.

The total number of B-cells in the germinal center, B_t, reaches a maximum of 1147 cells, eleven days after infection and the germinal center dies out 29 days after infection (see Figure 4.1, panel a). Over time, the germinal center is formed by B-cell clones of the highest somatic hypermutation, with the maximum ratio between the peaks of two consecutive clones $B_i/B_{i-1} = 2.91$ occurring for $i = 5$. There is a delay between the peaks of each clone ranging between 0.3 and 2.1 days. For the plasma cell production rate $\kappa = 1.2$ per day, plasma cells emerge 4.5 days following infection and reach a value of 4000 cells, 15 days following infection (see Figure 4.1, panel c).

The pre-Tfh and Tfh populations, H and G, reach their maximum density of 6.1×10^3 and 9.6×10^3 cells per ml, 5 and 7 days following infection, respectively. The $G : H$ ratio increases to 2.5, two days following infection and then levels off to 1.7 more Tfh than pre-Tfh cells (see Figure 4.2,

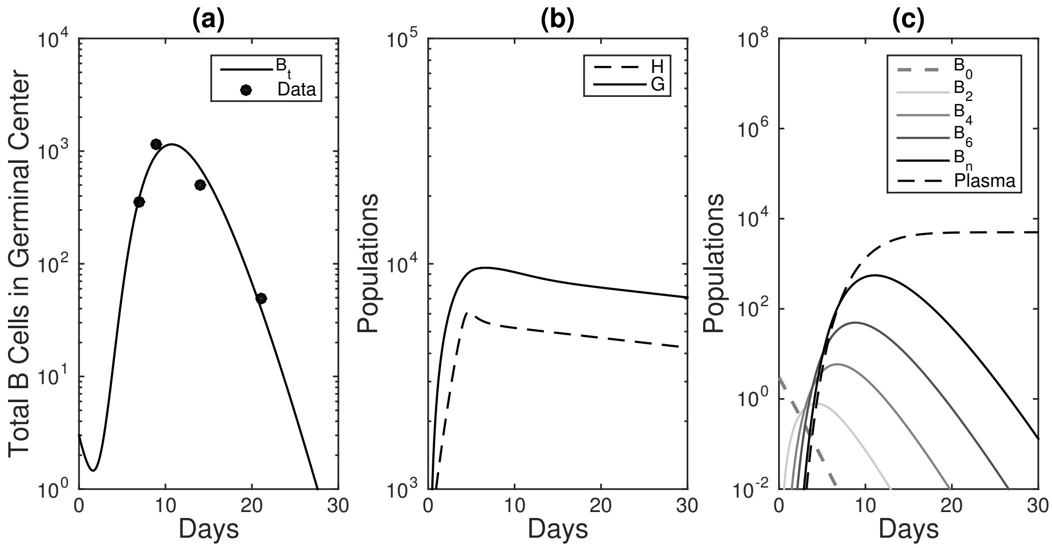

Figure 4.1: (a) B_t as given by (4.11) versus data (•); (b) Pre-Tfh cells H per ml and Tfh cells G per ml; (c) B cells that underwent different levels of somatic hypermutations and plasma cells. The parameter values are given in Tables 4.1 and 4.2.

panel c). A higher ratio, of as high as 4-times more Tfh than pre-Tfh cells, as predicted by [146], can be obtained if we increase γ, the pre-Tfh cell differentiation rate, by 50%. Once the antigen is eliminated, both H and G populations disappear.

For $\mu = 2$ per cell per day, the antigen is lost 5.9 days after infection. At that time V reaches 3×10^{-4} sRBC per ml (or 1 sRBC in the body). A reasonable concern is that varying this rate would affect the dynamics of the total B-cell population, as a prolonged antigenic stimuli would potentially lead to a larger germinal center that lasts for a longer period of time. To gain a deeper understanding of the role of μ, the antigen removal rate, in the B_t dynamics, we decrease μ by two and four orders of magnitude. As expected, when we decrease μ to 2×10^{-2} and 2×10^{-4} per cell per day, the time needed for the removal of antigen increases to 10 and 33 days following infection, respectively (see Figure 4.2, panel d). The maximum B_t increases by 28% and 32% respectively and germinal centers last for 30 days (see Figure 4.2, panel a). The μ effect on G population is not significant, but the H increases and exceeds the G population (see Figure 4.2, panel c).

We also investigated fitting α, the B-cell offspring production rate, and σ, the B-cell transition rate, using Markov chain Monte Carlo (MCMC) methods. MCMC is a technique used for generating

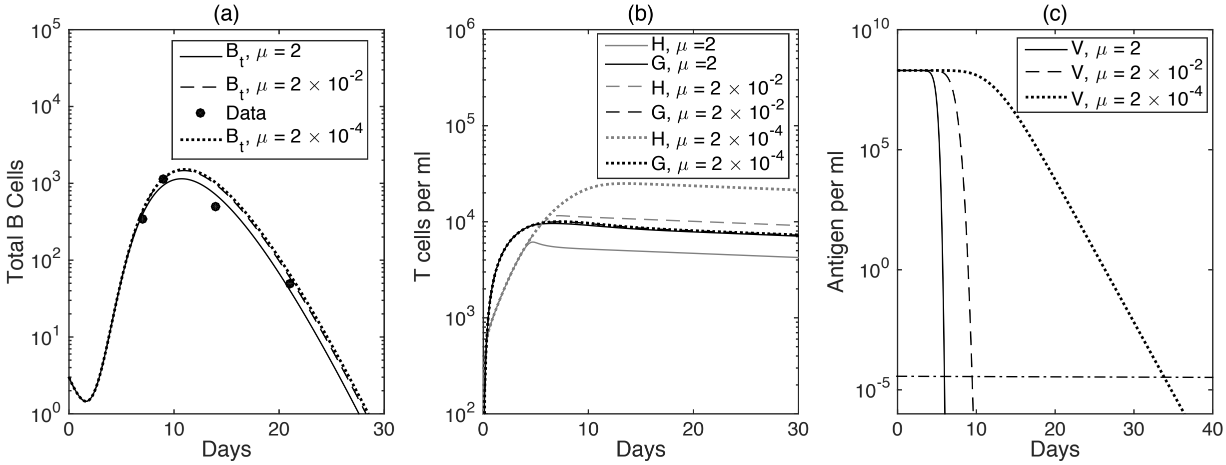

Figure 4.2: (a) B_t as given by (4.11) versus data (•); (b) Pre-Tfh cells H per ml and Tfh cells G per ml; and (c) Antigen per ml; for $\mu = 2$ per cell per day (solid lines), $\mu = 2 \times 10^{-2}$ per cell per day (dashed lines) and $\mu = 2 \times 10^{-4}$ per cell per day (dotted lines). The dashed-dotted line is the antigen limit of detection of 3×10^{-4} sRBC per ml. The other parameter values are given in Tables 4.1 and 4.2.

fair samples from a probability in high-dimensional space, using random numbers drawn from a uniform probability in a certain range. We developed a sum-of-squares function and minimized a gaussian likelihood function which we described in detail in Section 2.4.2. We utilized the MCMC toolbox for Matlab and selected an initial error variance of 230, which was derived based on the error bars of the collected data from [58]. We used our previous estimated parameters as initial guesses and our confidence intervals as upper and lower bounds from `nlinfit` (see Table 4.2). We performed 50,000 simulations. In Figure 4.3, we compare α vs σ and see that as σ decreases, α increases and see a correlation between the two parameters. This correlation occurs because α always appears in model (5.4) multiplied by σ, hence as σ decreases α increases to compensate. While, it is a possibility that α could be written as function of σ this would no longer biologically distinguish between the somatic hypermutations and birth rate of B cells. We also see that our original parameter estimate in Table 4.2 is a parameter estimate in our sample. In Figure 4.4 we plot the parameter ranges for α and σ, the parameter region with the highest probability of representing the data has the largest density.

It should be noted, it is concerning that the initial condition, specifically of $B_0(0) = 3$, is small

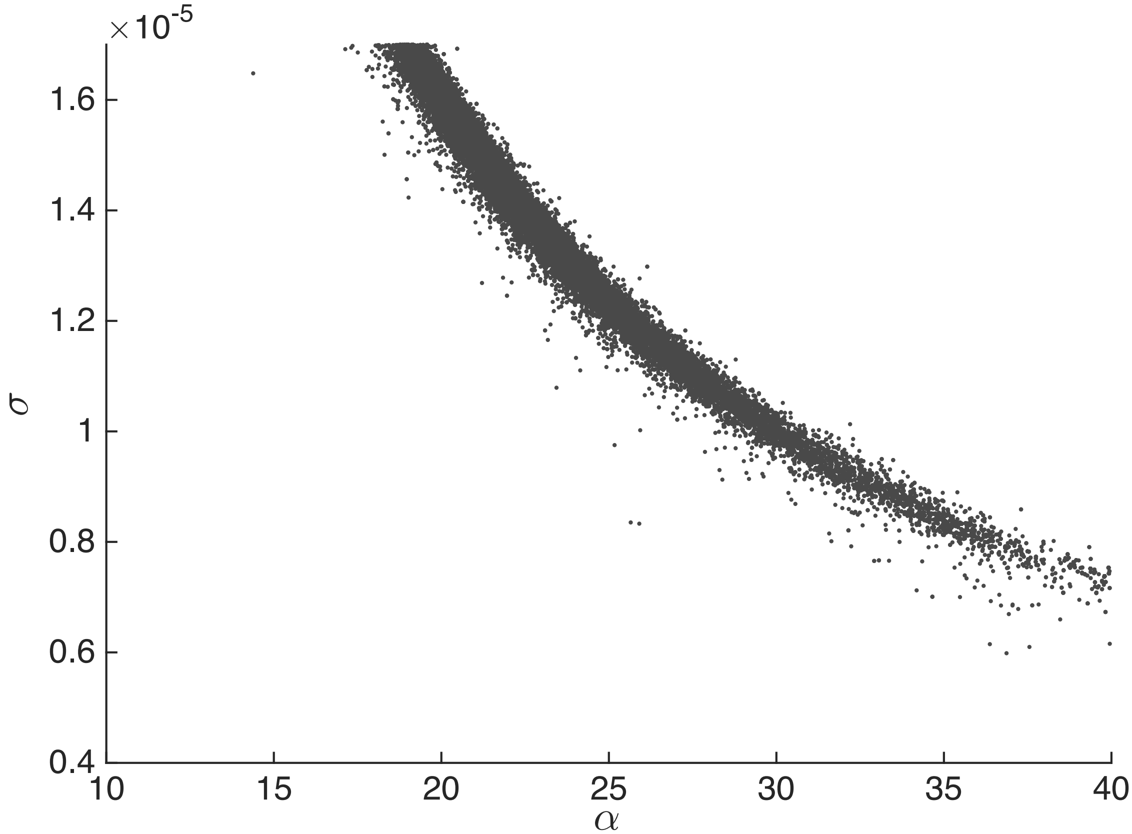

Figure 4.3: (a) Parameter estimates for α vs σ based on the data generated by MCMC; The other parameter values are given in Table 4.1.

compared to the large amount of antigen, i.e. $V(0) = 2 \times 10^8$, and other populations. To check for potential numerical error, we consider instead B_0 as a function to ensure the results would be maintained. We develop a mathematical model of B - Tfh cell dynamics that considers the interaction between the Tfh cells G and remove the pre-cursor T populations, Naive CD4 T cells and pre-Tfh cells.

Tfh cells G are produced at rate $\gamma h(t)$, based on a previous interaction with antigen, pre-Tfh and B cells, or die at per capita rate d_H. G cells are lost through natural death at per capita rate d_G. Moreover, we assume that competition between B cell clones B_i for Tfh cell-induced stimulation is limiting G population growth at rate η. This competition in return, will limit the number of B cells inside GCs and their transition between clones of higher affinity for the pathogen.

B cells move inside germinal centers where they undergo affinity maturation initiated by $h(t)$ which

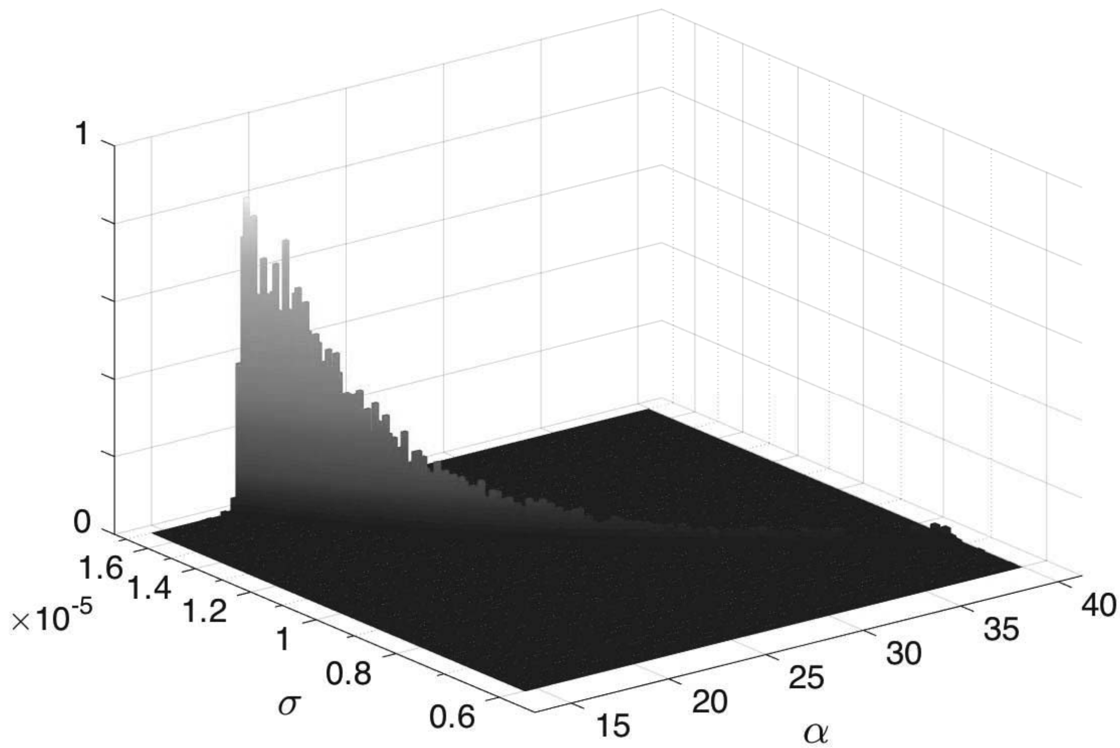

Figure 4.4: Density plot for the likelihood of α and σ based on the data generated by MCMC. The other parameter values are given in Table 4.1.

represents previous interaction with antigen, pre-Tfh and B cells. We assume that each stage of affinity maturation requires Tfh cell help at the same rate σ and that each population B_i produces α offsprings B_{i+1}, for $1 \leq 1 \leq n-1$. B_is die at the same per capita rate d as B blasts. Lastly, cells in clone B_n leave germinal centers and rate κ to become plasma cells P capable of removing antigen V at rate μ. Here $1 \leq i \leq n$ and n represents the maximum number of B cell clones inside a single germinal center.

The system describing these interactions is given by:

$$
\begin{aligned}
\frac{dG}{dt} &= \gamma h(t) - d_G G - \eta G \sum_{i=1}^{n} B_i, \\
\frac{dB_1}{dt} &= \alpha\sigma h(t) - \sigma B_1 G - dB_1, \\
\frac{dB_i}{dt} &= \alpha\sigma B_{i-1} G - \sigma B_i G - dB_i, \\
\frac{dB_n}{dt} &= \alpha\sigma B_{n-1} G - dB_n - \kappa B_n, \\
\frac{dP}{dt} &= \kappa B_n,
\end{aligned}
\tag{4.10}
$$

for $1 \leq i \leq n-1$ where all populations are initially absent. Our goal is to determine the dynamical evolution of the total B cell population in a single germinal center based on the availability of Tfh cells. That is, we look at:

$$
B_t = \sum_{i=1}^{n} B_i, \tag{4.11}
$$

for non-chronic infections and for chronic infections.

In Figure 4.5 we compare model (4.10) to model (5.4) and we see that the results are similar and the differences are negligible.

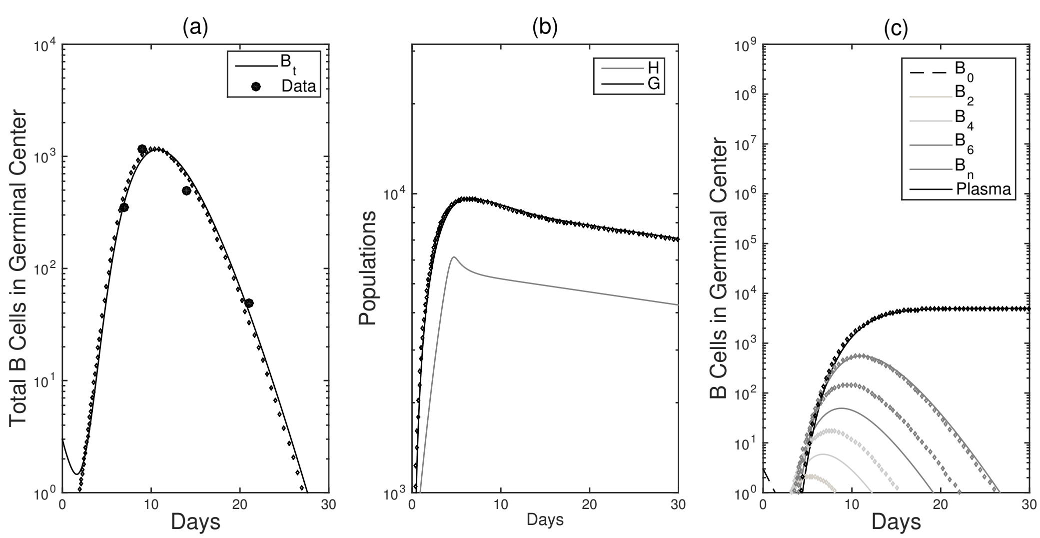

Figure 4.5: Original model (solid lines) and the proposed smaller model without small initial condition (diamond markers), where the parameters are the same in both cases.

4.4.3 Sensitivity analysis

We performed a focused analysis of the time-dependent sensitivity of model (5.4)'s trajectories to parameter variation, known as a semi-relative sensitivity analysis. We start by looking at the sensitivity of populations B_t and G to changes in the two fitted parameters α, the B-cell offspring production rate, and σ, the B-cell transition rate, as follows. We define the absolute sensitivity variables $B_{t,q} = \frac{\partial B_t(t,q)}{\partial q}$ and $G_q = \frac{\partial G(t,q)}{\partial q}$. They are obtained by differentiating both sides of system (5.4) with respect to q.

In Figure 4.6 we compared the semi-relative sensitivity curves $qB_{t,q}$ and qG_q for $q = \sigma$ and $q = \alpha$. These parameters have complementary effects on both B_t and G populations. As such, if α, the B-cell offspring production rate, and σ, the B-cell transition rate, are doubled, B_t increases by a maximum of 6121.6 and 5166.6 cells at day 10 following infection (see Figure 4.6, top panel). Varying parameters α and σ has no effect on G for the first 5 days. After that time, their effect is negative. In particular, if either of the two parameters is doubled, then the G population decreases by 5366 or 5504 cells per ml at day 17 for σ and α respectfully (see Figure 4.6, bottom panel).

We further compared the semi-relative sensitivity curves $qB_{t,q}$ and qG_q for $q = \kappa$ and $q = \mu$ (see Figure 4.7). These parameters have complimentary effects on the B_t population and a negligible effect on the G population. As such, if μ, the antigen removal rate, and κ, the plasma cell production rate, are doubled, B_t decreases by a maximum of 68 and 364 cells at day 11 following infection (see Figure 4.7, top panel). Varying parameters μ and κ has no effect on G for the first 5 days. After that time, their effect is opposite. In particular, if either of the two parameters is doubled, then the G population decreases by 120 or increases by 100 cells per ml after two weeks for μ and κ respectfully (see Figure 4.7, bottom panel).

Lastly we compared the semi-relative sensitivity curves $qB_{t,q}$ and qG_q for $q = \gamma$ and $q = \eta$ (see Figure 4.8). These parameters have opposite effects on both B_t and G population. As such, if γ, the pre-tfh cell differentiation rate, and η, the Tfh competition rate, are doubled, B_t increases by a maximum of 1739 cells at day 10 and decreases by a maximum of 90 cells at day 13 following

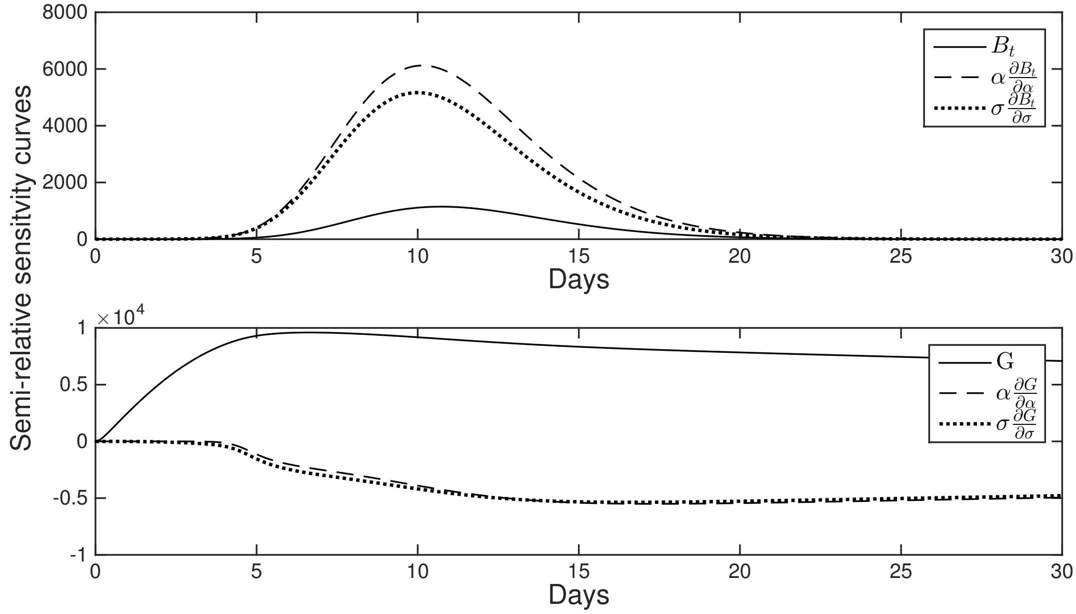

Figure 4.6: B_t and G (solid lines) and the semi-relative sensitivity curves, $q\frac{\partial B_t}{\partial q}$ and $q\frac{\partial G}{\partial q}$, over time for $q = \alpha$ (dashed lines), and $q = \sigma$ (dotted lines).

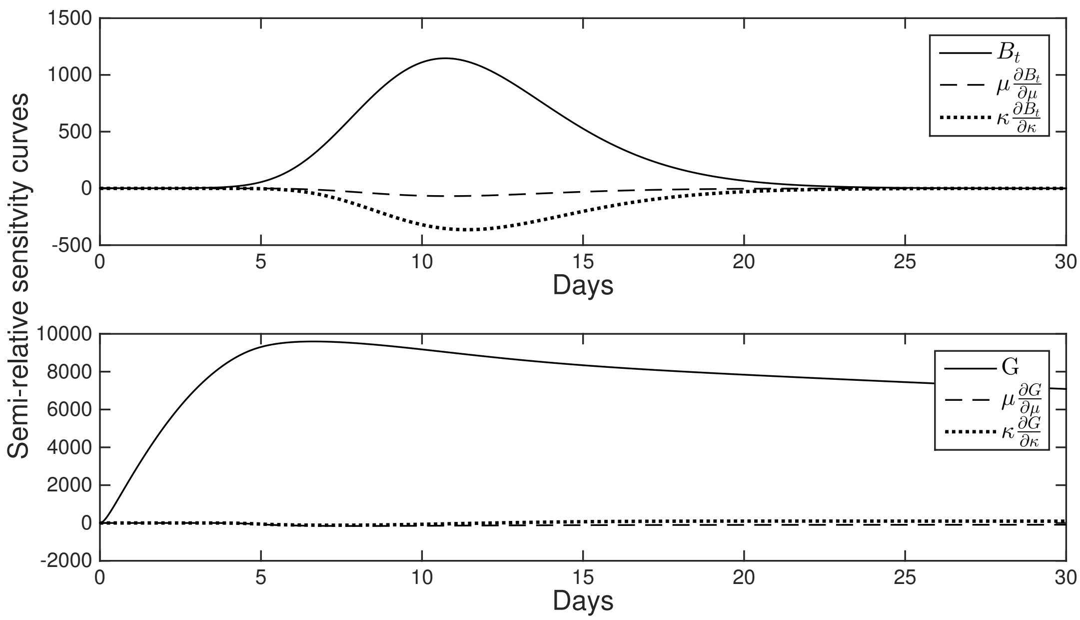

Figure 4.7: B_t and G (solid lines) and the semi-relative sensitivity curves, $q\frac{\partial B_t}{\partial q}$ and $q\frac{\partial G}{\partial q}$, over time for $q = \mu$ (dashed lines), $q = \kappa$ (dotted lines).

infection (see Figure 4.8, top panel). Varying γ was a positive effect on G within the first day. As such if γ is doubled G increases by a maximum of 2719 cells per ml at day 5 (see Figure 4.8, bottom panel). Varying parameter η has no effect on G for the first 5 days and after that time has a negative effect. In particular, if we double η, then the G population decreases by 628 cells per ml 19 days following infection.

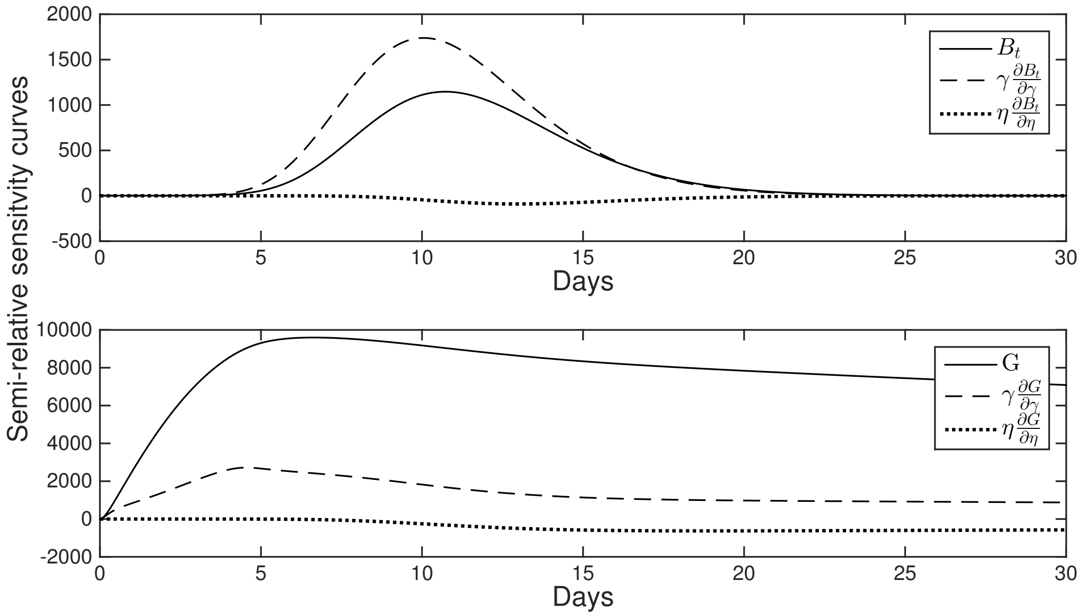

Figure 4.8: B_t and G (black lines) and the semi-relative sensitivity curves, $q\frac{\partial B_t}{\partial q}$ and $q\frac{\partial G}{\partial q}$, over time for $q = \gamma$ (dashed lines), $q = \eta$ (dotted lines).

4.5 Tfh-B-cell dynamics during chronic infections

We next want to understand the size and B-cell clone compositions of germinal centers during prolonged antigenic stimuli. During chronic virus infections with viruses like HIV, the immune protection occurs when antibodies are highly mutated. For example, the high-affinity human antibody VRC01 has 70-90 mutations [174]. We will use model (5.4) and parameters in Tables 4.1 and 4.2 as a starting point for understanding how the B-cell and Tfh cell dynamics change when many rounds of somatic hypermutations are allowed (as seen in the HIV patients). Most importantly, we want to determine the mechanistic interactions that allow for the emergence of a large enough B-clone with the highest level of mutation, which is capable of removing the antigen.

We represent highly mutated antibodies by increasing the level of admissible B-cell somatic hypermutations to $n = 50$ in model (5.4). We start by keeping all other parameters as in Tables 4.1 and 4.2. As expected, increasing n leads to an increase in the B_t population, with the B_t peak being two orders of magnitude higher and occurring two days earlier than in the $n = 8$ case. Such large germinal centers are not uncommon in persistent infections such as HIV [167], and subsequently we assumed the B-cell size to be reasonable and did not attempt to refit model (5.4) with $n = 50$ to the acute data. Under these assumptions, we predict that the germinal center terminates two days earlier, at 27 days following infection (see Figure 4.9, panel a).

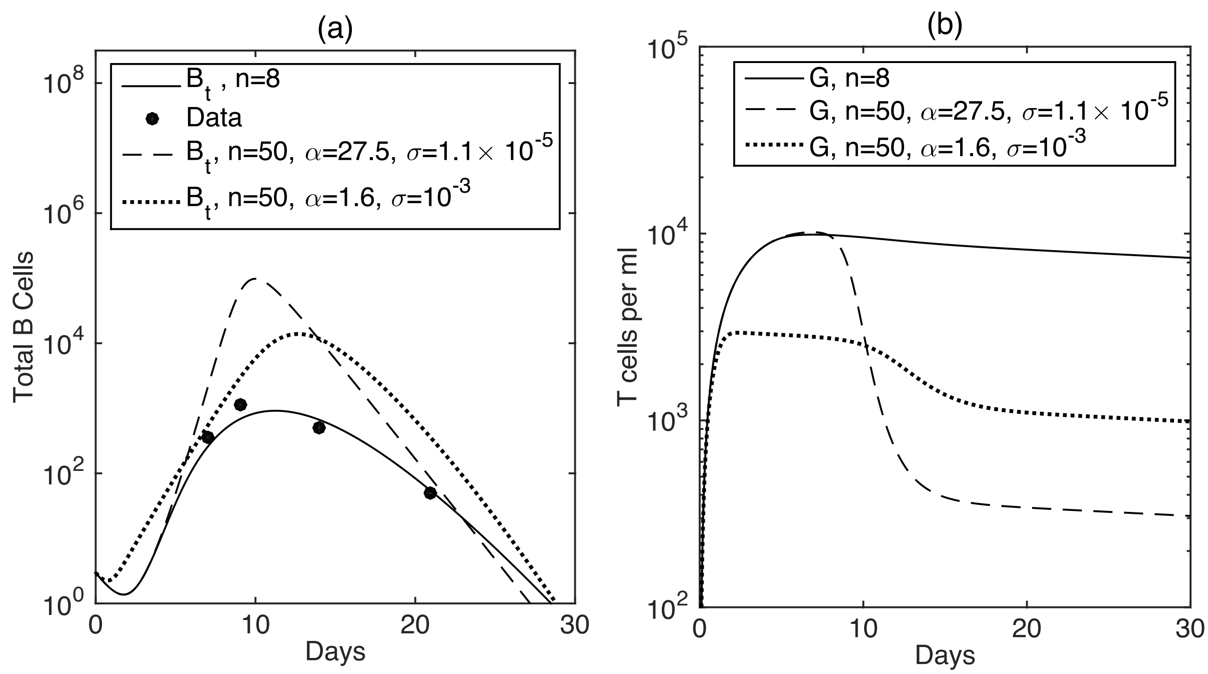

Figure 4.9: (a) B_t as given by (4.11) versus data (•); and (b) G per ml as given by model (5.4) for $n = 8$ (solid lines); $n = 50$, $\alpha = 27.5$, $\sigma = 1.1 \times 10^{-5}$ ml per cell per day (dashed lines); and $n = 50$, $\alpha = 1.6$, $\sigma = \times 10^{-3}$ ml per cell per day (dotted lines). The other parameters are given in Tables 4.1 and 4.2.

We observe that the Tfh cell population is smaller compared to the acute case during the contraction time, i.e. past 9 days following infection. This is due to competition between an increasing number of B-cell clones for Tfh cell stimuli as given by the term $\eta B_t G$ (see Figure 4.9, panel b).

To gain an understanding on the role of competition for Tfh cell help we compute and plot the distribution of B-cell clones for $n = 8$ and $n = 50$ at $t = 10$, $t = 20$, and $t = 30$ days after the germinal center initiation. For $n = 8$ and the three times considered, the late clones dominate the B_t population and, as time progresses, more and more of B_t is dominated by B_8, which is the clone that underwent the maximum rounds of hypermutations and the only clone giving rise to plasma cells (see Figure 4.10, top row). For $n = 50$, however, B_t is dominated by the clones that underwent $15-35$ rounds of somatic hypermutations at all times considered, and the B_{50} clone is never reached (see Figure 4.10, second row). Although there has been a slight movement to the later clones, there is very little change in the distribution between $t = 20$ and $t = 30$ days. Since only B_{50} produces plasma cells capable of eliminating virus, we predict that $dV/dt = 0$, and the virus remains at its initial value which is representative of a chronic infection.

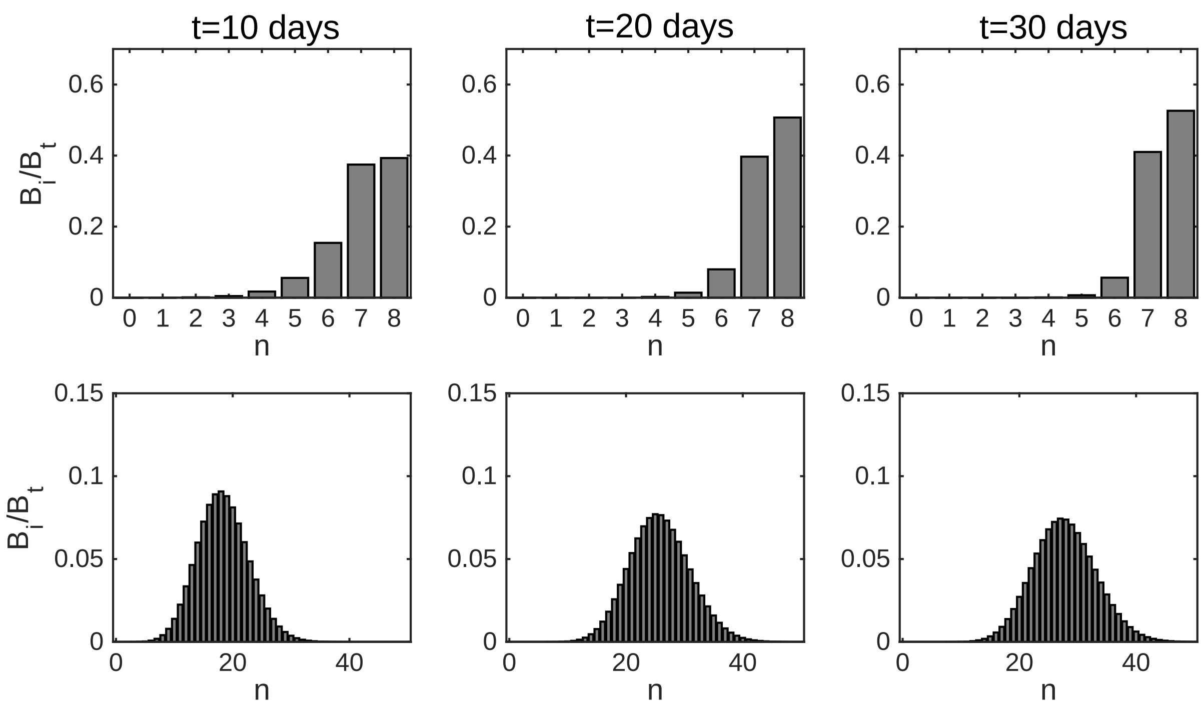

Figure 4.10: Clonal distribution B_i/B_t for $0 \leq i \leq n$, $t = 10$, $t = 20$, $t = 30$ days following infection for $n = 8$ (top) and $n = 50$ (bottom). B_t is given by (4.11) and the other parameters are given in Tables 4.1 and 2. Note that for $n = 8$ the germinal center contains the B clone with the highest level of somatic hypermutation B_8, while for $n = 50$ case the germinal center is dominated by middle clones and the B_{50} clone is absent.

Experimental data suggests that the key to developing therapies against chronic HIV infection lies in creating B-cells of the highest allowed level of somatic hypermutation [118]. Such later clones are instrumental for creating plasma and memory cells that produce highly mutated antibodies capable of clearing HIV infections. Our model is such that only the B-cells in the last clone become plasma cells that clear the virus, and since few B_{50} cells are being produced, the virus will not be eliminated. Therefore, we aim to understand what parameter changes will allow for the emergence of B-cell clones that underwent 50 rounds of affinity maturation, currently not observed in our predictions.

Not surprisingly, clone B_{50} can be achieved if the T follicular helper cells G are not a limiting value, in particular if we remove the competition term, *i.e.*, $\eta = 0$ per cell per day (see Figure 4.10, third row). Under this assumption, antigen V is eliminated 11.1 days following infection. In order to determine if additional interactions can lead to the same behavior, we keep $\eta = 10^{-5}$ per cell per day and adjust two different parameters. As such, if we increase 91-times the rate at which B-cell hypermutation is driven by interaction with Tfh cells, *i.e.* $\sigma = 0.001$ ml per cell per day, and we decrease 17.2-times the number of offspring produced during each clonal transition, *i.e.*, $\alpha = 1.6$ and keep the other parameters as in Tables 1 and 2, then the germinal center will contain the last clone B_{50} at all times. Moreover, B_{50} will become the dominant clone $t = 20$ days following infection (see Figure 4.10, bottom row). That means that decreasing the number of B-cells in each clone and speeding their transition rate into the next affinity class is sufficient in driving affinity maturation towards clones of the highest level of somatic hypermutation.

Under the adjusted values, $\alpha = 1.6$, the B-cell offspring production rate, and $\sigma = 10^{-3}$ ml per cell per day, the B-cell transition rate, the total germinal center B-cell population B_t peaks 13 days following infection and reaches a maximum of 1.39×10^4 cells, 12-times higher than in the acute case (see Figure 4.9, panel a). The Tfh population is 3.6-times smaller than in the acute and chronic cases for the first ten days, due to the decrease in offspring production. After day 10, the Tfh population decreases even further to 10^3 cells per ml (see Figure 4.9, panel b). However, this population is one order of magnitude higher than in the non-adjusted chronic case. This population is sufficient to provide help to all B-cell clones, such that the B_{50} clone can emerge, create plasma cells, and, most importantly, remove the antigen. For these adjusted parameters V is removed 9.5 days following infection.

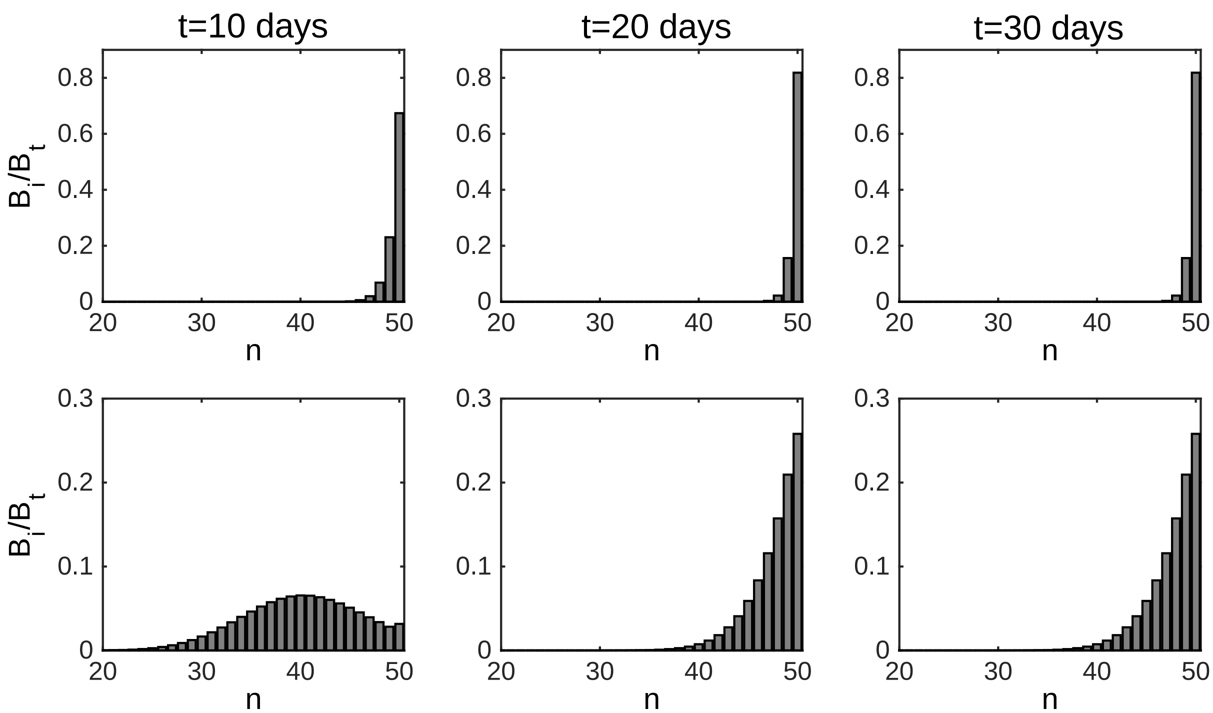

Figure 4.11: Clone distribution B_i/B_t for $0 \leq i \leq n$ at $t = 10$, $t = 20$, $t = 30$ days following infection for $n = 50$ and: (top) $\eta = 0$ and (bottom) $\alpha = 1.6$, $\sigma = 10^{-3}$ ml per cell per day, $\eta = 10^{-5}$ per cell per day. B_t is given by (4.11), and the other parameters are given in Tables 4.1 and 4.2. In both situations clone B_{50} dominates the germinal center B cell population 20 days following infection.

4.6 Alternative models

In the previous section we presented the models developed for our published paper [42]. These models were developed after trying many different modeling assumptions. The first alternative model we developed contained Naive CD4 T cells, N, pre-Tfh cells, H, Tfh cells, G, and B cells,

B_i,

$$
\begin{aligned}
\frac{dN}{dt} &= s_N - d_N N - \alpha_N V N, \\
\frac{dH}{dt} &= \alpha_N V N - d_h H - \gamma H \sum_{i=1}^{n} B_i, \\
\frac{dG}{dt} &= \beta \gamma H \sum_{i=1}^{n} B_i, - d_G G, \\
\frac{dB_0}{dt} &= -d_0 B_0 - \sigma B_0 G, \\
\frac{dB_i}{dt} &= 2\sigma\alpha B_{i-1} G - \sigma B_i G - d_i B_i, \\
\frac{dB_n}{dt} &= 2\sigma\alpha B_{n-1} G - d_n B_n.
\end{aligned}
\tag{4.12}
$$

This model had a germinal center population that lasted 50 plus days, very few Tfh cells, and early clones dominated the GC population. In this model the pre-Tfh cells transition to become Tfh cells based on the interaction with the germinal center, which is not seen biologically [171]. To adjust this we removed $\sum_{i=1}^{n} B_i$ in the transition from H to G and made the G production based only on B_0. We also assumed that each clone had a larger birth rate than the previously considered and instead of 2α for birth we used $2\alpha i$ because clones of higher somatic hypermutations are thought to proliferate faster [66]. Using these adjustments, we were able to successfully fit the model to data. During our model validation process, we found that the i's were not necessary and we also begin to include the formation of plasma, P, by adding the equation $\frac{dP}{dt} = kB_n$ to the system and $-kB_n$ to $\frac{dB_n}{dt}$. Germinal centers are develop to produce plasma and memory cells to fight specific pathogens (see section 1.3.1); the formation of plasma from the last clone is an indication of highly mutated germinal centers. While, this model fit the data well, it assumes that the Tfh cell population is not effected by all of the B cells, (i.e. no $G\sum_{i=1}^{n} B_i$ term) which we would expect to see biologically at the T:B border [171]. This lead us to make the Tfh population interact with all of the B cells in the germinal center, i.e. $\sum_{i=1}^{n} B_i$ was re-introduced to our model, however only within the G population and the system became:

$$
\begin{aligned}
\frac{dN}{dt} &= s_N - d_N N - \alpha_N V N, \\
\frac{dH}{dt} &= \alpha_N V N - d_H H - \gamma H B_0, \\
\frac{dG}{dt} &= \beta\gamma H B_0 - d_G G - \eta G \sum_{i=1}^{n} B_i, \\
\frac{dB_0}{dt} &= -\sigma B_0 G - d_0 B_0, \\
\frac{dB_i}{dt} &= 2\alpha\sigma B_{i-1} G - \sigma B_i G - d_i B_i, \\
\frac{dB_n}{dt} &= 2\alpha\sigma B_{n-1} G - \kappa B_n - d_i B_n, \\
\frac{dP}{dt} &= \kappa B_n.
\end{aligned}
\tag{4.13}
$$

For the next step we included an antigen population, $\frac{dV}{dt} = -\mu V P$, and dropped the 2 in the $2\alpha\sigma$ term. This became model (5.4) and the model we used for our publication [42].

We explored a source term in the B_0 equation and found this led to long lasting germinal centers. We also investigated the idea that selection was dependent on the total amount of B cells by replacing $\alpha\sigma$ with $\frac{\alpha\sigma}{K+B_t}$, which lead to the germinal center peaking within the first 5 days. We experimented with plasma formation, P, being dependent on every B cell clone but this had no effect on the model. This is a brief summary of the alternative models considered during the development phase of this work.

4.7 Modeling mutating antigen

Our model does not consider the effect of a mutating antigen, nor does it consider the need of both antigenic stimuli and Tfh cell help at each stage of B-cell somatic hypermutation. Previous studies predict that B-cell hypermutation is dependent on not only the ability of B-cells to recruit Tfh cell help, but also on the ability of the B-cells to retrieve and present antigen deposited on follicular dendritic cells [29, 95, 130, 167].

We extend model (5.4) to account for a mutating virus. In particular, we model a sequential mutation from virus V_0 to V_{n-1} at rate $0 < f < 1$. We only model the virus mutations that drive B-cell somatic hypermutations and all other mutations are ignored. Therefore, clone B_{i-1} is mutating into clone B_i due to stimuli from both Tfh cells and the respective virus variant V_{i-1} at rate $\sigma V_{i-1} G$, for $1 \leq i \leq n$. The T cell populations, N, H and G are modeled as before with the addition that total viral load, $V_t = \sum_{i=0}^{n-1} V_i$, can recruit pre-Tfh cells inside germinal centers to give rise to Tfh cells. As before, only the last clone, B_n, produces plasma cells, P. Under the assumption that broadly neutralizing antibody producing plasma cells are formed [167], P will remove all virus strains at rate μ. The modified model becomes

$$\frac{dV_0}{dt} = -fV_0 - \mu V_0 P, \tag{4.14a}$$

$$\frac{dV_i}{dt} = fV_{i-1} - fV_i - \mu V_i P, \tag{4.14b}$$

$$\frac{dV_{n-1}}{dt} = fV_{n-2} - \mu V_{n-1} P, \tag{4.14c}$$

$$\frac{dN}{dt} = s_N - d_N N - \alpha_N^{\phi} \sum_{i=0}^{n-1} V_i N, \tag{4.14d}$$

$$\frac{dH}{dt} = \alpha_N^{\phi} \sum_{i=0}^{n-1} V_i N - d_H H - \gamma H B_0, \tag{4.14e}$$

$$\frac{dG}{dt} = \gamma H B_0 - d_G G - \eta G \sum_{i=1}^{n} B_i, \tag{4.14f}$$

$$\frac{dB_0}{dt} = -d_0 B_0 - \sigma B_0 H V_0, \tag{4.14g}$$

$$\frac{dB_1}{dt} = \alpha\sigma B_0 H V_0 - \sigma V_1 B_1 G - dB_1, \tag{4.14h}$$

$$\frac{dB_j}{dt} = \alpha\sigma B_{j-1} G V_{j-1} - \sigma B_j V_j G - dB_j, \tag{4.14i}$$

$$\frac{dB_n}{dt} = \alpha\sigma B_{n-1} G V_{n-1} - dB_n - \kappa B_n, \tag{4.14j}$$

$$\frac{dP}{dt} = \kappa B_n, \tag{4.14k}$$

for $1 \leq i \leq n-2$ and $2 \leq j \leq n-1$. The initial conditions are $N(0) = s_N/d_N$, $B(0) = B_0$, $V(0) = V_0^{\phi}$

and all other populations are initially zero.

We numerically solve model (4.14), using parameters in Tables 4.1 and 4.2, $\alpha_N^{\phi} = 3.6 \times 10^{-6}$ ml per day per cell and $V_0^{\phi} = 10^3$ copies per ml (to account for an HIV-like antigen level). We vary mutation rate, f, to determine the effects of fast and slow mutating viruses on the GC's ability to produce broadly neutralizing antibodies and hence clear the virus. We compare the dynamics of B_t, V_t and G for $n = 8$ rounds of somatic hypermutation and varying mutation rates f. We see that fast viral mutation leads to the development of germinal centers containing large B_t populations. Indeed, for $f = 0.9$, germinal centers contain $B_t = 6.3 \times 10^4$ cells (see Figure 4.12, panel a, solid black lines). Moreover, fast mutation leads to fast production of clones with the highest degree of somatic hypermutation and consequently to plasma cell production (see Figure 4.12, panel a, solid grey line). As a result, virus is eliminated in the first two days after challenge (see Figure 4.12, panel c, solid line). For intermediate mutation rate, $f = 0.1$, the germinal center contains $B_t = 120$ cells (see Figure 4.12, panel a, dashed black line), plasma population is small and delayed (see Figure 4.12, panel a, grey dashed line), and, consequently, virus clearance is delayed (see Figure 4.12, panel c, dashed line). Lastly, for slow mutation, $f = 0.01$, the germinal center contains $B_t = 55$ cells (see Figure 4.12, panel a, dotted black line), plasma population is not produced at biological levels (cannot be seen in Figure 4.12, panel a) and, consequently, virus is not removed (see Figure 4.12, panel c, dotted line).

We look in detail at the slow mutation case. For $f = 0.01$, B_8, the clone with the highest affinity maturation level, is not produced. That is due to the fact that virus strain V_7, which is needed for B_8 activation, increases above the limit of detection (of 50 copies per ml) only at 230 days after infection (see Figure 4.13, panel a, black line). By that time, the germinal center has been terminated (see Figure 4.13, panel b). This is due to faster clearance of B-cells through natural death compared to B-cell production in the presence of antigenic stimulation, *i.e.* $d >> \alpha\sigma V_{i-1}G$. Therefore, higher order B-cell clones and, consequently, plasma cells are not produced and virus will persist. This result is independent of the competition between B-cell clones for T follicular helper cell stimulation and is maintained even when $\eta = 0$. To produce later B-cell clones, and

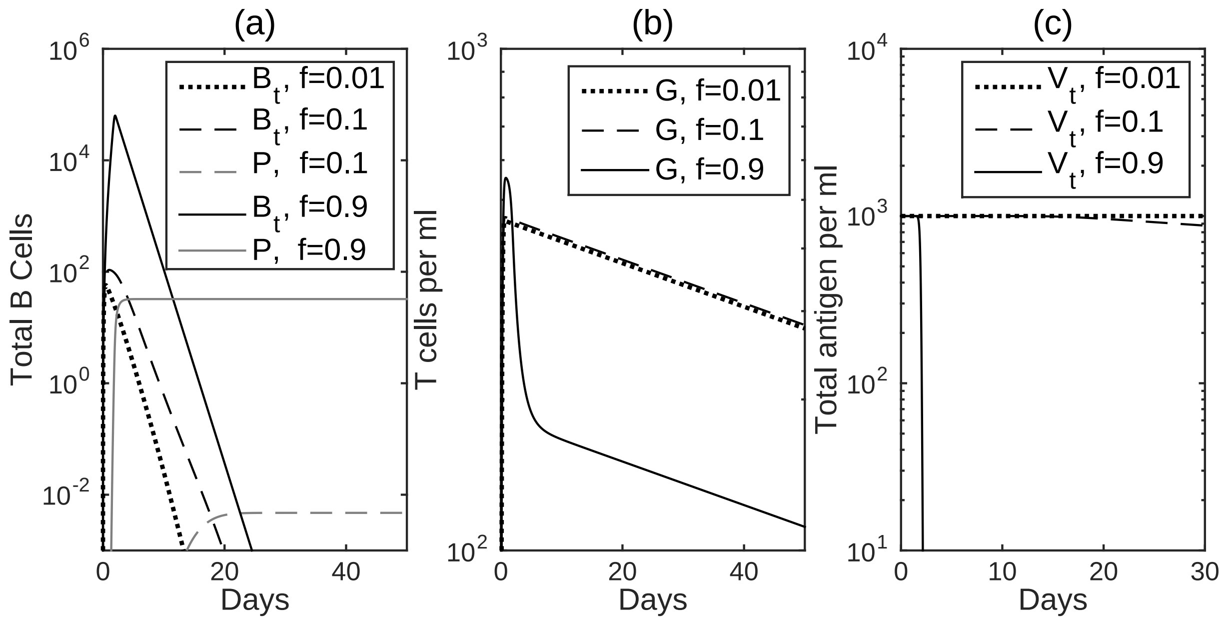

Figure 4.12: (a) B_t and P, (b) G per ml, and (c) $V_t = \sum_{i=0}^{n-1} V_i$ as given by (4.14) for $n = 8$ and $f = 0.9$ (solid lines); $f = 0.1$ (dashed lines); $f = 0.01$ dotted lines. The other parameters are given in Tables 4.1, 4.2, $\alpha_N^{\phi} = 3.6 \times 10^{-6}$ and $V_0^{\phi} = 10^3$. Note that P for $f = 0.01$ is negligible.

induce virus clearance, antigen-independent B-cell proliferation is needed. Such proliferation will compensate for B-cell loss. A possible form for the B_j population is:

$$\frac{dB_j}{dt} = \alpha\sigma B_{j-1} G V_{j-1} - \sigma B_j V_j G + rB_j - dB_j, \tag{4.15}$$

where $1 \leq j \leq n$ and r is the per capita B-cell growth rate. If the antigen-independent proliferation rate is high enough, *i.e.* $r = 0.75 < d$ or $r = 0.8 = d$ per day, model (4.14) with adjusted equations (4.15) predicts virus clearance for $n = 8$ and $f = 0.01$ (see Figure 4.14, panel c, dashed and dotted lines).

Lastly, when we consider that the number of somatic hypermutations needed to produce plasma cells is $n = 50$ (as in HIV patients that produce broadly neutralizing antibody [98, 151]), virus clearance requires both the antigen-independent B-cell proliferation given by (4.15) and lack of competition between B-cell clones for Tfh cell stimuli, *i.e.*, $\eta = 0$, for all $0.1 \leq f \leq 0.9$ (see Figure 4.14, panel c, dashed-dotted line).

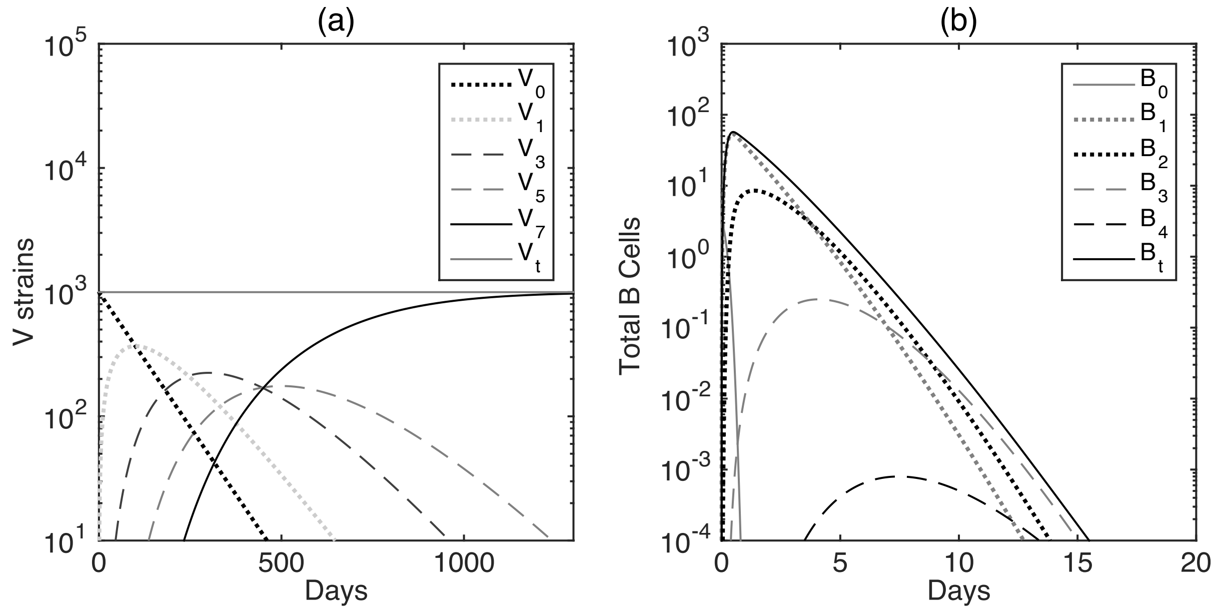

Figure 4.13: (a) V_i per ml, (b) B_i as given by (4.14) for $n = 8$ and $f = 0.01$. The other parameters are given in Tables 4.1, 4.2, $\alpha_N^{\phi} = 3.6 \times 10^{-6}$ and $V_0^{\phi} = 10^3$.

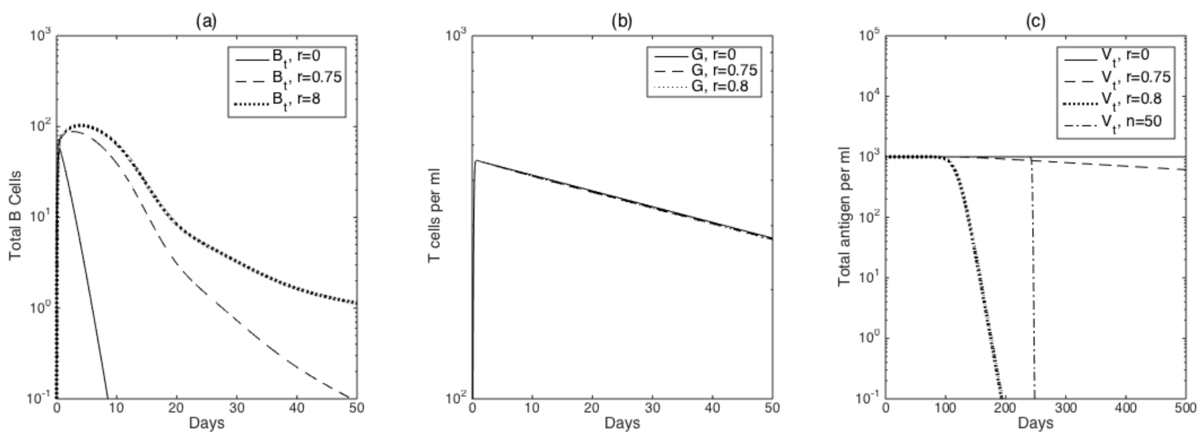

Figure 4.14: (a) B_t, (b) G per ml, and (c) $V_t = \sum_{i=0}^{n-1} V_i$ as given by (4.14) and (4.15) for $n = 8$, $f = 0.01$ and $r = 0$ (solid lines); $r = 0.75$ (dashed lines); and $r = 0.8$ (dotted lines). The other parameters are given in Tables 4.1, 4.2, $\alpha_N^{\phi} = 3.6 \times 10^{-6}$ and $V_0^{\phi} = 10^3$.

4.8 Discussion

We developed a mathematical model of germinal center formation that includes competition between B-cell clones for Tfh cell stimulation. When we model responses to an acute pathogen requiring eight rounds of somatic hypermutations, the model reproduces the dynamics observed during germinal center formation, such as the size of the B-cell population, the time of germinal center termination, and the ratio between pre-Tfh and Tfh populations following antigenic challenge. We fit the model to data, and found that there are enough Tfh cells to allow for B-cell clones of the highest level of somatic hypermutations to emerge.

We then extended our model to allow for as many as 50-rounds of somatic hypermutations which are needed to fight chronic infections such as HIV. By expanding the model to chronic infections we aimed to determine the possible mechanisms that regulate or limit germinal center dynamics during persistent disease. Our study predicts that, under the acute B_t and Tfh parameter values, B clones that undergo 50 rounds of somatic hypermutation cannot emerge, and the germinal center B-cell population is composed of cells that underwent a maximum of 35-rounds of somatic hypermutations. This is due to loss of specific Tfh cells due to interaction with an increasing number of B-cell clones. This effect can be reversed and B-cell protection can be achieved either through removal of competition between the B-cell clones or through emergence of smaller size clones that mutate at a faster pace.

When modeling a mutating antigen that drives the rate of B-cell somatic hypermutations, plasma cell production is dependent on the speed of viral mutation. For eight rounds of somatic hypermutations, fast and intermediate mutating plasma cells capable of removing the virus are always produced. A slow mutating virus, however, requires an additional antigen-independent B-cell expansion that maintains enough B-cells inside germinal centers to induce the next round of somatic hypermutation even when the antigenic stimulus is delayed. As in the non-mutating case Tfh are not limiting the emergence of all B-cell clones. For 50-rounds of somatic hypermutation, however, competition among the B-cell clones for Tfh cell stimuli prevents the emergence of plasma cell production regardless of the speed of virus mutation. In this case, both antigen-independent B-cell proliferation and the removal of competition for Tfh stimuli between the B-cell clones, as in the non-mutating case are needed for plasma cells to emerge.

Our models assume that the B-cell division rate is exponentially distributed (as in [6]), and disregarded the inherent cell cycle delay shown experimentally and considered in previous modeling studies [31, 79, 97]. One of the reasons for this assumption is the fact that the B_0 population represent primed pre-follicular B-cells, rather than naive B-cells. These cells take less than two days to transition into the B_1 class (given our parameters and model assumptions). This is consistent with the observation in [57], which states that the first B-cell division occurred at 48 h. If a delayed model is considered, where the $\alpha\sigma B_{i-1}G$ terms are replaced by $f(t)\alpha\sigma B_{i-1}G$ with

$$f(t) = \begin{cases} 0, & t < \tau, \\ 1, & t \geq \tau, \end{cases} \tag{4.16}$$

and $\tau = 2$ days as in [57], than the results of model (5.4) presented in Figures 1, 3 and 4 are preserved with limited change in the parameter values.

Our work assumes that B-cells must undergo a strict number of mutations before maturing into plasma cells. We found that modeling the breadth of the response, through creating plasma cells of different affinities at each stage of B-cell somatic hypermutations did not change our results. Further work is needed to determine the tradeoff between the need of high mutation numbers and the breadth of the immune response in fighting chronic infections.

In summary, we have developed models of Tfh-B cell interactions to examine the dynamics of germinal centers in both acute and chronic infections. We found that T follicular helper cells are a limiting factor in the emergence of extremely high rounds of B-cell somatic hypermutations for both non-mutating and mutating virus. Moreover, we found that this limitation can be removed by inducing faster transition between clones and limiting the sizes of individual clones. Lastly, for a mutating virus that drives the somatic hypermutations, additional factors such as antigen-independent B-cell proliferation may be needed for plasma cell production and virus neutralization. These results may provide insight into the germinal center role during chronic infections.

4.9 Future work

In our published model, we assume that a single germinal center is formed by as little as 2-3 B cells and evolves through affinity maturation and somatic hypermutation, in the presence of Tfh cells, into plasma capable of fighting pathogens [42]. Recently, its been shown through imaging that there may be multiple B cell progeny that in tandem go through rounds of somatic hypermutation and affinity maturations to develop into two different late stage clones. It was also shown that over time one progeny may take over the germinal center or both progenies may coexists. Understanding why homogenizing selection in individual germinal centers occur, or does not occur, will lead to a better understanding of germinal center development [159].

To address the developments in GC understanding we extend our model to create a germinal center with two B cell progenies. We develop a mathematical model of B - Tfh cell dynamics that considers the interaction between the Tfh cells G_1 and G_2, and two B cell progenies, B_{1i} and B_{2i}. Tfh cells, G_1 and G_2, are produced at rate $\gamma h(t)$, based on a previous interaction with antigen, pre-Tfh and B cells. G_1 and G_2 cells are lost through natural death at per capita rate d_G. Moreover, we assume that competition between B cell clones B_{ji} for Tfh cell-induced stimulation is limiting the G_1 and G_2 population growths at rate η. We assume G_1 is only affected by B_1 progeny whereas G_2 is affected by both the B_1 and B_2 progeny. This competition in return, will limit the number of B cells inside GCs and their transition between clones of higher affinity for the pathogen. B cells move inside germinal centers where they undergo affinity maturation initiated at rate $h(t)$ which represents previous interaction with antigen, pre-Tfh and B cells. We assume that each stage of affinity maturation requires Tfh cell help at rate σ_1 or σ_2 and that each population B_{ji} produces α offsprings B_{ji+1}, for $1 \leq i \leq n-1$ and $j = 1$ or 2. B_{ji}s die at the same per capita rate d as B blasts. Lastly, we assume, G_1 is involved in only the B_1 cell progeny selection, where as G_2 is involved in both the B_1 progeny and B_2 progeny.

The system describing these interactions is given by:

$$
\begin{aligned}
\frac{dG_1}{dt} &= \gamma h(t) - d_G G_1 - \eta G_1 \sum_{i=1}^{n} B_{1i}, \\
\frac{dB_{11}}{dt} &= \alpha\sigma_1 h(t) - \sigma_1 B_{11}(G_1+G_2) - dB_{11}, \\
\frac{dB_{1i}}{dt} &= \alpha\sigma_1 B_{1(i-1)}(G_1+G_2) - \sigma_1 B_{1i}(G_1+G_2) - dB_{1i}, \\
\frac{dB_{1n}}{dt} &= \alpha\sigma_1 B_{1(n-1)}(G_1+G_2) - dB_{1n} - \kappa B_{1n}, \\
\frac{dG_2}{dt} &= \gamma h(t) - d_G G_2 - \eta G_2 \sum_{i=1}^{n} B_{2i} + B_{1i}, \\
\frac{dB_{21}}{dt} &= \alpha\sigma_2 h(t) - \sigma_2 B_{21} G_2 - dB_{21}, \\
\frac{dB_{2i}}{dt} &= \alpha\sigma_2 B_{2(i-1)} G_2 - \sigma_2 B_{2i} G_2 - dB_{2i}, \\
\frac{dB_{2n}}{dt} &= \alpha\sigma_2 B_{2(n-1)} G_2 - dB_{2n} - \kappa B_{2n}, \\
\frac{dP}{dt} &= \kappa(B_{1n}+B_{2n})
\end{aligned}
\tag{4.17}
$$

for $1 \leq i \leq n-1$ with initial conditions

This model does not consider naive CD4 T cells or pre-Tfh cells. We use the parameters in Tables 4.1, 4.2 and investigate the model dynamics. We compare the total amount of B cells, the Tfh cells, plasma cells, and the clone mutations within each progeny. In Figure 4.15 we see coexistence of both progenies when $\sigma_1 = \sigma_2 = 10^{-4}$. In Figure 4.16 we see a dominate B_1 progeny where $\sigma_1 = 10^{-4}$ and $\sigma_2 = 10^{-5}$. In Figure 4.17 we see a dominate B_2 progeny where $\sigma_1 = 5 \times 10^{-6}$ and $\sigma_2 = 10^{-4}$. Particularly we look at the plasma formation for each of the three figures, the formation of plasma is an indication as to which progeny has undergone the highest rounds of somatic hypermutation and affinity maturation.

While we have shown these three cases numerically, for a future direction, we aim to better understand the trade off between each progeny analytically and investigate under what specific parameter conditions we develop a homogenous or diverse germinal center. This future direction project is in development with Dr. Stanca M. Ciupe and Dr. Lauren M. Childs.

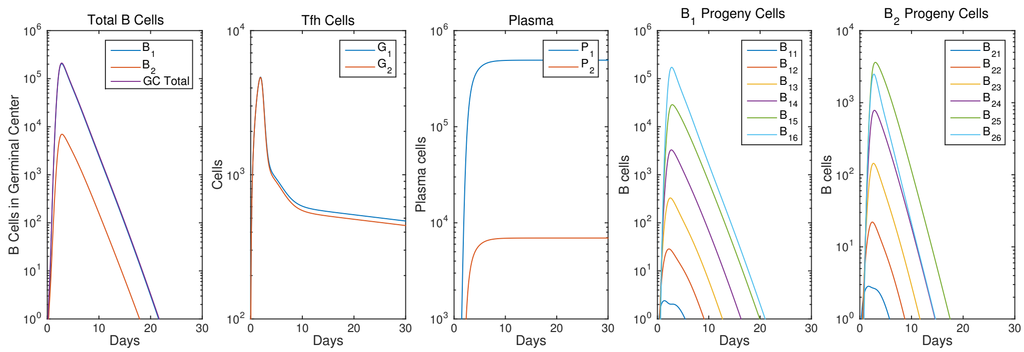

Figure 4.15: Germinal center dynamics during coexistence of two B cell progenies. B_t for each progeny; Tfh for each progeny; Plasma for each Progeny; clone development within progeny 1 and 2.

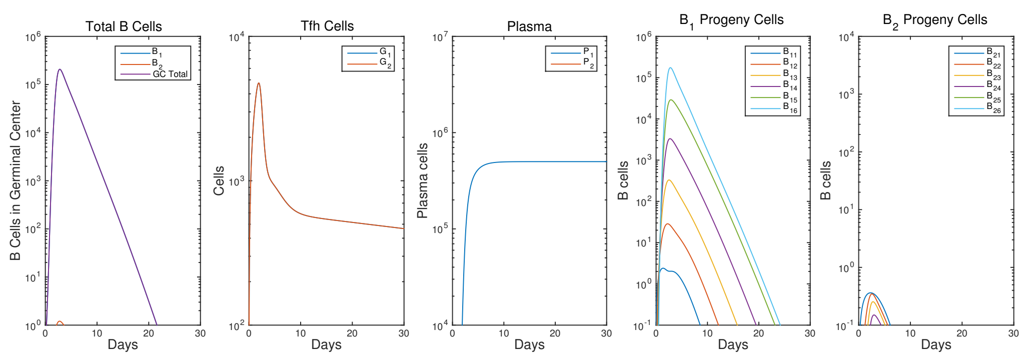

Figure 4.16: Germinal center dynamics for a dominating B_1 progeny. B_t for each progeny; Tfh for each progeny; plasma for each progeny; clone development within progeny 1 and 2.

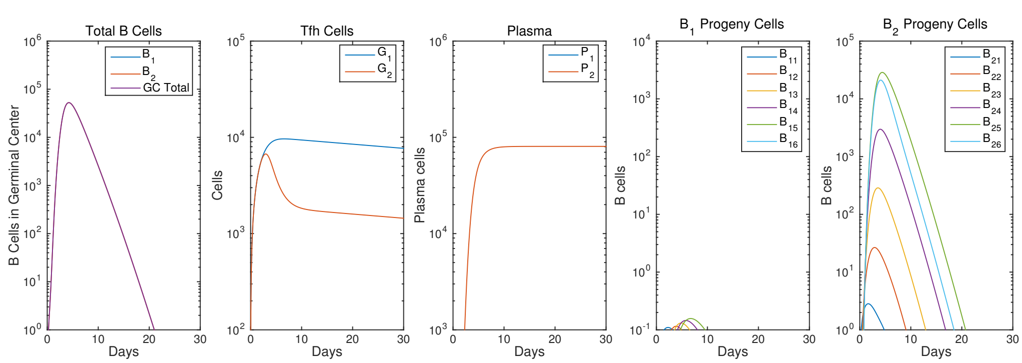

Figure 4.17: Germinal center dynamics for a dominating B_2 progeny. B_t for each progeny; Tfh for each progeny; plasma for each progeny; clone development within progeny 1 and 2.

Chapter 5

Modeling the HIV dynamics following 3BNC117 antibody infusion

This work was started during my summer at the Center for Nonlinear Studies at Los Alamos National Laboratory. It is in collaboration with Dr. Erwing Fabion Cardozo, Dr. Stanca M. Ciupe and Dr. Alan S. Perelson. The original idea stemmed from my time at Los Alamos with Fabion and Alan. Since then I have created the model, figures, and numerical simulations with supervision from Dr. Stanca M. Ciupe.

5.1 Abstract

Broadly neutralizing antibodies against HIV are able to act in many different ways in vivo: they can block viral entry, clear plasma virions, or lead to the death of virus-expressing cells. Recently, the 3BNC117 broadly neutralizing antibody has been tested in a phase I clinical trial as a potential alternative treatment of HIV. We test if 3BNC117 presents with one or a combination of these antiviral effects by developing both a pharmacokinetic model of 3BNC117 dynamics and a viral dynamics model. We fit the models to antibody and HIV RNA measurements from patients given

antibody therapy and conclude that 3BNC117 elicits both neutralizing and non-neutralizing effects. We predict that antibody binding is delayed and that the combined effects of initial CD4 T cell count, initial HIV levels, and virus production are strong indicators of a good response to 3BNC117 immunotherapy. We end by modeling the effect of antibody boosting on long-term viremia.

5.2 Introduction

The use of combination antiretroviral therapy (cART) as a treatment against human immunodeficiency virus (HIV) infection has lead to the suppression of viremia, as well as improvement and restoration of the immunological system of infected individuals [99]. This has, in turn, reduced incidence of mortality and morbidity among HIV infected individuals [82]. The presence of a latent reservoir, which cannot be purged by drugs, requires lifelong treatment without interruption [88]. The guidelines for therapy use are dependent on patients' virological response, tolerance, side effects, development of resistance due to genetic factors or non-compliance, and cost [78, 156]. The challenges in successful treatment administration include the strict dosing schedule, side effects, and drug resistance, encourages the exploration and development of new therapeutic alternatives.

Recently, broadly neutralizing antibodies (bnAbs) have been tested in phase 1 clinical trial as a potential alternative treatment of HIV. Such bnAbs have the advantage of an increased neutralizing potency against a large number of viral strains and clades, strong binding potential, and long half lives [60, 138]. Two bnAbs targeting the viral envelope, 3BNC117 and VRC01, suppressed viremia for the first month following single infusion. However, viral rebound from either resistant strains or preexistent strains that are refractory to treatment has been reported [19]. Understanding the pharmacokinetics of these bnAbs, their potential in suppressing viremia, the mechanisms behind virus rebound, and the role of boosting, are important steps that need to be addressed before they can be used as alternative therapies.

In this study, we investigate the antibody-virus dynamics after the 3BNC117 infusion in HIV infected individuals. This anti-HIV bnAb targets CD4 binding sites on the HIV virion envelope, blocking the infection of healthy CD4 T cells. However, HIV is highly mutating, and 3BNC117 does not neutralize all HIV strains. A recent human clinical trial investigated the effects of one infusion of 3BNC117 on the viral dynamics in HIV infected patients. It found that 3BNC117 was well tolerated, led to rapid decrease of viral loads, and induced sustained virological response for the first month [19]. Particularly, the 3BNC117 clinical trial consisted of a single antibody infusion in eight HIV infected individuals followed by measurements of their antibody and virus levels over the following 56 days. The virus decreased for the first 7 days in all patients but rebounded over the 7-28 days post infusion in all patients. Four patients' virus load returned to pre-infusion levels, three experienced virus rebound to up to 68% pre-infusion virus concentrations, and one's virus load remained below the limit of detection [19]. Surprisingly, the immunotherapy with 3BNC117 enhanced host-mediated humoral immunity to other HIV strains [140]. Moreover, it was suggested that administration in the early stages of HIV infection may elicit antibody responses similar to those of elite controllers [117]. This study was followed by a phase 2 clinical trial which investigated the efficacy of 3BNC117 in suppressing virus rebound after cART interruption, and addressed the role of antibody waning [137].

To gain new insight into the kinetics of virus decay and rebound following 3BNC117 infusion, we develop a mathematical model for the antibody-virus dynamics in HIV infected individuals and compare it with human temporal data of 3BNC117 and HIV RNA from eight patients from study [19] with the aim of assessing the potential of 3BNC117 as a therapeutic agent. Using the model and the patient data, we estimate the antibody kinetics and functions (neutralizing versus non-neutralizing [16, 117]) in each patient. We derive reasons behind the virus rebound, predict mechanisms associated to a good response to therapy, and address the effect of boosting.

5.3 Method

5.3.1 Patient data

The data consists of temporal measurements of 3BNC117 antibody concentration (in μg per ml) and HIV RNA concentrations (in copies per ml) in eight HIV-positive patients, seven of which were cART naive. It was collected at days $t = \{0,1,4,7,14,21,28,42,56\}$ following antibody infusion. The antibody levels were measured by a sandwich ELISA using an anti-3BNC117 specific antibody [19]. Patients 1-5 have antibody data for all nine times points, while patients 6-8 have incomplete antibody measurements. All patients have measurements at all nine data points for the HIV RNA concentrations. Lastly, the CD4 T cell concentrations (in cells per mm^3) were recorded at the time of antibody infusion.

5.3.2 Pharmacokinetic model of antibody dynamics

The first five patient's antibody data shows that, after one dose infusion, the 3BNC117 concentration decays in a bi-phasic manner. We utilize a two exponential bi-phasic decay model:

$$A(t) = D_1 e^{-k_1 t} + D_2 e^{-k_2 t}, \tag{5.1}$$

where the initial amount of the 3BNC117 antibody is $A(0) = D_1 + D_2$, and k_1 and k_2 represent the slopes of the first and second phase decays.

Model (5.1)'s parameters $\theta_A = \{k_1, k_2, D_1, D_2\}$ are estimated for each patient by fitting the antibody concentration $A(t)$ given by model (5.1) to individual 3BNC117 data from the clinical trial [19]. We use the `nlinfit` tool in MATLAB to minimize the objective function,

$$J_A = \sum_{i=1}^{n} [\log(D_{Ai}) - \log(A(t_i, \theta_A))]^2, \tag{5.2}$$

where n is the number of data points, D_{A_i} are the antibody concentrations at times t_i, $1 \leq i \leq n$ and $A(t)$ is the predicted antibody concentration as given by model (5.1). Moreover, if we let $M_A = 4$ be the number of estimated parameters, then the mean squared error is calculated by

$$MSE_A = \frac{J_A}{n - M_A}. \tag{5.3}$$

The best patient parameter estimates, their averages and the mean squared errors are listed in Table 5.1.

Patient	D_1 μg per ml	D_2 μg per ml	k_1 per day	k_2 per day	MSE$_A$
1	242.30	232.65	1.35	0.16	0.45
2	673.79	204.21	40.67	0.09	0.28
3	391.69	183.24	1.63	0.06	0.03
4	380.68	219.30	1.71	0.09	0.13
5	503.34	259.66	3.17	0.08	0.15
A	435.46	216.71	2.42	0.09	0.14
Average	437.27	219.91	8.49	0.1	

Table 5.1: Best fits of model (5.1) to the 3BNC117 data.

5.3.3 Virus dynamics model

To model the dynamics of HIV RNA following antibody infusion, we consider the interaction between uninfected CD4 T cells, T, infected CD4 T cells, I, HIV virus, V, antibody A and two types of immune complexes C_1 and C_2. Target CD4 T cells are produced at rate λ, die at per capita rate d, and become infected upon encountering HIV at rate β. Infected cells die at per capita rate δ and produce p virion per day. Virus is cleared at per capita rate c [121]. The formation of immune complexes between the infused 3BNC117 antibody, modeled by equation (5.1) and the virus is described by the following chemical interactions:

$$
\begin{aligned}
V + A \; &\underset{k_{off}}{\overset{k_{on1}}{\rightleftharpoons}} \; C_1, \\
C_1 + A \; &\underset{k_{off}}{\overset{k_{on2}}{\rightleftharpoons}} \; C_2,
\end{aligned}
$$

where C_i are immune complexes with bound antibodies. We assume that the binding rates are different, with $k_{on1} << k_{on2}$ accounting for a delay (immaturity) in the first immune complex formation. The unbinding rates are the same, k_{off}. The antibody has both neutralization effects, which reduce infectivity rate from β to $\beta/(1+\alpha A(t))$; and non-neutralization effects which remove complexes C_2 at rate $\gamma > c$. We model the immune complexes removal as a temporal density dependent function $\gamma = \frac{c_X t}{t+t_X}$, with c_X accounting for asymptotic complex removal and t_X for the time where the removal is half-maximal. The system describing these interactions is given by:

$$
\begin{aligned}
\frac{dT}{dt} &= \lambda - dT - \frac{\beta}{1+\alpha A(t)} TV, \\
\frac{dI}{dt} &= \frac{\beta}{1+\alpha A(t)} TV - \delta I, \\
\frac{dV}{dt} &= pI - cV - k_{on1} VA(t) + k_{off} C_1, \\
\frac{dC_1}{dt} &= k_{on1} VA(t) - k_{off} C_1 - k_{on2} C_1 A(t) + k_{off} C_2, \\
\frac{dC_2}{dt} &= k_{on2} C_1 A(t) - k_{off} C_2 - \gamma C_2,
\end{aligned}
\tag{5.4}
$$

with initial conditions $T(0) = T_0$, $I(0) = I_0$, $V(0) = V_0$ and $C_1(0) = C_2(0) = 0$.

The clinical trial data showed that, following a single antibody infusion, the virus decreased for the first 7 days in all patients, and rebounded over the 7-28 days post infusion in all patients. Four patients' viral load returned to pre-infusion virus levels, three experienced virus rebound to up to 68% pre-infusion concentrations, and one remained below the limit of detection [19]. We will use model (5.4) to address the mechanisms of decay and rebound, in particular the role the neutralizing and non-neutralizing antibody functions.

Parameters

We use data from the 3BNC117 clinical trial and previously published studies to parametrize model (5.4). We assume that 1% of the CD4 T cell population is susceptible to HIV [149], uninfected CD4 T cells die at rate 0.01 per day [100], productively infected cells die at rate 1 per day [113], and HIV virus in the plasma is cleared at rate 23 per day [131]. The binding and unbinding rates to HIV envelope of broadly neutralizing IgG antibodies are 3.04×10^4 per mol per sec and 1.99×10^{-4} per sec, respectively [138]. We convert these in ml per μg per day and per day, as follows:

$$k_{on2} = \frac{3.04 \times 10^4}{Ms} = \frac{3.04 \times 10^4 L}{mol\ s} \cdot \frac{1000ml}{L} \cdot \frac{86400s}{day} \cdot \frac{mol}{150000g} \cdot \frac{g}{10^6 \mu g} = 17.51 \frac{ml}{\mu g \times day},$$

and

$$k_{off} = \frac{1.99 \times 10^{-4}}{s} = \frac{1.99 \times 10^{-4}}{s} \cdot \frac{86400s}{day} = 17.19 \frac{1}{day}.$$

These calculations are based on the assumption that the molecular weight of IgG is approximately 150kDa where $1kDa = \frac{10^3 g}{mol}$. We assume that the initial antibody binding rate k_{on1} is unknown, and estimate it through fitting. However, once a first complex C_1 is formed, antibodies bind to C_1 to form a second stage complex C_2 at the reported bnAb binding rate of 17.51 ml per μg per day. Antibodies disassociate from complexes C_1 and C_2 at rate 17.19 per day, and the immune complexes C_2 are cleared through phagocytosis. We assume that, in the long-run, the immune complexes are removed four times faster than free virus as reported experimentally [62], *i.e*, $c_X = 4c = 92$ per day. The immune complexes removal is half-maximal when patients reached their minimum viral measurement, *i.e*, on average $t_X = 14$ days.

Individual patient's concentrations of uninfected CD4 T cells and HIV virus at the time of antibody infusion were reported in the clinical trial [19]. We assume that the reported virus values are the values of V_0 and 1% of the reported CD4 T cell values are the values of T_0. Moreover, we derive parameters β, λ, and I_0, by assuming that both the virus load and the uninfected cell concentration reached equilibria values at the start of treatment. That is, $\beta = \frac{\delta c}{T_0 p}$, $\lambda = (d + \beta V_0)T_0$, and $I_0 = \frac{cV_0}{p}$. These fixed parameters are summarized in Table 5.2.

Name	Description	Value	Units	Citation
δ	Productively infected cell decay rate	1	per day	[113]
c	Clearance rate of virus in plasma	23	per day	[131]
d	Death rate of target cells	0.01	per day	[100]
k_{on2}	3BNC117 binding rate	17.51	ml per μg per day	[138]
k_{off}	3BNC117 unbinding rate	17.19	per day	[138]
γ	Complex clearance rate	$\dfrac{4ct}{t+14}$	per day	
β_a	Density dependent infection rate for sensitive virus	$\delta c/T(0)p$	ml per copies per day	calculated
λ	Target cell production rate	$(d+\beta_a V(0))T(0)$	cells per ml per day	calculated

Table 5.2: Fixed parameters used in (5.4).

Data Fitting

The remaining parameters $\theta_v = \{p, \alpha, k_{on1}\}$, corresponding to virus production rate, p; 3BNC117 neutralization effect, α; and probability of a first antibody binding a virion, k_{on1}; are estimated for each patient by fitting the total virus load $V_T(t) = V(t) + C_1(t) + C_2(t)$ given by model (5.4) to post 3BNC117 infusion HIV RNA patient data from [19]. We use the `nlinfit` tool in MATLAB to minimize the objective function,

$$J_V = \sum_{i=1}^{n} [\log(D_{Vi}) - \log(V_T(t_i, \theta_v))]^2, \tag{5.5}$$

where n are the number of data points, D_{Vi} are the virus data at times t_i for $1 \leq i \leq n$, and $V_T = V + C_1 + C_2$ is the total virus concentration as given by model (5.4). Moreover, if we let $M_V = 3$

be the number of estimated parameters, then the mean squared error is calculated by

$$MSE_V = \frac{J_V}{n - M_V}. \tag{5.6}$$

Table 5.3 presents the estimated parameters and the mean squared error for each patient.

Patient	p virions/day	α ml/μg	k_{on1} ml per μg per day	MSE$_V$
1	1072.41	6.4×10^{-3}	1.3×10^{-2}	0.575
2	122833.03	0	3.1×10^{-2}	0.347
3	608.71	1.8×10^{-3}	1.2×10^{-3}	0.080
4	548.18	6.2×10^{-3}	3.1×10^{-2}	0.576
5	1902.85	1.8×10^{-3}	8.2×10^{-5}	0.167
6	1495.85	0	9.9×10^{-2}	0.299
7	7512.18	0	6.3×10^{-2}	0.409
8	4610.16	7.9×10^{-4}	3.7×10^{-2}	0.721
Average	17572.92	2.1×10^{-3}	3.6×10^{-2}	

Table 5.3: Best fits of model (5.4) to the HIV data.

5.4 Numerical results

5.4.1 Antibody dynamics

We found a good agreement between model (5.1) (with the values from Table 5.1) and the antibody data, for the first five patients (see Figure 5.1, first five panels). Since no antibody data is reported for the last three patients, we generated a data set consisting of average values among the first five patients at each time point, patient A. We then fit model (5.1) to this new, patient A, data and use the results as a proxi for the antibody dynamics in patients 6-8 (see Figure 5.1, panel 6).

For the estimated parameters, we compute the half lives of the first and second phase decays to be on average $\frac{ln(2)}{k_1} = 0.1$ days and $\frac{ln(2)}{k_2} = 7.2$ days, respectively. The average D_1 is 437.3 μg per ml and the average D_2 is 219.9 μg per ml. The antibody decays below the ELISA assay's level of detection of 2 μg per ml, on average, 54 days post infusion. Patient 1, who has the lowest D_1, also has the quickest antibody loss. The time to antibody loss is directly correlated with k_2, i.e. the patient with the lowest k_2 clears the antibody first, and the patient with highest k_2 keeps the antibody longest (with a maximum of 81 days).

To determine the relationship between the antibody dynamics and HIV kinetics, we incorporate the individual antibody curves into model (5.4).

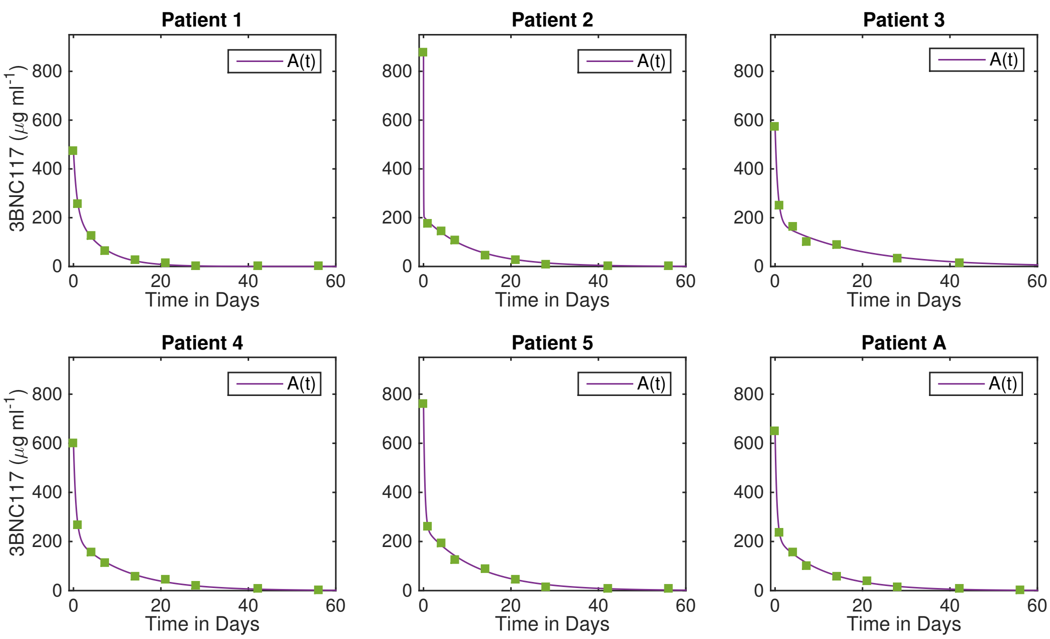

Figure 5.1: Antibody as given by model (5.1) against 3BNC117 data (o). The parameters are given in Table 5.1. Patient A is the average data set across the 5 patients at each time point.

5.4.2 Virus dynamics

Using the parameters in Tables 5.2 and 5.3 we plot the total HIV concentrations $V_T(t) = V(t) + C_1(t) + C_2(t)$ given by model (5.4) against the HIV data in [19] (see Figure 5.2). The model describes the virus data in [19] well. However, unlike [19], we report virus rebound to individual's initial viral levels in five patients (1, 4, 5, 6 and 7) and virus that stays below the initial value in three patients (2, 3, and 8). By contrast, [19] reported viral rebound in four patients (4, 5, 6, 7) and a sustained viral control in four patients (1, 2, 3, and 8).

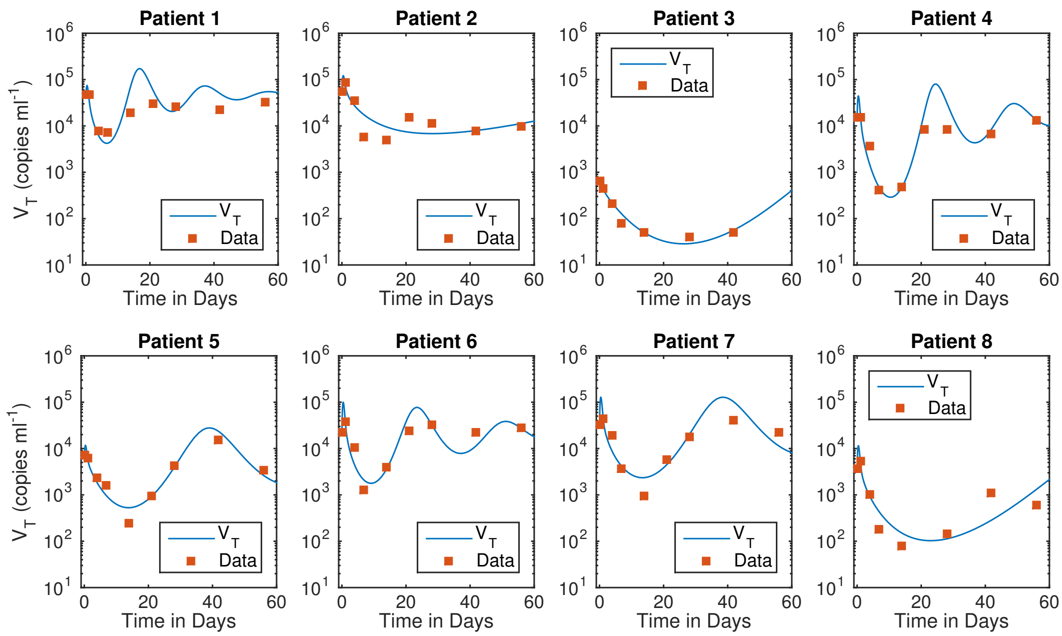

Figure 5.2: Virus given by (5.4) against HIV RNA date. Parameters are given in Tables 5.2 and 5.3.

We predict that the viral production rate, p, is on average 1.8×10^4 virions per cell per day, with patient 4 having the lowest production rate of 548.2 virions per cell per day and patient 2 having the highest production rate of 1.2×10^5 virions per cell per day.

The average binding rate, k_{on1}, is 0.035 ml per μg per day, which is much lower than the bnAbs binding rate, $k_{on2} = 17.5$ ml per μg per day. This suggests that there is an initial delay in antibody binding. Patient 3 has the lowest binding rate of 0.001 ml per μg per day and patient 6 has the highest binding rate of 0.1 ml per μg per day.

Finally, the average neutralizing effect α is 2.1×10^{-3} ml per μg, with the highest value of 6.4×10^{-3} ml per μg in patient 1, and no neutralizing effects in patients 2, 6, and 7. To determine the relative contributions of α and $A(t)$ in each patient, we plotted the temporal changes in infectivity in the presence of antibody, $\beta_a = \beta/(1+\alpha A(t))$ (see figure 5.3). We found an average maximum β_a value of 2.5×10^{-6} ml per virion per day, with ranges of 1.7×10^{-8} ml per virion per day in patient 2 and 4.9×10^{-6} ml per virion per day patient 3.

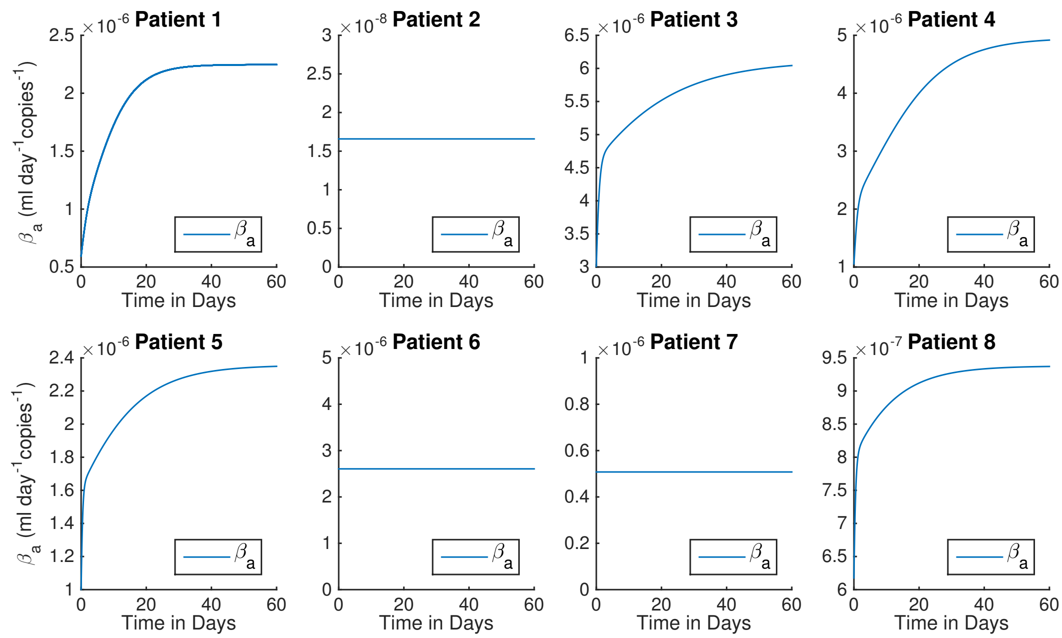

Figure 5.3: Infectivity rate in the presence of neutralizing antibody, $\beta_a = \frac{\beta}{1+\alpha A(t)}$. Parameters are given in Tables 5.2 and 5.3.

Model (5.4) predicts that $V_T(t)$ increases for the first 9.6 hours to an average 6.1×10^4 virions/ml among the patients (see Figure 5.4). This initial increase is due to the delay in initial antibody binding given by low k_{on1} values. Indeed, patients 3 and 5, which have the smallest increase (of 7 and 5.1×10^3 virions per ml), have the lowest k_{on1} values (1.2×10^{-3} ml per μg per day) and 8.2×10^{-5} ml per μg per day).

The long term dynamics of V_T show that it takes, on average, 3.1 years for patients to return to their post infusion virus set point. Patient 1 returns to set point 0.8 years post infusion, while patient 2 returns to set point 9.7 years post infusion.

We investigated the composition of the total virus $V_T(t) = V(t) + C_1(t) + C_2(t)$ over time (see Figure 5.5). In the first day after antibody infusion, on average 55.7% of total virus is bound, with patient 6 (and 3) having the highest (lowest) percentage of immune complexes $C_1(t) + C_2(t)$. By days 30 and 60, however, the immune complexes and the antibody are removed and the total virus is composed of 97.6% and 99% free virus $V(t)$, with patient 3 (and 6) having the highest (lowest)

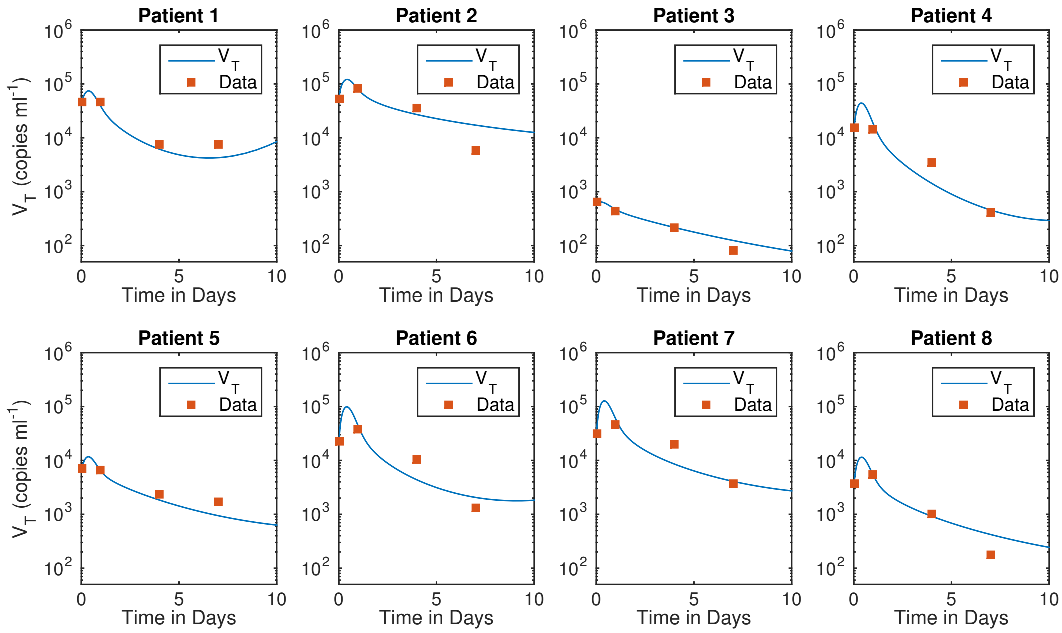

Figure 5.4: Virus given by (5.4) and HIV RNA data for the first 10 days. The parameters are given in Table 5.2 and 5.3.

amount of free virus. The intermediate immune complex, $C_1(t)$, is small at all times, and accounts for less that 0.7% of the total virus load for all patients. The total amount of immune complexes $C_1(t)+C_2(t)$ is positively correlated with the binding rate k_{on1} (with p-values of $p = 6.2\times10^{-3}$ at day 30 and $p = 8.9\times10^{-4}$ at day 60), with the patient with the lowest k_{on1} having the lowest amount of $C_1(t)+C_2(t)$.

We investigated the inter-patients correlation between the fitted parameters, the initial CD4 T cells and the initial virus. We found that the ratio between the product of initial CD4 T cell count and virus production rate and the initial virus load, $\frac{pT_0}{V_0}$, is linearly correlated (p-value of $p = 3.8\times10^{-6}$) with the overall post-infusion time needed for the virus to rebound to the original set point (see Figure 5.6). We found no statistically significant correlations between parameters p, α and k_{on1}; initial conditions V_0, T_0 and A_0; maximum, minimum and percentage changes in β_a; and the time of V_T rebound to set point (see Table 5.4).

To determine whether both the neutralizing and non-neutralizing antibody effects are needed in model (5.4), we compare the full model, with those where only neutralization is considered, *i.e.*,

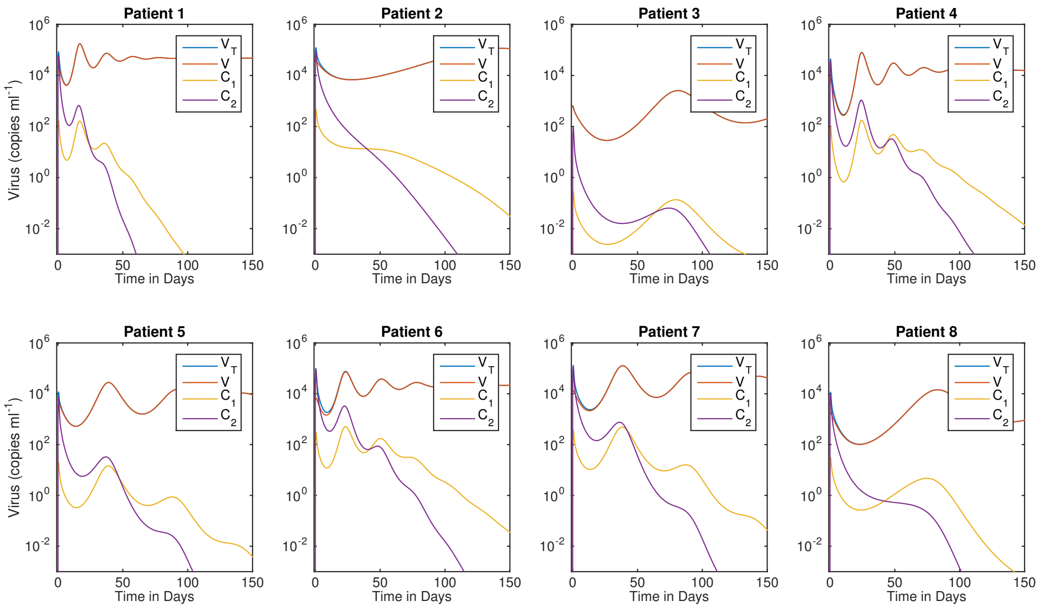

Figure 5.5: Plot of V_T (blue line), V (red line), C_1 (yellow line) and C_2 (purple line) over time. The parameters are given in Table 5.2 and 5.3.

	p	α	k_{on}	V_0	T_0	A_0	min β	max β	β change	V_T rebound to set point
p	1	0.40	0.93	0.10	0.06	0.03	0.24	0.20	0.37	0.001
α	0.40	1	0.25	0.84	0.35	0.09	0.81	0.23	3×10^{-5}	0.21
k_{on}	0.93	0.25	1	0.71	0.62	0.82	0.74	0.41	0.24	0.70
V_0	0.10	0.84	0.71	1	0.01	0.71	0.15	0.15	0.90	0.41
T_0	0.06	0.35	0.62	0.01	1	0.77	0.24	0.68	0.48	0.23
A_0	0.03	0.09	0.82	0.71	0.77	1	0.40	0.19	0.16	0.04
min β	0.24	0.81	0.74	0.15	0.24	0.40	1	0.04	0.86	0.49
max β	0.20	0.23	0.41	0.15	0.68	0.19	0.04	1	0.16	0.38
β change	0.37	3×10^{-5}	0.24	0.90	0.48	0.16	0.86	0.16	1	0.20
V_T rebound to set point	0.001	0.21	0.70	0.41	0.23	0.04	0.49	0.35	0.20	1

Table 5.4: P values for parameter correlations

$k_{on1} = k_{on2} = k_{off} = 0$; and with those where only non-neutralizing effects are considered, *i.e.*, $\alpha = 0$ (see Figure 5.7). We plot model (5.4) (see Figure 5.7, solid blue lines), compared to (5.4) where $\alpha = 0$ (see Figure 5.7, purple dotted line) and (5.4) where $k_{on1} = 0$ (see Figure 5.7, red dashed line). Figure 5.7 shows that without k_{on1} we are unable to capture the increase in the first data points (red dashed line). Similarly, if we do not model neutralization, i.e. $\alpha = 0$ we cannot

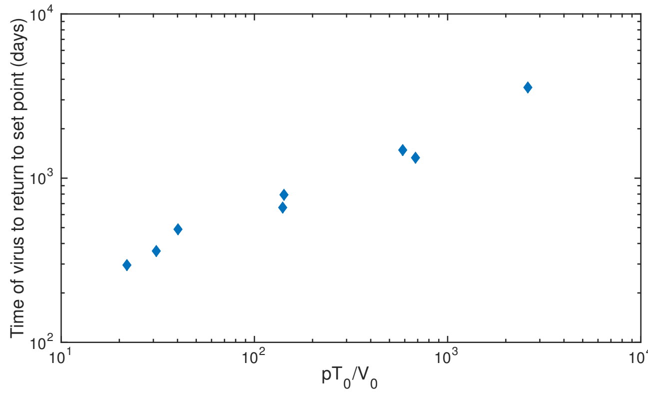

Figure 5.6: Plot of the time to virus return to set point in (5.4) vs. pT_0/V_0 for each patient. The parameters are given in Table 5.2 and 5.3.

capture the magnitude of the HIV drop in patients 1, 3, 4, 5, 8, and 9 (see Figure 5.7 purple dotted line).

We also fit for all 8 patients a neutralization only model ($k_{on1} = k_{on2} = k_{off} = 0$), and a non-neutralization only model ($\alpha = 0$). These parameter fits are listed in Table 5.5 and 5.6, respectively. To compare the three models we used Akaike's information criterion (AIC),

$$AIC_i = n\ln(MSE_V) + 2k, \tag{5.7}$$

n is the number of data points, k is the number of parameters we fit, and MSE_V is the mean squared error. We calculate the AIC_i for each patient for model (5.4), a non-neutralizing only model (i.e fixed $\alpha = 0$) and a neutralizing only model (i.e. fixed $k_{on1} = k_{on2} = k_{off} = 0$) with the parameters of best fit for each case. We then normalize the AIC_i to the lowest value and average the AIC across the patient cohort for each of the three cases. For model (5.4) $AIC_{ave} = 14.93$, for fixed $\alpha = 0$ $AIC_{ave} = 16.64$, and for fixed $k_{on1} = k_{on2} = k_{off} = 0$ $AIC_{ave} = 16.09$. We find that the full model (5.4) gives the best fit to the data.

Patient	p virions/day	k_{on1}	MSE_V
1	5656.21	4.8×10^{-2}	0.613
2	4465.56	8.6×10^{-2}	1.332
3	670.47	4.1×10^{-2}	0.217
4	10719.61	3.3×10^{-2}	1.744
5	1912.30	5.0×10^{-2}	0.216
6	1490.27	1.1×10^{-1}	0.290
7	7454.22	6.8×10^{-2}	0.395
8	6307.31	5.2×10^{-2}	0.724
Average	4834.49	6.1×10^{-2}	

Table 5.5: Parameters for (5.4) fit to patient data when $\alpha = 0$.

Patient	p virions per day	α ml per μg per day)	MSE_V
1	1030.51	7.8×10^{-2}	0.529
2	1018.21	4.9×10^{-2}	2.870
3	604.20	1.9×10^{-2}	0.065
4	521.82	8.9×10^{-2}	0.555
5	1870.08	2.2×10^{-2}	0.160
6	1501.10	4.6×10^{-1}	0.482
7	8040.84	2.8×10^{-2}	0.497
8	525.92	7.5×10^{-2}	1.518
Average	1889.08	5.1×10^{-2}	

Table 5.6: Parameters for (5.4) fit to patient data when $k_{on1} = k_{on2} = k_{off} = 0$.

5.4.3 Boosting

In all patients the antibody decays below the limit of detection by day 81 and, consequently, the virus rebounds. To determine how the virus long-term dynamics change when the antibody is still present, we are considering the effects of antibody boosting. We consider weekly antibody infusion of 30 mg per kg for up to 5 weeks. We model $A(t)$ using model (5.1) and parameters in

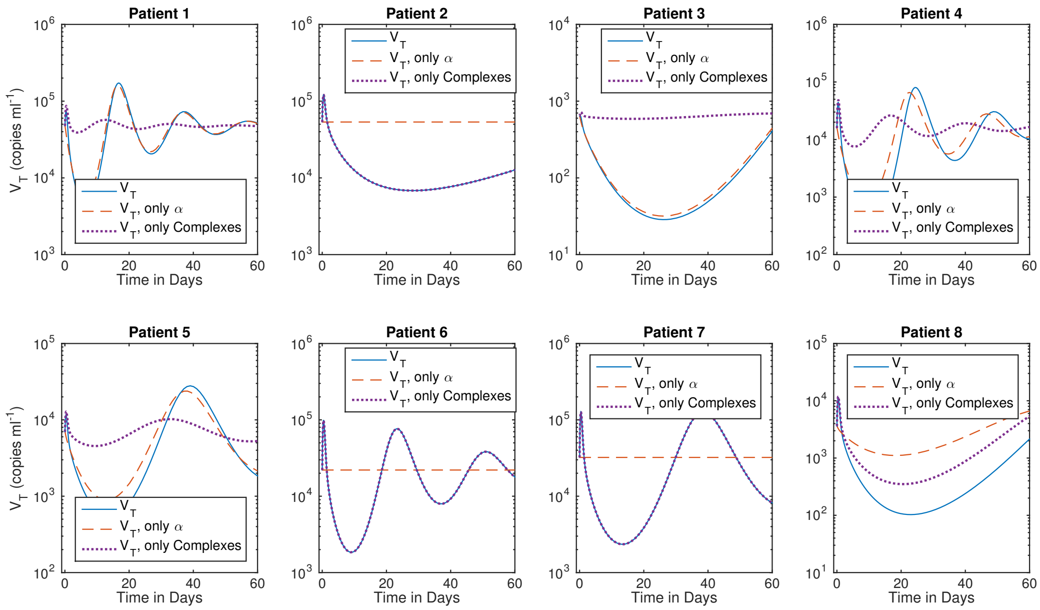

Figure 5.7: Plot of V_T for (5.4) (solid blue line), (5.4) when $\alpha = 0$ (dotted purple line), (5.4) when $k_{on1} = k_{on2} = k_{off} = 0$ (dotted purple line). The remaining parameters are given in Table 5.2 and 5.3.

Table 5.1 and repeated rounds of infusion by

$$A_i(t) = D_1 e^{-k_1(t-\tau\times i)} + D_2 e^{-k_2(t-\tau\times i)}, \quad \text{when} \quad \tau \times i < t, \tag{5.8}$$

$$A_T = \sum_{i=0}^{n} A_i(t) \tag{5.9}$$

where τ is the time between infusion and n is the rounds of infusion. We model $V(t)$ using model (5.4) and the parameters in Tables 5.2 and 5.3.

After 5 rounds of boosting, patient 1 achieves a minimum total virus load $V_T(t)$ of 529 virions per ml at day 17.2 (see Figure 5.8 left panel, light blue line). By contrast, patient 8's virus load V_T goes below one virion (*i.e.* 3×10^{-4} virions per ml), at day 40 (see Figure 5.8, right panel, light blue line). These two patients represent the best and the worst case scenarios. As noted previously, patient 1 had the shortest effect from the 3BNC117 therapy and the lowest amount of antibody. This is correlated to patient 1 responding the worst to repeated boosting.

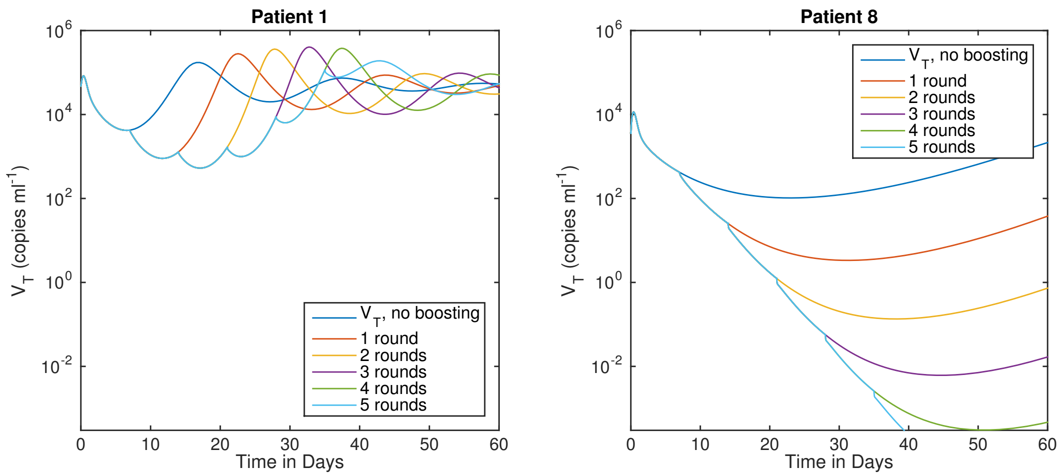

Figure 5.8: V_T after 5 rounds of weekly 3BNC117 antibody boosting in Patient 1 (left panel) and Patient 8 (right panel).

To address whether we can achieve virus clearance on a different boosting regime in patient 1, we investigate other boosting frequencies and found that boosting every 2 days leads to virus decay below one virion by day 26 (see Figure 5.9, left panel, light blue line). Similarly, boosting every two days for 5 rounds leads to virus clearance in patient 8 (see Figure 5.9, right panel).

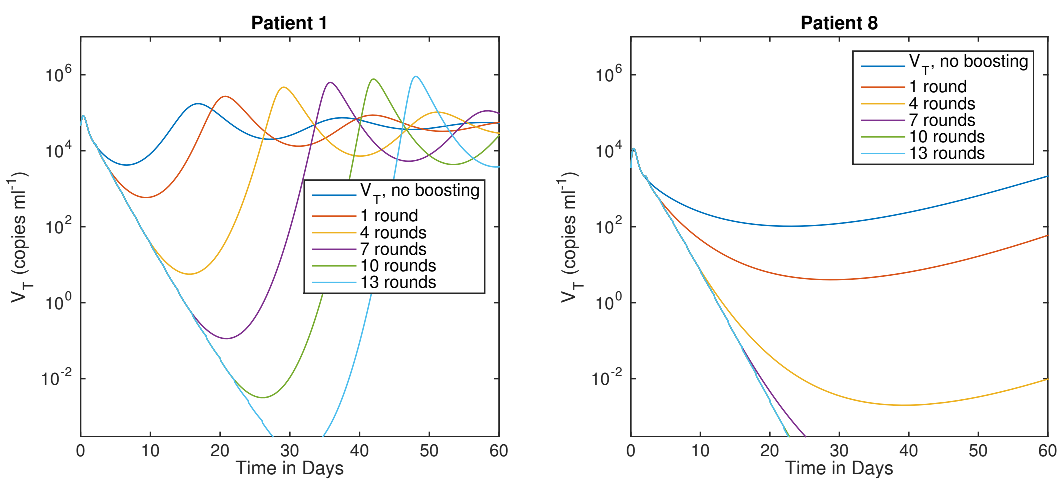

Figure 5.9: V_T after 13 rounds of every 2 days of 3BNC117 antibody boosting in Patient 1 (left panel) and Patient 8 (right panel).

5.5 Alternative Models

Throughout the model development process, we have always used (5.1) to model the bi-phasic decay of monoclonal antibodies. The original viral dynamic model was developed during my time at Los Alamos National Lab with a confidential data set. Our original data had more patients and more frequent data points. The initial idea was to develop a two strain model that had a viral strain that was sensitive to monoclonal antibody therapy and resistant to monoclonal antibody. While this model fit the data and may add biological insight to the development of resistance; it had limitations due to the large numbers of parameters to fit. We returned to the basic HIV model and assumed 3BNC117 has two effects on HIV dynamics: i) reduced virus infectivity through initial antibody binding and neutralization, $\beta_a(t)$ and ii) antibody mediated viral clearance $g(t)$. These dynamics are described by the system:

$$\begin{aligned}\frac{dT}{dt} &= \lambda - dT - \beta_a TV,\\ \frac{dI}{dt} &= \beta_a TV - \delta I, \\ \frac{dV}{dt} &= pI - cV - g(t)V.\end{aligned} \tag{5.10}$$

$$\beta_a = \frac{\beta}{1+\alpha A(t)} \tag{5.11}$$

$$g(t) = \begin{cases} 0 & \text{if } t < \tau_2, \\ \dfrac{\gamma A(t)}{A(t)+\kappa} & \text{if } t > \tau_2, \end{cases} \tag{5.12}$$

where α is the rate the antibodies reduce β, the HIV infectivity rate due to neutralizing effects and γ is the antibody mediated clearance due to non-neutralizing effects. We assumed that the antibody therapy doesn't take effect until τ_1. We fit p, the virus production rate, γ, the rate antibodies induce viral clearance, and τ_2 the delay in antibody effect. While again this model fit the data well (see figure 5.10) the time delay τ_2 creates a sharp point in the viral load, that is not seen *in vivo*. After further thought, we decided the time delays manufactured delays in the model that were

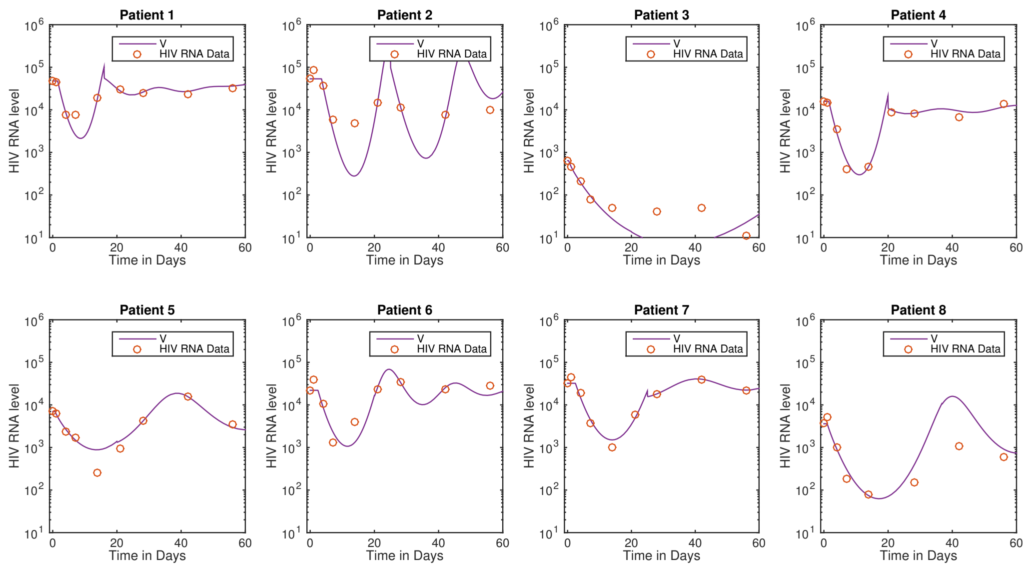

Figure 5.10: V(t) as given by (5.10) versus HIV data (o).

not known to happen *in vivo*. Next, we created a model similar to (5.4), but with only one viral complex. However, this limited our ability to capture the initial data points in the viral load, and we hypothesize that there was a delay in formation of viral complexes, and developed model (5.4).

5.6 Discussion

In this study, we developed a novel mathematical model of HIV dynamics in the presence of infused monoclonal antibody therapy. We assume that the antibody has two distinct effects: (i) virus neutralization and (ii) increased removal of virus-antibody immune complexes. Using the models and published data from a recent phase I clinical trial with broadly neutralizing antibody 3BNC117 [19], we fit unknown parameters in order to determine the host-antibody characteristics that can explain the observed patient dynamics.

While it was suggested that 3BNC117 only elicits neutralization effects [138], we found that neutralization alone is not enough to explain patient dynamics observed in the experimental data. Instead, increased clearance of antibody-virus immune complexes is needed in order to explain the early dynamics in HIV in all patients. Moreover, we found that antibody binding is delayed and it leads to an increase in the virus load.

Our model predicts that patients 2, 3, 8 are the best responders to the therapy and maintain reduced HIV viral levels for the longest period of time; this is different than the clinical trial conclusions [19], which found patients 1, 2, 3, and 8 maintained reduced viremia, albeit patient 1 was the worst of the 4 "good responders". We found that the combined effects of virus production, initial CD4 T cell count and initial virus load, as given by the ratio pT_0/V_0, correlates with the increased duration of virus control during antibody treatment. It would be of interest to identify how these results change when monoclonal antibody therapy is given to patients on cART, who already have an increased T_0/V_0 ratio, In that situation, the monoclonal antibody therapy will give us information about the effects the antibody has on the HIV latent reservoir.

We found virus rebound in all patients following the degradation of the infused antibody. To determine whether virus decays below one virion when antibody boosting is considered, we numerically simulated the effects of multiple infusions and found that, while five rounds of boosting each week may be enough for some patients to achieve virus decay below one virion, other, more frequent boosting regimes may be needed to achieve virus clearance in all patients.

Our model does not take into account a patient's own antibody response, which we consider to be inefficient in removing contemporary virus. Nor does it consider virus mutation away from the infused antibody, which we neglect due to the short period of treatment. Patients used in this study were all sensitive to the 3BNC117 therapy and, while resistance may play a factor, we show that antibody excretion from the body is enough to explain the observed virus rebound.

In conclusion, we developed a model of virus dynamics in the presence of 3BNC117 therapy and showed that the antibody elicits both neutralizing and non-neutralizing functions. We showed that the antibody binding is delayed and that a high ratio between initial CD4 T cell and initial virus ratio is a key component of a good response to the therapy. We hypothesize that through repeated antibody boosting HIV may reach below one copy level in the blood.

Chapter 6

Conclusion

My expertise in immunological modeling converges with my experiences in the livestock industry in rural Kentucky. I spent a good portion of my adolescence on farms where I observed first-hand the movement and mannerisms of livestock, primarily horses. I have had an incredibly rewarding career as a competitive equestrian, earning the title of National Champion in horsemanship at the 2011 Intercollegiate Horse Show Association National Championship. I have gone on to compete in show jumping competitions against riders who ship their horses internationally from their training facilities to major venues in Florida, Texas, Kentucky, and Virginia. In each of these situations, the horses share stabling with other animals from around the world where the potential for infectious disease transmission can be high.

While significant care is given to individual competition horses, it is unfeasible to give the same standard of care to a herd of stock animals raised for beef or dairy production, making proper control of infection imperative to a successful farming operation. Similar to horses, cattle are shipped in tightly packed trailers and are raised in groups with common feeding and drinking facilities. Upon entering the farm-to-table pipeline, an asymptomatic individual could potentially infect other individuals with which it comes into contact. As these secondarily infected cattle continue through the pipeline to other stockyards, processing plants, and eventually to slaughter, greater populations are at risk of exposure to disease that could ultimately contaminate the human food supply. The problem of an infected individual traveling between several discrete populations through multiple geographic locations is complex and has tangible impacts on the health of both the exposed cattle and the humans who consume infected meat.

Although the models in this dissertation are focused on understanding human diseases, my longer-term career goal is to apply similar mathematical techniques in animal diseases, such as bovine immunodeficiency virus, escherichia coli, and equine hepres virus. Addressing these problems through quantitatively based solutions will improve animal livelihood and help target critical points within the farm-to-table pipeline that will enable infectious disease management in livestock populations to be more efficient and economical. The study of herd infection across geographic boundaries bridges immunology and epidemiology with agricultural practice in complex, multiscale biological systems.

Over the course of my career, connections and collaborations with veterinary immunologists and epidemiologists will help me to develop my research career in mathematical modeling of multi-scale disease propagation in animals. Typically, veterinary researchers amass large pools of data during the course of their studies. However, the interactions between many of these datasets remain obscured by the highly controlled experimental conditions under which they are obtained. Post-hoc mathematical modeling is able to elucidate connections between variables investigated under vastly different conditions and explain from a theoretical perspective the results of a study. The mathematical modeling of complex systems enables researchers to perform critical experiments in a more cost-effective and time-efficient manner. Additionally, and especially with regard to infectious disease, mathematical models are able to make predictions using sparse datasets and under experimental conditions that may be otherwise difficult or unethical to perform in vivo. Through collaborations that I develop during my postdoctoral work and the proximity in which I will work with veterinary researchers, I will be able to more easily obtain data specific to the problems and interactions I describe mathematically. Ideally, the models I develop over the course of my career will impact the management of livestock pathologies to reduce the burden they place on the agricultural economic sector, as well as general human and animal health.

This dissertation represents the beginning of what is hopefully a long career in infectious disease modeling across many different species. Within this work, we discuss multiple studies that highlight the utility of mathematical modeling to investigate hypotheses in biological systems that may be unfeasible or unethical to carry out experimentally. In the first chapters, we review mathematical appliations in the life sciences, provide an introduction to virology, and specifically discuss HIV and HPV. We highlight major advances in immunology developed from modeling work and discuss the fine immunological details of germinal centers, Tfh cells, and antibodies. We also provide a detailed background of the modeling tools used throughout this dissertation.

We develop a mathematical model of an HIV HPV co-infection to identify conditions where HIV infections alters HPV persistence. We also investigate HPV outcomes in a co-infection scenario during ART. Next we explore the generic immunological process by which a host responds to any foreign pathogen. In chapter 4 we develop a mathematical model for germinal centers during acute disease and estimate parameters based on germinal center B cell data. We extend this model for chronic disease and predict that T follicular helper cells are the limiting factor and investigate germinal center formation for a mutating virus and hypothesize what might lead to the development of broadly neutralizing antibodies.

Finally, we model monoclonal antibody therapy in HIV infected individuals. We develop a mathematical model to elucidate the underpinnings of 3BNC117. Using patient data we fit our parameters and hypothesize why patients rebound after treatment. With the therapy model, we then predict the effect of repeated 3BNC117 therapy boosting on patients.

In summary we have developed mathematical models for the immune responses to infectious diseases. We studied immune response in context to a specific virus as well as for a generic pathogen, and gained insight to successful immune responses. With in the projects we have drawn new conclusions by combining previously published worked, we have developed a completely new model, and we have adjusted a published model for treatments and fit published patient data to the model.

Bibliography

[1] R. Albrecht and J. Oliver. Labeling considerations for confocal microscopy. In Basic Confocal Microscopy, pages 79–114. Springer, 2011.

[2] C. Allen, T. Okada, and J. Cyster. Germinal-center organization and cellular dynamics. Immunity, 27(2):190–202, 2007.

[3] ART Cohort Collaboration. Life expectancy of individuals on combination antiretroviral therapy in high-income countries: a collaborative analysis of 14 cohort studies. Lancet, 372:293–9, 2008.

[4] E. Arts and D. Hazuda. HIV-1 antiretroviral drug therapy. Cold Spring Harb Perspect Med, 2:1–23, 2012.

[5] B. Asquith and C. Bangham. Review: An introduction to lymphocyte and viral dynamics: the power and limitations of mathematical analysis. Proceedings of the Royal Society of London B: Biological Sciences, 270:1651–7, 2003.

[6] B. Asquith, C. Debacq, A. Florins, N. Gillet, T. Sanchez-Alcaraz, A. Mosley, and L. Willems. Quantifying lymphocyte kinetics in vivo using carboxyfluorescein diacetate succinimidyl ester (CFSE). Proc Biol Sci, 273:1165–71, 2006.

[7] R. Aster, B. Borchers, and C. Thurber. Parameter Estimation and Inverse Problems. Elsevier, 2005.

[8] P. Baccam, C. Beauchemin, C. Macken, F. Hayden, and A. Perelson. Kinetics of influenza a virus infection in humans. J Virol, 80:7590–9, 2006.

[9] D. Beachler and G. D'Souza. Oral HPV infection and head and neck cancers in HIV-infected individuals. Curr Opin Onco, 25:503–10, 2013.

[10] D. Beachler, E. Sugar, J. Margolick, K. Weber, and et al. Risk factors for acquisition and clearance of oral human papillomavirus infection among HIV-infected and HIV-uninfected adults. Am J Epidemiol, pages 40–53, 2014.

[11] C. Beauchemin and A. Handel. A review of mathematical models of influenza a infections within a host or cell culture: lessons learned and challenges ahead. BMC Public Health, 11:S7, 2011.

[12] M. Beaumont and B. Rannala. The bayesian revolution in genetics. Nat Rev Genet, 5:251–61, 2004.

[13] G. Bocharov and A. Romanyukha. Mathematical model of antiviral immune response iii. influenza a virus infection. J Theor Biol, 167:323–60, 1994.

[14] D. Bortz and P. Nelson. Sensitivity analysis of a nonlinear lumped parameter model of hiv infection dynamics. Bull Math Biol, 66:1009–26, 2004.

[15] F. Broere, S. Apasov, M. Sitkovsky, and W. van Eden. A2 t cell subsets and t cell-mediated immunity. In Principles of immunopharmacology, pages 15–27. 2011.

[16] D. Burton. Antibodies, viruses and vaccines. Nat Rev Immunol, 2:706–13, 2002.

[17] D. Burton and J. Mascola. Antibody responses to envelope glycoproteins in HIV-1 infection. Nat Immunol, 16:571–6, 2015.

[18] J. Cameron, D. Mercante, M. O'Brien, A. Gaffga, J. Leigh, P. J. Fidel, and et al. The impact of highly active antiretroviral therapy and immunodeficiency on human papillomavirus

infection of the oral cavity of human immunodeficiency virus–seropositive adults. Sexually Transm Dis, 32:703–9, 2005.

[19] M. Caskey, F. Klein, J. Lorenzi, M. Seaman, and et al. Viremia suppressed in HIV-1-infected humans by broadly neutralizing antibody 3BNC117. Nature, 522:487–91, 2015.

[20] T. Chun, L. Carruth, D. Finzi, S. X, J. DiGiuseppe, H. Taylor, and et al. Quantification of latent tissue reservoirs and total body viral load in HIV-1 infection. Nature, 387:183–8, 1997.

[21] S. Ciupe, B. Bivort, D. Bortz, and P. Nelson. Estimating kinetic parameters from HIV primary infection data through the eyes of three different mathematical models. Math Biosci, 200:1–27, 2006.

[22] S. Ciupe, P. De Leenheer, and T. Kepler. Paradoxical suppression of poly-specific broadly neutralizing antibodies in the presence of strain-specific neutralizing antibodies following hiv infection. J Theor Biol, 277:55–66, 2011.

[23] S. Ciupe, R. Ribeiro, P. Nelson, G. Dusheiko, and A. Perelson. The role of cells refractory to productive infection in acute hepatitis B viral dynamics. Proc Natl Acad Sci U S A, 104:5050–5, 2007.

[24] S. Ciupe, R. Ribeiro, and A. Perelson. Antibody responses during hepatitis b viral infection. Math Biosci, 263:83–92, 2015.

[25] J. Conway and D. Coombs. A stochastic model of latently infected cell reactivation and viral blip generation in treatedHIVpatients. PLoS Comput Biol, 7:1–15, 2011.

[26] A. Cormack. Recollections of my work with computer assisted tomography. Mol Cell Biochem, 32:57–61, 1980.

[27] A. Corthay. How do regulatory T cells work? Scand J Immunol, 70:326–36, 2009.

[28] S. Crotty. Follicular helper CD4 T cells (Tfh). Annu. Rev. Immunol., 29:621–63, 2011.

[29] R. Cubas, J. Mudd, A. Savoye, M. Perreau, J. van Grevenynghe, and et al. Inadequate T follicular cell help impairs B cell immunity during HIV infection. Nat Med, 19:494–9, 2013.

[30] H. Dahari, E. Shudo, R. Ribeiro, and A. Perelson. Modeling complex decay profiles of Hepatitis B virus during antiviral therapy. Hepatology, 49:32–8, 2009.

[31] R. De Boer and A. Perelson. Quantifying T lymphocyte turnover. J Theor Biol, 327:45–87, 2013.

[32] R. De Boer, R. Ribeiro, and A. Perelson. Current estimates for hiv-1 production imply rapid viral clearance in lymphoid tissues. PLoS Comput Biol, 6:1–9, 2010.

[33] S. De Flora and S. La Maerstra. Epidemiology of cancers of infectious origin and prevention strategies. J Prev Med Hyg, 56:E15–20, 2015.

[34] L. Denny, S. Franceschi, S. de Sanjose, I. Heard, A. Moscicki, and J. Palefsky. Human papillomavirus, human immunodeficiency virus and immunosuppression. Vaccine, 30:F168–74, 2012.

[35] J. Doorbar. Molecular biology of human papillomavirus infection and cervical cancer. Clin Sci, 110:525–41, 2006.

[36] J. Doorbar, W. Quint, L. Banks, I. Bravo, and et al. The biology and life-cycle of human papillomaviruses. Vaccine, 30:F55–70, 2012.

[37] G. D'Souza, C. Fakhry, E. Sugar, E. Seaberg, K. Weber, H. Minkoff, and et al. Six-month natural history of oral versus cervical human papillomavirus infection. Int J Cancer, 121:143–50, 2007.

[38] G. D'Souza, A. Kreimer, R. Viscidi, M. Pawlita, C. Fakhry, W. Koch, and et al. Case study of human papillomavirus and oropharyngeal cancer. N Engl J Med, 356:1944–56, 2007.

[39] R. Eftimie, J. Gillard, and D. Cantrell. Mathematical models for immunology: Current state of the art and future research directions. Bull Math Biol, 78:2091–134, 2016.

[40] N. Egawa, K. Egawa, H. Griffin, and J. Doorbar. Human papillomaviruses; epithelial tropisms, and the development of neoplasia. Viruses, 7:3863–90, 2015.

[41] M. Einstein, J. Schiller, R. Viscidi, H. Strickler, and et al. Clinician's guide to human papillomavirus immunology: knowns and unknowns. Lancet Infect Dis, 9:347–56, 2009.

[42] S. Erwin and S. Ciupe. Germinal center dynamics during acute and chronic infection. Mathematical Biosci Eng, 14:655–71, 2017.

[43] C. for Disease Control and Prevention. Prevention of genital human papillomavirus infection. Department of Health and Human Services, 2004.

[44] W. Fuchs, A. Kreuter, M. Hellmich, A. Potthoff, J. Swoboda, N. Brockmeyer, and et al. Asymptomatic anal sexually transmitted infections in HIV positive men attending anal cancer screening. Br J Dermatol, pages 1–8, 2015.

[45] G. Galfre and C. Milstein. Preparation of monoclonal antibodies: Strategies and procedures. Methods Enzymol, 73:3–46, 1981.

[46] R. Geskus, C. Gonzalez, M. Torres, J. Del Romero, P. Viciana, M. Masia, and et al. Incidence and clearance of anal high-risk human papillomavirus in HIV-positive men who have sex with men: estimates and risk factors. AIDS, 30:37–44, 2016.

[47] P. Gravitt. The known unknowns of HPV natural history. J Clin Invest, 121(12):4593–9, 2011.

[48] J. Grierson, R. Koelmeyer, A. Smith, and M. Pitts. Adherence to antiretroviral therapy: factors independently associated with reported difficulty taking antiretroviral therapy in a national sample of HIV-positive australians. HIV Med, 12:562–9, 2011.

[49] J. Grivel, M. Penn, D. Eckstein, B. Schramm, R. Speck, N. Abbey, and et al. Human immunodeficiency virus type 1 coreceptor preferences determine target T-cell depletion and cellular tropism in human lymphoid tissue. J Virol, 74:5347–51, 2000.

[50] D. Groves, W. Lever, and T. Makinodan. Stochastic model for the production of antibody-forming cells. Nature, 222, 1969.

[51] R. Gupta and R. K. Global epidemiology of drug resistance after failure of WHO recommended first-line regimens for adult HIV-1 infection: a multicentre retrospective cohort study. Lancet Infect Dis, 15:1–11, 2016.

[52] A. Hauser, M. Shlomchik, and A. Haberman. In vivo imaging studies shed light on germinal-centre development. Nat Rev Immunol, 7:499–504, 2007.

[53] B. Haynes. New approaches to HIV vaccine development. Curr Opin Immunol, 35:39–47, 2015.

[54] D. Henrard, E. Daar, H. Farzadegan, S. Clark, and et al. Virologic and immunologic characterization of symptomatic and asymptomatic primary HIV-1 infection. J Acquir Immune Defic Syndr Hum Retrovirol, 9:305–10, 1995.

[55] H. Hethcote. The mathematics of infectious diseases. SIAM Rev, 42:599–653, 2000.

[56] A. Hodgkin and A. Huxley. A quantitative description of membrane current and its application to conduction and excitation in nerve. J Physiol, 117:500–44, 1952.

[57] P. Hodgkin, J. Lee, and A. Lyons. B cell differentiation and isotype switching is related to division cycle number. J Exp Med, 184:277–81, 2005.

[58] K. Hollowood and J. Macartney. Cell kinetics of the germinal center reaction - a stathmokinetic study. Eur J Immunol, 22:261–6, 1992.

[59] F. Hoppensteadt and C. Peskin. Mathematics in medicine and the life sciences, volume 10. Springer Science & Business Media, 2013.

[60] J. Horwitz, A. Stromberg, H. Mouquet, A. Gitlin, A. Tretiakova, T. Eisenreich, and et al. HIV-1 suppression and durable control by combining single broadly neutralizing antibodies and antiretroviral drugs in humanized mice. Proc Natl Acad Sci U S A, 110:16538–43, 2013.

[61] D. Iber and P. Maini. A mathematical model for germinal centre kinetics and affinity maturation. J Theor Biol, 219:153–75, 2002.

[62] T. Igarashi, C. Brown, A. Azadegan, N. Haigwood, and et al. Human immunodeficiency virus type 1 neutralizing antibodies accelerate clearance of cell–free virions from blood plasma. Nat Med, 5:211–6, 1999.

[63] C. Janeway, P. Travers, M. Walport, and M. Shlomchik. Immunobiology. 6. Garland Science, 2005.

[64] A. Jemal, M. Center, C. DeSantis, and E. Ward. Global patterns of cancer incidence and mortality rates and trends. Cancer Epidemiol, 19:1893–907, 2010.

[65] A. Jung and D. Paauw. Diagnosing HIV-related disease: using the CD4 count as a guide. J Gen Intern Med, 13:131–6, 1998.

[66] T. Kepler and A. Perelson. Cyclic re-entry of germinal center B cells and the efficiency of affinity maturations. Immunol Today, 14:412–5, 1993.

[67] C. Kesmir and R. De Boer. A mathematical model on germinal center kinetics and termination. J Immunol, 163:2463–9, 1999.

[68] C. Kesmir and R. de Boer. A spatial model of germinal center reactions: cellular adhesion based sorting of B cells results in efficient affinity maturation. J Theor Biol, 222:9–22, 2003.

[69] R. Kim, J. Yochim, M. Kang, K. Shin, R. Christensen, and N. Park. HIV-1 Tat enhances replicative potential of human oral keratinocytes harboring HPV-16 genome. Int J Oncol, 33:777–82, 2008.

[70] C. King, S. Tangye, and C. Mackay. T follicular helper (TFH) cells in normal and dysregulated immune responses. Annu. Rev. Immunol., 26:741–66, 2008.

[71] J. Kravchenko, I. Akushevich, S. Sudenga, C. Wilson, and et al. Transitional probability-based model for HPV clearance in HIV-1-positive adolescent females. PloS one, 7:1–11, 2012.

[72] F. Kroese, A. Wubbena, H. Seijen, and P. Nieuwenhuis. Germinal centers develop oligoclonally. Eur J Immunol, 17:1069–72, 1987.

[73] R. Kuppers, M. Zhao, M. Hansmann, and K. Rajewsky. Tracing B cell development in human germinal centers by molecular analysis of single cells picked from histological sections. Embo J, 12:4955–67, 1993.

[74] P. Kwong and J. Mascola. Human antibodies that neutralize HIV-1: identification, structures, and B cell ontogenies. Immunity, 37:412–425, 2012.

[75] V. L and M. Diaz. Autoreactivity in HIV-1 broadly neutralizing antibodies: implications for their function and induction by vaccination. Curr OpinHIVAIDS, 9:224–34, 2014.

[76] A. Layton. Mathematical modeling of kidney transport. Wiley Interdiscip Rev Syst Biol Med, 5:557–73, 2013.

[77] M. Lederman, A. Penn-Nicholson, M. Cho, and D. Mosier. Biology of ccr5 and its role inHIVinfection and treatment. Jama, 296(7):815–26, 2006.

[78] F. Lee, J. Amin, and A. Carr. Limited reporting of major harms in studies of initial combination antiretroviral therapy: a systematic review. AIDS, 29:921–9, 2005.

[79] H. Lee, E. Hawkins, M. Zand, T. Mosmann, H. Wu, and et al. Interpreting CFSE obtained division histories of B cells in vitro with Smith-Martin and cyton type models. Bull Math Biol, 71:1649–70, 2009.

[80] I. LeGrice, P. Hunter, and B. Smaill. Laminar structure of the heart: a mathematical model. Am J Physiol, 272:H2466–76, 1997.

[81] G. Levi, J. Feldman, S. Holman, A. Salarieh, H. Strickler, S. Alter, and et al. Relationship between HIV viral load and langerhans cells of the cervical epithelium. J of Obstet and Gynaecol Res, 31:178–84, 2005.

[82] C. Lewden, G. Chene, P. Morlat, F. Raffi, and et al. HIV-infected adults with a CD4 cell count greater than 500 cells/mm3 on long-term combination antiretroviral therapy reach same mortality rates as the general population. J Acquir Immune Defic Syndr, 46:72–7, 2007.

[83] M. Lindqvist, J. van Lunzen, D. Soghoian, B. Kuhl, S. Ranasinghe, and et all. Expansion of HIV-specific T follicular helper cells in chronic HIV infection. J Clin Invest, 122:3271–80, 2012.

[84] S. Luria and M. Delbrück. Mutations of bacteria from virus sensitivity to virus resistance. Genetics, 28:491, 1943.

[85] I. MacLennan. Germinal centers. Annu Rev Immunol., 12:117–39, 1994.

[86] G. Maglennon, P. McIntosh, and J. Doorbar. Persistence of viral dna in the epithelial basal layer suggests a model for papillomavirus latency following immune regression. Virology, 414:153–63, 2011.

[87] J. Marchalonis and V. Gledhill. Elementary stochastic model for the induction of immunity and tolerance. Nature, 220, 1968.

[88] D. Margolis, J. Garcia, D. Hazuda, and B. Haynes. Latency reversal and viral clearance to cure HIV-1. Science, 353:aaf6517, 2016.

[89] L. Markowitz, E. Dunne, M. Saraiya, H. Chesson, and et al. Human papillomavirus vaccination: recommendations of the advisory committee on immunization practices (ACIP). MMWR Recomm Rep, 63:1–30, 2014.

[90] R. McDougal, T. Morse, T. Carnevale, L. Marenco, and et al. Twenty years of ModelDB and beyond: building essential modeling tools for the future of neuroscience. J Comput Neurosci, pages 1–10, 2016.

[91] Merck Co Inc. Gardasil9 safety information. Merck Sharp and Dohme Corp, pages 1–23, 2016.

[92] M. Meyer-Hermann. A mathematical model for the germinal center morphology and affinity maturation. J Theor Biol, 216:273–300, 2002.

[93] M. Meyer-Hermann, M. Figge, and K. Toellner. Germinal centres seen through the mathematical eye: B-cell models on the catwalk. Trends in Immunol, 30:157–64, 2009.

[94] M. Meyer-Hermann and P. Maini. Cutting edge: back to one-way germinal centers. J Immunol, 174:2489–93, 2005.

[95] M. Meyer-Hermann, P. Maini, and D. Iber. An analysis of B cell selection mechanisms in germinal centers. Math Med Biol, 23:255–77, 2006.

[96] M. Meyer-Hermann, E. Mohr, N. Pelletier, Y. Zhang, G. Victoria, and K. Toellner. A theory of germinal center B cell selection, division, and exit. Cell Reports, 2:162–174, 2012.

[97] H. Miao, X. Jin, A. Perelson, and H. Wu. Evaluation of multitype mathematical models for CFSE-labeling experiment data. Bull Math Biol, 74:300–26, 2012.

[98] I. Mikell, D. Sather, S. Kalams, M. Altfeld, G. Alter, and L. Stamatatos. Characteristics of the earliest cross-neutralizing antibody response to HIV-1. PLoS Pathog, 7:1–15, 2011.

[99] A. Mocroft, S. Vella, T. Benfield, A. Chiesi, and et al. Changing patterns of mortality across europe in patients infected with HIV-1. The Lancet, 352:1725–30, 1998.

[100] H. Mohri, A. Perelson, K. Tung, R. M. Ribeiro, and et al. Increased turnover of T lymphocytes in HIV-1 infection and its reduction by antiretroviral therapy. The Jour of Exp Med, 194:1277–88, 2001.

[101] M. Moody, R. Zhang, E. Walter, C. Woods, G. Ginsburg, and et al. H3N2 influenza infection elicits more cross-reactive and less clonally expanded anti-hemaglutinin antibodies than influenza vaccination. PLoS One, 6:1–14, 2011.

[102] S. Mooij, D. van Santen, R. Geskus, M. van Der Sande, R. Coutinho, I. Stolte, and et al. The effect of HIV infection on anal and penile human papillomavirus incidence and clearance: a cohort study among MSM. AIDS, 30:121–32, 2016.

[103] J. Moore. Coreceptors–implications for HIV pathogenesis and therapy. Science, 276(5309):51–2, 1997.

[104] J. Moreira and J. Faro. Modelling two possible mechanisms for the regulation of the germinal center dynamics. J Immunol, 177:3705–10, 2006.

[105] A. Moscicki, M. Schiffman, S. Kjaer, and L. Villa. Chapter 5: updating the natural history of HPV and anogenital cancer. vaccine 24 (suppl): S3, s42–s51, 2006.

[106] K. Mosegaard and M. Sambridge. Monte carlo analysis of inverse problems. Inverse Problems, 18:R29–54, 2002.

[107] C. Murall, C. Bauch, and T. Day. Could the human papillomaviurs vaccines drive virulence evolution. Proc Biol Sci, 282:1–10, 2015.

[108] C. Murall, K. McCann, and C. Bauch. Revising ecological assumptions about human papillomavirus interactions and type replacement. J Theor Bio, 350:98–109, 2014.

[109] M. Nakagawa, D. Stites, S. Patel, S. Farhat, and et al. Persistence of human papillomavirus type 16 infection is associated with lack of cytotoxic T lymphocyte response to the E6 antigens. J Infect Dis, 182:595–8, 2000.

[110] A. Nelson, E. Dhimolea, and J. Reichert. Development trends for human monoclonal antibody therapeutics. Nat Rev Drug Discov, 9:767–74, 2010.

[111] R. Nikin-Beers and S. Ciupe. The role of antibody in enhancing dengue virus infection. Math Biosci, 263:83–92, 2015.

[112] M. Nowak and C. Bangham. Population dynamics of immune responses to persistent viruses. Science, 272:74–9, 1996.

[113] K. NR, S. E, O. AM, E. JC, and et al. CD8+ lymphocytes control viral replication in SIVmac239-infected rhesus macaques without decreasing the lifespan of productively infected cells. PLoS Pathog, 6:1–11, 2010.

[114] M. Oprea and A. Perelson. Somatic mutation leads to efficient affinity maturation when centrocytes recycle back to centroblasts. J Immunol, 158:5155–62, 1997.

[115] M. Oprea, E. van Nimwegen, and A. Perelson. Dynamics of one-pass germinal center models: implications for affinity maturation. Bull Math Biol, 62:121–53, 2000.

[116] W. H. Organization. Comprehensive cervical cancer control: A guide to essential practice. 2:1–393, 2014.

[117] J. Overbaugh and L. Morris. The antibody response against HIV-1. Cold Spring Harb perspect Med, 2:1–18, 2012.

[118] S. Pallikkuth, A. Parmigiani, and S. Pahwa. The role of interleukin-21 in HIV infection. Cytokine growth factor rev, 23:173–80, 2012.

[119] A. Perelson, P. Essunger, Y. Cao, M. Vesanen, and et al. Decay characteristics of hiv-1-infected compartments during combination therapy. Nature, 387:188–191, 1997.

[120] A. Perelson, D. Kirschner, and R. de Boer. Dynamics ofHIVinfection of cd4+ t cells. Math Biosci, 114:81–125, 1993.

[121] A. Perelson, A. Neumann, M. Markowitz, J. Leonard, and et al. HIV-1 dynamics in vivo: virion clearance rate, infected cell life-span, and viral generation time. Science, 271:1582–6, 1996.

[122] A. Perelson and R. Ribeiro. Estimating drug efficacy and viral dynamic parameters: HIV and HCV. Stat Med, 27:4647–57, 2008.

[123] A. Perelson and R. Ribeiro. Modeling the within-host dynamics of HIV infection. BMC Biol, 11:1–10, 2013.

[124] M. Perreau, A.-L. Savoye, E. De Crignis, J. Corpataux, R. Cubas, and et al. Follicular helper T cells serve as the major CD4 T cell compartment for HIV-1 infection, replication, and production. J Exp Med, 210:143–56, 2013.

[125] A. Picard, C. Badoual, M. Hourseau, C. Halimi, H. Pere, F. Dib, and et al. HPV prevalence in HIV patients with head and neck squamous cell carcinoma. AIDS, 30:1257–66, 2016.

[126] A. Pratama and C. Vinuesa. Control of tfh cell numbers: why and how & quest. Immunol Cell Biol, 92:40–8, 2014.

[127] A. Proudfoot, T. Wells, and P. Clapham. Chemokine receptors-future therapeutic targets for HIV? Biochem Pharmacol, 57:451–64, 1999.

[128] J. Publicover, A. Gaggar, S. Nishimura, C. Van Horn, A. Goodsell, and et al. Age-dependent hepatic lymphoid organization directs successful immunity to Hepatitis B. J Clin Invest, 123:3728–39, 2013.

[129] J. Publicover, A. Goodsell, S. Nishimura, S. Vilarinho, Z. Wang, and et al. IL-21 is pivotal in determining age-dependent effectiveness of immune responses in a mouse model of human hepatitis B. J Clin Invest, 121:1154–62, 2011.

[130] M. Radmacher, G. Kelsoe, and T. Kepler. Predicted and inferred waiting times for key

mutations in the germinal centre reaction: evidence for stochasticity in selection. Immunol and Cell Bio, 76:373–81, 1998.

[131] B. Ramratnam, S. Bonhoeffer, J. Binley, A. Hurley, and et al. Rapid production and clearance of HIV-1 and Hepatitis C virus assessed by large volume plasma apheresis. Lancet, 354:1782–5, 1999.

[132] D. Rosenbloom, A. Hill, S. Rabi, R. Siliciano, and M. Nowak. Antiretroviral dynamics determines HIV evolution and predicts therapy outcome. Nat med, 18:1378–85, 2012.

[133] A. Rositch, A. Burke, R. Viscidi, M. Silver, and et al. Contributions of recent and past sexual partnerships on incident human papillomavirus detection: acquisition and reactivation in older women. Cancer Res, 72:6183–90, 2012.

[134] M. Ryser, E. Myers, and R. Durrett. HPV clearance and the neglected role of stochasticity. PLoS Comput Biol, 11:1–16, 2015.

[135] S. Sakaguchi. Naturally arising CD4+ regulatory T cells for immunologic self-tolerance and negative control of immune responses. Annu. Rev. Immunol., 22:531–62, 2004.

[136] T. Sasagawa, H. Takagi, and S. Makinoda. Immune responses against human papillomavirus (HPV) infection and evasion of host defense in cervical cancer. J Infect Chemother, 18:807–15, 2012.

[137] J. Scheid, J. Horwitz, Y. Bar-On, E. Kreider, C. Lu, J. Lorenzi, and et al. HIV-1 antibody 3BNC117 suppresses viral rebound in humans during treatment interruption. Nature, 00:1–8, 2016.

[138] J. Scheid, H. Mouquet, B. Ueberheide, R. Diskin, F. Klein, T. Oliveira, and et al. Sequence and structural convergence of broad and potent HIV antibodies that mimic CD4 binding. Science, 333:1633–1637, 2011.

[139] M. Schnell, J. Johnson, L. Buonocore, and J. Rose. Construction of a novel virus that targets HIV-1-infected cells and controls HIV-1 infection. Cell, 90(5):849–57, 1997.

[140] T. Schoofs, F. Klein, M. Braunschweig, E. Kreider, and et al. HIV-1 therapy with monoclonal antibody 3BNC117 elicits host immune responses against HIV-1. Science, 352:997–1001, 2016.

[141] T. Schwickert, G. Victoria, D. Fooksman, A. Kamphorst, M. Mugnier, and et al. A dynamic T cell-limited checkpoint regulates affinity-dependent B cell entry into the germinal center. J Exp Med, 208:1243–52, 2011.

[142] A. Scott, J. Allison, and J. Wolchok. Monoclonal antibodies in cancer therapy. Cancer Immun, 12:1–8, 2012.

[143] M. Scott, M. Nakagawa, and A. Moscicki. Cell-mediated immune response to human papillomavirus infection. Clin Diagn Lab Immunol, 8:209–20, 2001.

[144] P. Sharp and B. Hahn. Origins of HIV and the AIDS pandemic. Cold Spring Harb Perspect Med, 1:1–23, 2011.

[145] C. Shiboski, A. Lee, H. Chen, J. Webster-Cyriaque, T. Seaman, R. Landovitz, and et al. Human papillomavirus infection in the oral cavity of HIV patients is not reduced by initiating antiretroviral therapy. AIDS, [Epub ahead of print], 2016.

[146] Z. Shulman, A. Gitlin, S. Targ, M. Jankovic, G. Pasqual, and et al. T follicular helper cell dynamics in germinal centers. Science, 341:673–77, 2013.

[147] G. Siskind and B. Benacerraf. Cell selection by antigen in the immune response. Adv. Immunol., 10:1–50, 1969.

[148] A. Smith, F. Adler, R. Ribeiro, R. Gutenkunst, and et al. Kinetics of coinfection with influenza A virus and streptococcus pneumoniae. PLoS Pathog, 9:1–12, 2013.

[149] M. Stafford, L. Corey, Y. Cao, E. Daar, D. Ho, and A. Perelson. Modeling plasma virus concentration during primary HIV infection. J Theor Biol, 203:285–301, 2000.

[150] L. Stamatatos. HIV vaccine design: the neutralizing antibody conundrum. Curr Opin Immunol, 24:315–23, 2012.

[151] L. Stamatatos, L. Morris, D. Burton, and J. Mascola. Neutralizing antibodies generated during natural HIV-1 infection: good news for an HIV-1 vaccine? Nat Med, 15:866–70, 2009.

[152] M. Stanley. Epithelial cell responses to infection with human papillomavirus. Clin Microbiol Rev, 25:215–22, 2012.

[153] H. Strickler, R. Burk, M. Fazzari, K. Anastos, and et al. Natural history and possible reactivation of human papillomavirus in human immunodeficiency virus–positive women. J Natl Cancer Inst, 97(8):577–86, 2005.

[154] W. Suh. Life of T follicular helper cells. Mol Cells, 38:195–201, 2015.

[155] S. Syrjänen. Human papillomavirus infection and its association with HIV. Adv Dent Res, 23:84–9, 2011.

[156] C. T and F. M. Current status and prospects of HIV treatment. Curr Opin in Virol, 18:50 – 6, 2016.

[157] T. Tanaka, Y. Hishitani, and A. Ogata. Monoclonal antibodies in rheumatoid arthritis: comparative effectiveness of tocilizumab with tumor necrosis factor inhibitors. Biologics, 8:141–53, 2014.

[158] E. Tansey and P. Catterall. Monoclonal antibodies: a witness seminar in contemporary medical history. Med Hist, 38:322–7, 1994.

[159] J. Tas, L. Mesin, G. Pasqual, S. Targ, and et al. Visualizing antibody affinity maturation in germinal centers. Science, 351:1048–54, 2016.

[160] G. Tomaras, N. Yates, P. Liu, L. Qin, and et al. Initial b-cell responses to transmitted human immunodeficiency virus type 1: virion-binding immunoglobulin IgM and IgG antibodies followed by plasma anti-gp41 antibodies with ineffective control of initial viremia. J Virol, 82:12449–63, 2008.

[161] S. Tugizov, R. Herrera, P. Chin-Hong, P. Veluppillai, D. Greenspan, J. Michael Berry, and et al. HIV-associated disruption of mucosal epithelium facilitates paracellular penetration by human papillomavirus. Virology, 446:378–88, 2013.

[162] UNAIDS. Global HIV statistics. World AIDS Day, pages 1–8, 2016.

[163] A. Venuti, F. Paolini, L. Nasir, A. Corteggio, and et al. Papillomavirus E5: the smallest oncoprotein with many functions. Mol Cancer, 10:1–18, 2011.

[164] L. Verkoczy, G. Kelsoe, M. Moody, and B. Haynes. Role of immune mechanisms in induction of HIV-1 broadly neutralizing antibodies. Curr Opin Immunol, 23:383–90, 2011.

[165] M. Verma, S. Erwin, A. Abedi, R. Hontecillas, and et al. Modeling the mechanisms by which HIV-associated immunosuppression influences HPV persistence at the oral mucosa. PlosOne, 12:e0168133, 2016.

[166] S. Vernon, C. Hart, W. Reeves, and J. Icenogle. The HIV-1 tat protein enhances E2-dependent human papillomavirus 16 transcription. Virus Res, 2:133–45, 1993.

[167] G. Victora and L. Mesin. Clonal and cellular dynamics in germinal centers. Curr Opin Immunol, 28:90–6, 2014.

[168] G. Victora and M. Nussenzweig. Germinal centers. Ann Rev Immunol, 30:429–57, 2012.

[169] C. Vinuesa. HIV and T follicular helper cells: a dangerous relationship. J Clin Invest, 122:3059–62, 2012.

[170] C. Vinuesa, I. Sanz, and M. Cook. Dysregulation of germinal centres in autoimmune disease. Nat Rev Immunol, 9:845–57, 2009.

[171] J. Weinstein, S. Hernandez, and J. Craft. T cells that promote B-cell maturation in systemic autoimmunity. Immunol Rev, 247:160–171, 2012.

[172] R. A. Weiss. HIV receptors and cellular tropism. IUBMB life, 53:201–5, 2002.

[173] I. Wollenberg, A. Agua-Doce, A. Hernandez, C. Almeida, V. Oliveira, and et al. Regulation of the germinal center reaction by Foxp3+ follicular regulatory T cells. J Immunol, 187:4553–4560, 2011.

[174] X. Wu, T. Zhou, J. Zhu, B. Zhang, I. Georgiev, and et al. Focused evolution of HIV-1 neutralizing antibodies revealed by structures and deep sequencing. Science, 333:1593–602, 2011.

[175] X. Zhang, S. Ing, A. Fraser, M. Chen, O. Khan, J. Zakem, and et al. Follicular helper T cells: new insights into mechanisms of autoimmune diseases. Ochsner J, 13:131–9, 2013.

[176] S. Zhao, Z. Xu, and Y. Lu. A mathematical model of hepatitis B virus transmission and its application for vaccination strategy in China. Int J Epidemiol, 29:744–52, 2000.